Department of Materials Science and Engineering

A computational framework for coupled modelling of three-phase systems with soluble surfactants

Gijsbert Alexander Wierink

Aalto University

DOCTORAL DISSERTATIONS

Aalto University publication series
DOCTORAL DISSERTATIONS 57/2012

A computational framework for coupled modelling of three-phase systems with soluble surfactants

Gijsbert Alexander Wierink

Doctoral dissertation for the degree of Doctor of Science in Technology to be presented with due permission of the School of Chemical Technology for public examination and debate in Auditorium V1 at the Aalto University School of Chemical Technology (Espoo, Finland) on the 25th of May 2012 at 12:00 noon (at 12 o'clock).

Aalto University
School of Chemical Technology
Department of Materials Science and Engineering
Research Group for Mechanical Processing and Recycling

Supervisor
Prof. Dr. Kari Heiskanen

Instructor
Prof. Dr. Kari Heiskanen

Preliminary examiners
Priv.Doz. Dr. Stefan Pirker, Johannes Keppler University, Linz, Austria
Dr. Mikko Manninen, VTT, Espoo, Finland

Opponent
Prof. Dr. Johannes Cilliers, Imperial College London, United Kingdom

Aalto University publication series
DOCTORAL DISSERTATIONS 57/2012

ISBN 978-952-60-4617-4 (printed)
ISBN 978-952-60-4618-1 (pdf)
ISSN-L 1799-4934
ISSN 1799-4934 (printed)
ISSN 1799-4942 (pdf)

Unigrafia Oy
Helsinki 2012

Finland

The dissertation can be read at http://lib.tkk.fi/Diss/

441 697
Printed matter

Aalto University

Aalto University, P.O. Box 11000, FI-00076 Aalto www.aalto.fi

Abstract

Author
Gijsbert Alexander Wierink

Name of the doctoral dissertation
A computational framework for coupled modelling of three-phase systems with soluble surfactants

Publisher School of Chemical Technology

Unit Department of Materials Science and Engineering

Series Aalto University publication series DOCTORAL DISSERTATIONS 57/2012

Field of research Mineral processing - Modelling of mineral froth flotation

Manuscript submitted 14 February 2012 **Manuscript revised** 17 April 2012

Date of the defence 25 May 2012 **Language** English

☒ **Monograph** ☐ **Article dissertation (summary + original articles)**

Abstract

Bubble-particle interaction is a key phenomenon in many industrial applications, for example in mineral froth flotation. Flotation systems are typically characterised by high void fraction of dispersed phases and often multiple surface active compounds are present. The complexity of bubble-particle interaction has lead researchers to develop simplified models for dilute systems and typically physical and physico-chemical aspects are left out.

This work discusses a modelling framework for analysis of bubble-particle interaction in the presence of soluble surfactants. The model includes full momentum coupling between gas, liquid, and solid phases using a coupling between Computational Fluid Dynamics (CFD) and the Discrete Element Method (DEM) named CFDEM. CFDEM is an open source modelling framework where the CFD code OpenFOAM and the DEM code LIGGGHTS interact.

To accommodate topological changes of the bubble surface during break-up and coallescence the Volume Of Fluid (VOF) method was used. Solid particles are tracked in a Lagrangian frame of reference and experience forces due to collisions and the presence of the gas-liquid interface. A comprehensive model has been developed where particle-interface forces are modelled as a hyperbolic function of the gradient of the phase fraction. Particles can be captured within the interfacial region and can detach from the bubble when the balance of forces so dictates. DLVO and non-DLVO forces, as well as inertial forces, form part the total stress balance and contribute to the momentum equation of all phases. Variable interfacial tension is taken into account by implementation of a volumetric transport equation for soluble surfactant in the bulk fluid and within the interfacial gas-liquid region. The method is fully mass conservative and combines higher order physical momentum coupling with physico-chemical momentum. The sub-models used need further study, but to the authors knowledge the model presented is the first to couple all momenta in a comprehensive modelling framework for bubble-particle interaction.

The main value of this work is that the computational framework is modular and easily extensible to include more accurate sub-models. The Lagrangian particles are in fact dynamic lists that can be populated by the properties appropriate to the system. These properties accommodate further development and help to identify future research needs in the field of flotation modelling.

Keywords Mineral froth flotation, modelling, CFD, DEM, three-phase flow

ISBN (printed) 978-952-60-4617-4 **ISBN (pdf)** 978-952-60-4618-1

ISSN-L 1799-4934 **ISSN (printed)** 1799-4934 **ISSN (pdf)** 1799-4942

Location of publisher Espoo **Location of printing** Helsinki **Year** 2012

Pages 118 **The dissertation can be read at** http://lib.tkk.fi/Diss/

Preface

This thesis was completed at the Research Group for Mechanical Processing and Recycling at Aalto University, School of Chemical Technology, in Espoo, Finland between January 2007 and September 2011. This work would not have been possible without the continued support from many people around me. I would like to extend my gratitude to all my teachers, in the broadest sense of the word.

I thank my supervisor Prof. Kari Heiskanen for making my Doctoral studies possible in the first place, continuously challenging me, and supporting me in the pursuit of my studies and research. Prof. Heiskanen introduced me to modelling of mineral froth flotation and the problems concerning various aspects of momentum coupling. I have had the privilege of continued scientific and financial support and academic freedom to explore experimental, theoretical, and computational topics related to flotation modelling. I greatly appreciate this support and thank Prof. Heiskanen for the opportunities that I have had.

During the later stage of my Doctoral studies I have had to honour to spend half a year at the Laboratory for Thermal-Hydraulics (LTH) at the Paul Scherrer Institute (PSI) in Villigen, Switzerland. This visit was made possible by the positive and open attitude of Prof. Horst-Michael Prasser of ETH-Zürich and PSI and Dr. Bojan Ničeno of LTH at PSI. I deeply thank Prof. Prasser and Dr. Ničeno for their warm welcome, scientific support, supervision, and financial support that have made my visit possible. During my stay at LTH I have learnt a lot and had a great time doing so. I would like to thank my direct supervisor and colleagues at LTH, in particular Dr. Ničeno, Dr. Badillo, and Dr. Sato.

A key element of my research has been the open source CFD code OpenFOAM. I would like to thank all those who have contributed to the development and maintenance of the code. I thank my colleagues and friends that have helped and supported me in the development of my research using OpenFOAM. In particular I extend my gratitude to Mr. Mikko Au-

vinen, Dr. Ville Vuorinen, and Lic. Esko Järvinen for help, training, and useful discussions. I have also enjoyed the opportunity to learn about OpenFOAM at the OpenFOAM Summer School in Zagreb, Croatia, in 2009. For that thanks are due to Prof. Hrvoje Jasak and Dr. Željko Tuković.

Thanks to Dr. Christoph Goniva and Dr. Christoph Kloss of the Johannes Keppler University in Linz, Austria, I have been able to use the CFD-DEM coupled code CFDEM. I have very much enjoyed working with Dr. Goniva and Dr. Kloss and thank them deeply for their enthusiasm, help, and friendship.

My studies have been part of several research projects involving the School of Chemical Technology at Aalto University, VTT, and a consortium of companies through the Finnish Funding Agency for Technology and Innovation Tekes. I thank all colleagues in these projects for their collaboration and support. In particular I would like to thank Mr. Juha Tiitinen, Mr. Janne Vuori, and Dr. Marja Oja of the School of Chemical Technology, (late) Mr. Timo Niitti, Mr. Sami Grönstrand, Mr. Antti Rinne, and Dr. Kari Saloheimo of Outotec Oyj. Thanks are also due to Mrs. Tuija Mäkinen for many organisational matters she gracefully arranged without needing to do so.

Finally, I extend my gratitude to my family, family-in-law, and friends for their support during my studies and work. I thank my parents for providing me with the opportunity and support to pursue a university degree. A final and very special word of thanks is reserved for my wife Maaria and my son Theodor, who have supported me so much during easy and difficult times. Thank you all, I owe this work and experience to you.

Wokingham, United Kingdom, April 19, 2012,

Gijsbert Alexander Wierink

Contents

List of Figures

List of Tables

List of Symbols

Roman symbols

Symbol	Description	SI Unit
A	Hamaker constant	J
b_m	Machine accelaration	m s^{-2}
Bo	Modified Bond number $\left(\frac{G}{2\pi r_p \gamma}\right)$	-
C	Concentration	mol m^{-3}
d	Diameter	m
$\mathcal{D}$	Diffusion coefficient	m^2 s^{-1}
e	Elementary charge (1.602176565)	C
E_c	Collision efficiency	-
$\mathbf{E}_n$	Surface normal electric field strength	kg m s^{-3} A^{-1}
Eo	Eötvös number $\left(\frac{g(\rho_l-\rho_g)d_b^2}{\sigma}\right)$	-
F	Faraday constant (96485.34), force	A s mol^{-1}, kg m s^{-2}
$\mathbf{F}$	Force	kg m s^{-2}
G	Non-dimensional particle settling velocity $\left(\frac{2r_p^2(\rho_p-\rho_f)g}{9\mu_f U}\right)$	-
h	Pulp height in Eq.(2.3) and separation distance in Eq.(3.36)	m
H	Particle-particle separation distance in Eq.(3.22)	m
$\mathbf{H}$	H-operator (see Eq.(3.62))	
$\mathbf{I}$	Identity tensor	-
J_g	Superficial gas velocity	m s^{-1}
k	Flotation rate constant, Boltzmann constant (1.3806488·10^{-23})	-, J K^{-1}

K	Stokes number $\left(\frac{\tau_p}{\tau_f} = \frac{2\rho_p r_p^2 U}{9\mu_f r_b}\right)$, critical Stokes number	-
K_c	Critical Stokes number	-
K'	Function of Stokes number in Eq.(2.46): $K' = K\left(1 + \frac{\rho_p}{2\rho_f}\right)$	-
K''	Function of Stokes number in Eq.(2.46): $K'' = \frac{3K\rho_p}{2\rho_f}$	-
K'''	Function of Stokes number in Eq.(2.55): $K''' = \frac{(\rho_p - \rho_f)}{\rho_f} K$	-
K_{123}	Kinetic interaction constant	J
L	Capillary length	m
M	Morton number $\left(\frac{g\mu_l^4(\rho_l - \rho_g)}{\rho_l^2 \sigma^3}\right)$	-
$\mathbf{n}$	Interface normal vector	-
N	Number density	m^{-1}
p	Pressure	kg m^{-1} s^{-2}
$\tilde{q}$	Non-dimensionalised for of quantity q	-
$\overline{Q}$	Average of quantity Q	
r	Radius, polar coordinate	m
Re	Reynolds number $\left(\frac{Ud}{\nu}\right)$	(-)
$\mathbf{S}$	Source term	mol m^{-3} s^{-1}
$\mathbf{S}_f$	Surface area vector	m^2
t	Time	s
$\mathbf{t}$	Tangential surface vector	
T	Temperature, Tenacity	K, kg m s^{-2}
$\mathbf{U}$	Velocity	m s^{-1}
V	Volume, potential, energy	m^3, J, J
We	Weber number $\left(\frac{\rho U l}{\gamma}\right)$	-
w_r	Radial component of relative fluid velocity between two colliding particles, see Eq.(2.105)	m s^{-1}
z	Electro-valence, distance in Eq.(2.13)	-, m
Z	Collision frequency	s^{-1}

Greek symbols

Symbol	Description	SI Unit
α	Phase fraction	-
γ	Surface tension	kg s^{-2}
Γ	Surface surfactant concentration	mol m^{-2}
δ	Diffusive boundary layer thickness	m
ϵ	Characteristic amplitude of perturbation	m
ε	Turbulent kinetic energy dissipation rate, dielectric constant	m^2 s^{-3}, -
θ	Contact angle or polar coordinate	rad
κ	Curvature	m^{-1}
λ_p	Particle range in Eq.(2.39), characteristic wave length of perturbation Eqs.(3.35) and (3.41)	m
μ	Dynamic viscosity	kg m^{-1} s^{-1}
ν	Kinematic viscosity	m^2 s^{-1}
ϕ	Face flux	m^3 s^{-1}, -
Ψ	Stream function, surface potential	m^3 s^{-1}, V
ρ	Density	kg m^{-3}
σ	Stress tensor	kg m^{-1} s^{-2}
τ_p, τ_f	Particle (p) and fluid (f) response time	s

Indices

Symbol	Description
a, att	Attachment
b	Bubble, bulk, buoyancy
c	Compression, collision, critical
ca	Capillary
d	Drag
e	Electric
det	Detachment
eff	Effective
f	Fluid
g	Gas
h	Hydrophobic interaction
hyd	Hydrostatic pressure
i	Component i, induction
p	Particle, pressure
r	Radial
s	Surface, stability, solid
t	Tangency
vdW	Van der Waals
σ	Surface
θ	Tangential
τ	Shear stress
∞	Far-field

List of Abbreviations

CFD	Computational Fluid Dynamics	20
DEM	Discrete Element Method	20
$DLVO$	Derjaguin-Landau-Verwey-Overbeek (theory)	28, 64
GSE	Generalised Sutherland Equation	40
$LAMMPS$	Large-scale Atomic/Molecular Massively Parallel Simulator	20
LHS	Left-hand side	49
$LIGGGHTS$	LAMMPS Improved for General Granular and Granular Heat Transfer Simulations	20
$OpenFOAM$	Open Field Operation And Manipulation	20
PBM	Population Balance Model	19, 23
RHS	Right-hand side	31

1. Introduction

1.1 Mineral froth flotation

Mineral froth flotation may be defined as a physico-chemical process in which mineral particles, suspended in an aqueous solution, selectively adhere to dispersed air bubbles (Rehbinder, 1940). Mineralised bubbles rise to the top of the flotation cell where minerals are recovered as a froth concentrate (Rehbinder, 1940; Gaudin, 1957; Glembotskii et al., 1963). The flotation process can be divided into groups based on how air is delivered into the pulp and how the fine solid suspension is mixed. The most common type of flotation machine is the mechanically agitated flotation cell, where air is blown into the pulp through or nearby a rotor-stator mechanism.

1.2 Scope

The area of flotation modelling is of great interest since it is of major importance to both fundamental research and industrial application. Accurate flotation models can help engineers and scientists to design and control flotation equipment in an optimised way. Until date the fundamental mechanisms that govern bubble-particle interaction in flotation are still not understood well enough to develop a mathematical model from first principles. For this reason, most flotation models lean heavily on empirical knowledge (Tuteja et al., 1994) and are often (semi-)statistical in nature. It has been widely accepted that the rate of flotation is determined by the temporal efficiency at which bubbles and particles interact (Gaudin, 1932, p. 88). Gaudin (1932) took a deterministic approach and considered bubble-particle interaction as a multi-step process that can be analysed in discrete steps. Some of the authors (e.g. Gaudin (1932) and Sutherland (1948)) of seminal flotation papers openly criticised this approach and its shortcomings, but pointed out that these concessions were needed to produce workable results. The central point in these simplifications is the underlying exclusion of momentum coupling from the

models. It is important to note that momentum coupling, here, concerns the physical moments of inertia as well as interactions between momentum and chemical potential. A notable example of the latter coupling is the Marangoni effect.

In the context of this thesis it is instructive to consider three different scales, as schematically depicted in Fig. 1.1. These scales are the micro-scale, the meso-scale, and the macro-scale, respectively, and it must be noted that the length scales are indicative only and by no means discrete. The characteristic length scale of the nano/micro-scale is in the order of 10^{-10} to 10^{-5} m. At this scale, many important (molecular) physico-chemical phenomena take place and processes are often discrete in nature. The other end of the spectrum is the macro-scale, at the level of industrial processes and length scales larger than about 10^{-2} m, where hydrodynamic processes are dominant. Clearly, a critical part of modelling of mineral froth flotation is how information is transferred between the micro- and macro-scales. The coupling between the different spatial and temporal scales determines how hydrodynamics and (surface) physico-chemistry interact and how momentum is transferred between these scales. The scale that provides coupling between the micro- and macro-scales is referred to as the meso-scale. Meso-scale modelling can provide a valuable transfer function for the dynamic interaction between the very small and very large scales. The focus of this thesis is therefore on modelling of the dynamics at the meso-scale.

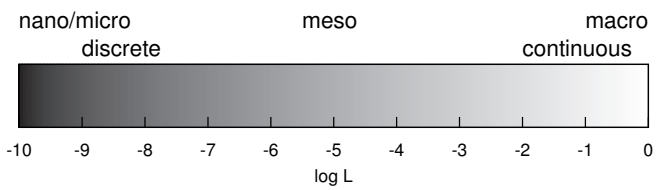

Figure 1.1. Schematic diagram of the different scales in modelling of mineral froth flotation. The log of the characteristic length scale L is indicated below the bar. The meso-scale forms the bridge between the (discrete) nano/micro-scale and the (continuous) macro-scale.

1.3 Objectives

The main objective of this thesis is to create a framework where different models of mineral froth flotation sub-processes can be developed and tested in a computational context. The model discussed in this thesis is not a flotation model in itself, but rather a test harness to investigate the appropriate physical and chemical fundamentals for the process at hand. Hydrodynamics at the scale of swarms of bubbles and particles can inter-

act with the physico-chemistry of surfactant dynamics at the gas-liquid interface and phenomena such as film rupture. This coupling of scales give the model a bridging property in flotation modelling. In summary, the general aims of this study are:

i. to develop a computational framework at the *meso-scale* to bridge the gap between the micro- and macro-scales (see Fig. 1.1) with features allowing full momentum coupling;

ii. to provide a testing ground for physico-chemical and kinetic models of flotation (sub-)processes;

iii. to couple physico-chemical and hydrodynamic phenomena, e.g. include the Marangoni effect to couple surface chemistry and interfacial momentum;

iv. to create a tool that can provide input for macro-scale (semi-)statistical models that can be validated at smaller scales.

This thesis includes the key elements that are necessary to implement full momentum coupling between phases with the Marangoni effect. However, to keep focus on the development of the modelling framework, some elements of interest are not included at this stage. The modelling framework discussed in this thesis does not include the following topics:

- Population Balance Modelling (PBM),
- molecular processes, and
- quantum dynamic effects.

1.4 Method

Historically, modelling of mineral froth flotation can be divided into two schools of thought; hydrodynamics (or mixing) and (surface) chemistry. It is important to understand that these two groups of phenomena occur simultaneously and in the same space. For example, the distribution of surfactants in the bulk is governed by hydrodynamics, changing surface tension and bubble drag locally. The latter is strongly coupled to hydrodynamics, in particular in more dense multiphase systems. At the level of individual particles and bubbles, surface chemistry determines the strength and direction of forces between particles and the gas-liquid interface and thus an important part of bubble-particle interaction in flotation. It is clear that an integrated modelling framework is needed for detailed and more holistic modelling of the flotation process.

The work presented in this thesis is a modelling framework using both Computational Fluid Dynamics (CFD) and the Discrete Element Method (DEM). Selection of a suitable development environment is of great importance to model transparency, code efficiency and portability, as well as knowledge retention. The CFD package used in this work is OpenFOAM®[1] (OpenCFD Ltd., 2011a), a mature open source CFD package produced by OpenCFD Ltd. The open and modular structure of OpenFOAM® allows for efficient model development and the use of readily parallelised solvers.

The motion of particles in the gas-liquid system is solved for using a DEM code coupled to the CFD solver. The CFD-DEM coupled framework is the open source CFD-DEM project CFDEM[2] (Goniva et al., 2011; Kloss et al., 2011). Within CFDEM, OpenFOAM® is coupled to the open source DEM code LIGGGHTS[3]. LIGGGHTS stands for "LAMMPS Improved for General Granular and Granular Heat Transfer Simulations" and is a fork of the molecular dynamics code LAMMPS (Large-scale Atomic/Molecular Massively Parallel Simulator)[4] (Plimpton, 1995).

[1] OpenFOAM - The open source CFD toolbox: `http://www.openfoam.com`
[2] CFDEM - Open Source CFD, DEM, and CFD-DEM: `http://www.cfdem.com`
[3] LIGGGHTS Open Source Discrete Element Method Particle Simulation Code: `http://www.liggghts.com`
[4] LAMMPS: `http://lammps.sandia.gov/`

1.5 Structure

To clarify the motivation of this thesis and the background of many flotation models in the literature, Chapter 2 covers a review of flotation modelling found in literature. First, kinetic modelling and dominant physicochemical phenomena are treated in Sections 2.1 and 2.2, respectively. The interaction between bubbles and particles is commonly divided into three sub-processes, namely bubble-particle collision, attachment of particles to bubbles, and bubble-particle aggregate stability. These three processes are discussed in Section 2.3. The key parameter in kinetic modelling of froth flotation is the flotation rate constant. The probabilistic sub-processes discussed in Section 2.3 and the collision frequency in Section 2.4 are the two building blocks to formulate the flotation rate constant. The assumptions made in the derivations in Chapter 2 result in limited applicability and predictive power of models. To apply the knowledge available in literature in an integral and coupled way, a new modelling approach is proposed in Chapter 3. The modelling approach (Section 3.5), the surfactant transport model (Section 3.6), particle motion and particle-particle collision (Section 3.7), and forces that occur between particles and the gas-liquid interface (Section 3.8) are discussed. In Chapter 4 the results of the coupled bubble-particle model are discussed. Finally, concluding remarks and an outlook on further work is given in Chapter 5.

2. Modelling of mineral froth flotation

2.1 Kinetics and the rate of flotation

Due to the large range of spatial scales involved in the flotation process (see Fig. 1.1 on p. 18), commonly a kinetic approach is chosen to model flotation. That is, a characteristic kinetic parameter is formulated to describe the rate at which material is recovered from the flotation cell over time. The flotation rate equation is a direct application of the "law of mass action" (see Asimov (1982, p. 474)) and the temporal change of equilibrium conditions. The flotation rate equation can be a useful engineering tool, although one must be aware that the method is integral and that much information is lost due to averaging and integration. During the 1930s (Gaudin, 1932; Garcia Zuñiga, 1935) the flotation rate equation took the form of the solution of:

$$\frac{dC}{dt} = -kC, \tag{2.1}$$

where k is the flotation rate constant and C the concentration of the mineral species targeted for recovery. Gaudin (1932) also observed that different particle size distributions characterised different flotation rate constants. Sutherland (1948) formulated this observation more explicitly as[1]:

$$\frac{dC}{dt} = -k_i C_i. \tag{2.2}$$

Eq.(2.2) can also be employed to model the exchange between different populations of species in the flotation cell, i.e. free bubbles, free particles, and bubble-particle aggregates. This discrete method is commonly called the Population Balance Model (PBM), the basis of which was probably laid by Bascur (1982) (Herbst et al., 2002, p. 397). The modelling framework discussed in Chapters 3 and 4 can be integrated with PBM. However, this is beyond the scope of this thesis.

From Eqs.(2.1) and (2.2) it can readily be seen that in the kinetic approach

[1] In Eq.(2.2), Einstein notation is used.

the key parameter is the flotation rate constant k. Typically, k is modelled as a constant and is of deterministic and probabilistic nature. Modelling of k and its constituents forms the core of flotation modelling in literature. Many researchers have developed expressions for k. For example, Jameson et al. (1977) derived an expression that links local and global parameters as:

$$k = \frac{3\dot{\varphi}_g h E_{coll}}{2 d_b V}, \tag{2.3}$$

where $\dot{\varphi}_g$ is the gas flow rate, h is the pulp height, E_{coll} is the collection efficiency, d_b bubble diameter, and V a reference volume. Eq.(2.3) relates kinetics of small scales, e.g. bubble diameter, to parameters of industrial scales, e.g. tank cell volume. It should be noted that Eq.(2.3) is not applicable to turbulent systems (Pyke, 2004). More attempts have been made in literature to formulate an equation for the flotation rate constant. In literature, the rate constant is usually related to the respective probabilities of bubble-particle collision, attachment, and aggregate stability. The temporal scale of the rate constant is commonly provided by including an expression for the collision frequency. The interaction probabilities are discussed in Section 2.3 and relations for the collision frequency are treated in Section 2.4.

Yet another method to model k has been to relate the rate constant to probabilistic bubble-particle kinetics and a time average interface flux (Gorain et al., 1995a,b, 1996, 1998). The latter parameter has been named the bubble surface area flux. Gorain et al. (1995a) realised that an important factor in flotation recovery is the bubble surface area available for particle collision and attachment. In the work by Gorain and co-workers, summarised in Gorain et al. (1999), the bubble surface area flux S_b is defined as:

$$S_b = \frac{6 J_g}{d_b}, \tag{2.4}$$

where J_g is the superficial gas velocity of the flotation cell. That is, J_g represents the ratio of the volumetric gas flow rate through the cell to the cell's cross sectional surface area. Note that S_b scales with the surface-to-volume ratio of a spherical bubble, i.e. with $\frac{6}{d_b}$. The flotation rate constant is then calculated as a function of S_b (Gorain et al., 1998):

$$k = P_f S_b, \tag{2.5}$$

where P_f is the probability of flotation, including collision and attachment efficiencies. Gorain et al. (1999) later included also the froth recovery of

Dobby and Finch (1987) in Eq.(2.5). Before going into the constituents of P_f in Section 2.3, it is instructive to consider the hydrodynamic and physico-chemical phenomena that act in different zones around the rising bubble. This is the topic of the following section.

2.2 Physico-chemical phenomena

One of the complexities that modelling of mineral froth flotation presents, is that the process is governed by hydrodynamics as well as physico-chemical forces. An extensive treatment of the chemistry involved is beyond the scope of this thesis. However, it is helpful to highlight some of the most important physico-chemical aspects of flotation to understand bubble-particle attachment and aggregate stability. The observation of the hydrodynamic-chemical complexity may seem obvious, but leads to significant challenges in the formulation of accurate models. In addition to the hydrodynamic aspects of flotation, such as drag, mixing, and collision frequency, the main physico-chemical parameters are:

- Eh-pH condition,
- concentration of:
  - electrolytes,
  - depressants,
  - activators, and
  - frothers
- mineral surface structure.

The main effect of the parameters listed above is their control of the multi-component adsorption dynamics at gas-liquid and liquid-solid interfaces. The Eh-pH condition of the pulp controls the chemical species in solution and on the mineral surface. Electrolyte concentration is an important factor for the zeta-potential of mineral surface exposed to aqueous solution, which in turn determines how and what species deposit and are formed on the mineral surface. Depressants and activators are chemicals that are used to push the equilibrium concentration of certain species in solution in a desired direction. For example, in the combined flotation of galena (PbS) and sphalerite ((Zn,Fe)S) zinc sulfate can be added to increase the amount of zinc species in solution and so actually depress sphalerite flotation by preventing the sphalerite surface to oxidise and become more hydrophobic. Finally, frothers are chemicals that change the surface tension of the system and so control bubble size and rheological properties. It is clear that the above mentioned physico-chemical properties are in close

relation to the hydrodynamic behaviour of the cell. For example, bubble size distribution has a strong coupling with the cell hydrodynamics.

Derjaguin and Dukhin (1961) recognised that at different distances from a bubble rising in liquid, different groups of forces are dominant. They introduced a division into three zones, schematically depicted in Fig. 2.1.

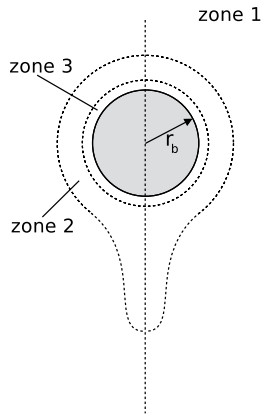

Figure 2.1. Three zones of interaction around a bubble, characterised by the dominant forces in each zone (after Derjaguin and Dukhin (1961)).

In zone 1, many particle diameters away from the bubble surface, hydrodynamic forces are dominant and collision theory applies. This is the reason that the probabilities of collision and attachment may be treated separately (Ralston et al., 1999). A discussion on hydrodynamic collision models follows in Section 2.3.1. In zone 2, the particle has approached the bubble surface so close that surface forces become relevant. This distance is typically in the order of 10^{-8}-10^{-7} m (Israelachvili, 1992, p. 152). The forces in zone 2 are mostly of electrophoretic nature, as heterogeneous surface charge distribution can generate a field strength in the order of 3000 V/cm (Ralston et al., 1999). Also, the gradient of surface surfactant concentration, the so-called Marangoni effect (Scriven and Sternling, 1960), plays an important role in interfacial charge and rheology. In zone 2, hydrodynamics still play a role as it is a transition zone between hydrodynamics and surface chemistry. As such, it is important to note that the transition between these zones is gradual (Nguyen et al., 1997a).

The transitional zone 2 is characterised by diffusiophoretic interactions, where the local equilibrium of surfactant adsorption and desorption equilibrium is disturbed (Schulze, 1983, p. 75). The thickness δ of zone 2 for flotation size bubbles is $\mathcal{O}\left(r_b Pe^{-\frac{1}{2}}\right) \equiv \sqrt{\frac{r_b \mathcal{D}}{U_\infty}}$ (Derjaguin and Dukhin, 1961). For a bubble diameter of 1 mm with a rise velocity of 0.2 m/s, and diffusion coefficient of 10^{-10} m/s, thickness δ is in the order of 500 nm.

The main aim of accurate modelling results in zone 2 is the prediction of surfactant concentration and bubble surface mobility (Derjaguin and Dukhin, 1961). The surface normal flux of surfactant is described by (Derjaguin and Dukhin, 1961):

$$\mathcal{D}_{eff} \left| \frac{\partial c(r,\theta)}{\partial r} \right|_{r=r_b} = \nabla_s \left(\Gamma U_s \right), \tag{2.6}$$

where $\mathcal{D}_{eff}$ is the effective ion diffusivity coefficient, r is the bubble radial coordinate, Γ the equilibrium bubble surface surfactant concentration, and U_s is the bubble surface velocity. Derjaguin and Dukhin (1961) recognised that Eq.(2.6) is not trivial to solve in general. To simplify the solution procedure for Eq.(2.6), they assumed that surfactant mass transfer in the boundary layer of the bubble, i.e. in zone 2, is diffusion dominated. This constraint thus becomes:

$$\begin{cases} \frac{\Gamma}{\overline{C}_b} & \ll \delta \\ \frac{C_b(\theta)-\overline{C}_b}{\overline{C}_b} & \ll 1 \\ \frac{\Gamma(\theta)-\overline{\Gamma}}{\overline{\Gamma}} & \ll 1 \end{cases} \tag{2.7}$$

Now, under the set of conditions in Eqs.(2.7), they considered Γ constant and moved it out of the gradient term in Eq.(2.6). To compute U_s in Eq.(2.6), Derjaguin and Dukhin (1961) used a simplified version of the Hadamard-Rybczynski (Hadamard, 1911; Rybczynski, 1911) solution, after Fuks (1955, p. 211):

$$U_s \approx \tfrac{3}{2} U_\infty \sin\theta, \tag{2.8}$$

where U_∞ is the far-field fluid velocity, and θ the polar angle of the bubble. It is important to note that Eq.(2.8) is a solution for potential flow around a hard sphere. Fuks (1955, p. 221) extended the hard-sphere analysis of Levich (1952, Ch. 6) by assuming the gas sphere to rise in ideal liquid, with a no-slip boundary condition at the gas-liquid interface. It must also be assumed that the interface is perfectly clean.

Using the conditions in Eqs.(2.7) and substituting Eq.(2.8) into Eq.(2.6), Derjaguin and Dukhin (1961) obtained the concentration gradient normal to the bubble surface as:

$$\mathcal{D}_{eff}\left|\frac{\partial c(r,\theta)}{\partial r}\right|_{r=r_b} = \nabla_s\left(\Gamma U_s\right) \equiv 3\overline{\Gamma}\frac{1}{r_b}U_\infty\cos\theta \tag{2.9}$$

Note that in Eq.(2.9) the term $\frac{1}{r}$ appears because all elements of the unit vector of position are taken into account in the gradient operator in a cylindrical coordinate system. Since Eq.(2.9) is evaluated at the bubble surface, $\frac{1}{r}$ becomes $\frac{1}{r_b}$ in Eq.(2.9). After applying the divergence in polar coordinates, a factor 2 appears in addition to $\frac{1}{r}$ so that factor $\frac{3}{2}$ in Eq.(2.8) becomes 3 on the RHS of Eq.(2.9). The condition for this operation is that the Cauchy-Riemann equations hold at the origin of the coordinate system. In fact, when the Cauchy-Riemann equations hold, the divergence term represents the flux density (Shurman, 2010, p. 468-469). A consequence of the validity of the Cauchy-Riemann condition is that the velocity field is irrotational, i.e. the potential flow assumption applies (Chanson, 2007). Fuks (1955, p. 221) also mentions his assumption of potential flow around a hard sphere, or rather cylinder, explicitly.

Derjaguin and Dukhin (1961) then write the electric field strength as a function of electrolyte concentration gradient. Assuming a constant field strength within zone 2 and substituting the concentration gradient with the right-hand term in Eq.(2.9), the surface normal electric field strength becomes:

$$\mathbf{E}_n = \frac{2RT}{F}\frac{\left(\mathcal{D}_+ - \mathcal{D}_-\right)}{\mathcal{D}_+\mathcal{D}_-\left(z_+ + z_-\right)}\frac{U_\infty\overline{\Gamma}}{r_b\overline{C}_b}\cos\theta, \tag{2.10}$$

where $\mathcal{D}_+$ and $\mathcal{D}_-$ are the ion diffusivity coefficients, z_+ and z_- the respective valences, and F the Faraday constant. From Eq.(2.10) the surface normal electromotoric force for very small particles can be derived. It must be noted, however, that Eq.(2.10) applies only to dilute electrolyte solutions. For more dense solutions Derjaguin and Dukhin (1961) suggest to approximate the radial concentration field by a definite Gaussian integral. Integration leads to an error function on the domain $\langle r_b, r_b + \delta]$.

When the separation between particle surface and gas-liquid interface is further reduced to about 10^{-8} m (Israelachvili, 1992, p. 246-248), forces due to steric effects and interaction of the electric double-layers occur. These forces are commonly modelled by the (extended) DLVO theory, after the colloidal stability theory of Derjaguin and Landau (1941) and Verwey and Overbeek (1948). The DLVO theory as applied to bubble-particle in-

teraction is discussed in Section 3.8.

2.3 Probabilistic modelling of sequential events

The "total probability of flotation", cf. P_f in Eq.(2.5), is commonly simplified by considering the interaction between a single bubble and a single particle. Such single bubble models are typically further reduced in complexity by dividing the process into three sub-processes (Gaudin, 1932, p. 86). Schuhmann (1942) used the analysis of Gaudin (1932, p. 88-92) to write the probability of flotation P as it is currently found in the literature, as the product of the probabilities of sub-processes:

$$P_f = P_c P_a P_s, \tag{2.11}$$

where P_c is the probability of particle-bubble collision, P_a the probability of attachment, and P_s the probability of particle-bubble aggregate stability. Eq.(2.11) only considers bubble-particle interaction in the flotation pulp, probability of froth recovery is not considered here. The flotation rate constant k is then modelled as the product of the probability of flotation and the frequency at which bubbles and particles interact (Schulze, 1983, p. 259):

$$ZP_f = ZP_c P_a P_s \models k, \tag{2.12}$$

where Z is the bubble-particle collision frequency. As a background to this thesis, the following sections cover the fundamental derivation of and assumptions behind models of the sub-processes in Eq.(2.12).

2.3.1 Deterministic modelling of collision probability

2.3.1.1 Geometric collision probability

The process of first contact between bubble and particle is accepted to be the key element in Eq.(2.12). This process of "first encounter" was a widely debated subject (Pyke, 2004) and it was not until cinematographic evidence of Bogdanov and Filanovski (1940) and the seminal paper of Sutherland (1948), that the "encounter" theory of Gaudin (1932) became widely accepted. Schuhmann (1942) was probably the first to consider bubble-particle collision efficiency as a fundamental parameter in the calculation of the flotation rate constant (Yoon and Luttrell, 1989).

Gaudin (1932, p. 88-92) made a geometric analysis of the probability of

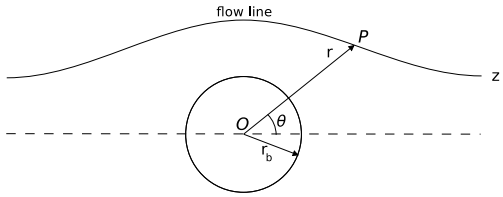

Figure 2.2. Flow line around a spherical obstacle (after Gaudin (1957, p. 344)).

collision between a bubble and a particle, reasoning that if bubble and particle do not collide, subsequent adhesion cannot occur. Gaudin (1932) followed the analysis of stream lines around a cylinder by Houstoun (1925, p. 55) and assumed:

1. that water is incompressible, non-viscous, and infinitely divisible,
2. that bubble and particle can be modelled as hard spheres,
3. that the bubble is the only disturbing factor in the quiescent liquid, and
4. fluid flow is irrotational, i.e. a potential flow solution applies.

Gaudin (1932) noted that the combination of in particular assumptions 2 and 4 is erroneous, but due to the complexity of the problem, these assumptions were needed at the time. Nevertheless, Gaudin's model can give a first indication of collision probability. The analysis of Gaudin (1932, p. 88-92) was later extended (Gaudin, 1957, p. 340-347) to both laminar and turbulent flow, using a Stokesian stream line function of Lamb (1932, art. 94, p. 125). Gaudin (1957) considered analytically the "path of [viscous fluid] elements" along a spherical obstacle. The equation for flow pathlines past a spherical obstacle is of the form (Gaudin, 1957, p. 344):

$$z = \left[2\left(\frac{r}{r_b}\right)^2 - 3\frac{r}{r_b} + \frac{r_b}{r} \right] \sin^2\theta, \tag{2.13}$$

where the angle θ and distance r from the bubble centre are shown in Fig. 2.2. The pathline function z is derived from the Stokesian stream function Ψ. Gaudin (1957, p. 344) relate z to Ψ as:

$$z = \frac{-4\Psi}{U_\infty r_b^2}, \tag{2.14}$$

where U_∞ is the far-field flow speed.

Gaudin (1957) noted that there is a relation between the stream line far from the obstacle and the position close to the obstacle surface, i.e. follow-

ing the stream line downstream until the obstacle's equator. At the equator, the maximum normalised distance s_{max} from the obstacle's centre (O in Fig. 2.2) is $1 + \frac{r_p}{r_b}$. Far away from the obstacle, the minimum distance s_{min} from the centre axis, for the same stream line, is $\frac{r}{r_b}\sin\theta$. By substituting these distances, s_{min} and s_{max}, into Eq.(2.13) Gaudin obtained for $r \to \infty$:

$$z_\infty = \underbrace{\left(2 - \frac{3r_b}{r} + \left(\frac{r_b}{r}\right)^3\right)}_{\approx 2} \underbrace{\left[\left(\frac{r}{r_b}\right)^2 \sin^2\theta\right]}_{\mathrm{s}^2_{\mathrm{min}}} \tag{2.15}$$
$$\approx 2s^2_{min},$$

with the rather crude approximation of $2 - \frac{3r_b}{r} + \left(\frac{r_b}{r}\right)^3 \approx 2$. Substituting s_{max} into Eq.(2.13), with $\theta = \frac{\pi}{2}$ and thus $\sin^2\theta = 1$ at the obstacle's equator, we obtain:

$$z_0 = \left[2\left(\frac{r}{r_b}\right)^2 - 3\frac{r}{r_b} + \frac{r_b}{r}\right]\sin^2\theta \tag{2.16}$$
$$= \left[2 + 4\frac{r_p}{r_b} + 2\left(\frac{r_p}{r_b}\right)^2\right] - \left(3 + 3\frac{r_p}{r_b}\right) + \frac{1}{1 + \frac{r_p}{r_b}}$$

Then, Gaudin (1957, p. 347) used a Taylor expansion of the last term in Eq.(2.16), neglecting third order terms and accepting the approximation $\frac{1}{1+\frac{r_p}{r_b}} \to 1 - \frac{r_p}{r_b} + \left(\frac{r_p}{r_b}\right)^2$. Note that this approximation means that $r_p \approx 0.1r_b$ for the numerical error to be less than about 10%. With this approximation, Eq.(2.16) reduces to:

$$z_0 \approx 3\frac{r_p}{r_b} \tag{2.17}$$

Equating the RHS of Eq.(2.15) with the RHS of Eq.(2.17), we obtain for viscous flow:

$$3\left(\frac{r_p}{r_b}\right)^2 = 2s^2_{min} \tag{2.18}$$

For turbulent flow Gaudin (1957, p. 247) used the pathline equation of Lamb (1932, art. 94, p. 125) for potential flow:

$$z = \left[2\left(\frac{r}{r_b}\right)^2 - \frac{2r_b}{r}\right]\sin^2\theta. \tag{2.19}$$

At the equator $\frac{r}{r_b} = 1 + \frac{r_p}{r_b}$, and using again the approximation $\frac{1}{1+\frac{r_p}{r_b}} \rightarrow 1 - \frac{r_p}{r_b} + \left(\frac{r_p}{r_b}\right)^2$, Eq.(2.19) can be writen as (Gaudin, 1957, p. 347):

$$\begin{aligned} z_0 &= \left[2\left(\frac{r}{r_b}\right)^2 - 2\frac{r_b}{r}\right]\sin^2\theta \\ &= \left[2 + 4\frac{r_p}{r_b} + 2\left(\frac{r_p}{r_b}\right)^2\right] - \left[2 - 2\frac{r_p}{r_b} + 2\left(\frac{r_p}{r_b}\right)^2\right] \\ &= 6\frac{r_p}{r_b}. \end{aligned} \tag{2.20}$$

Now, equating the RHS of Eq.(2.15) with the RHS of Eq.(2.20), we obtain for turbulent flow:

$$6\frac{r_p}{r_b} = 2s_{min}^2. \tag{2.21}$$

Here it is assumed that high Reynolds number flow can be modelled as inviscid so that the Navier-Stokes equation reduces to the Euler equation. When Kelvin's theorem is accepted, i.e. the total derivative of circulation vanishes, the fluid is considered irrotational and its motion can be described by the gradient of a scalar potential. Consequently, Eq.(2.21) is only valid for an incompessible, inviscid, ideal fluid.

The probability P_c of a particle colliding with the cylindrical obstacle when following a random stream line is s_{min}^2 (Gaudin, 1957). The collision probability, or efficiency E_c thus becomes:

$$E_c = \frac{3}{2}\left(\frac{r_p}{r_b}\right)^2, \qquad \text{for viscous flow} \tag{2.22}$$

$$E_c = 3\frac{r_p}{r_b}, \qquad \text{for turbulent flow} \tag{2.23}$$

Eq.(2.22) has been derived for Stokes flow and is valid for very small bubbles, while Eq.(2.23) has been derived for potential flow and is valid for bubbles much larger than typical for flotation size bubbles (Yoon, 1993). Yoon (1991) found experimental evidence that the Gaudin model is applicable for bubbles of around 100 μm. The for and aft flow fields are considered to be symmetric and the bubble must rise with constant velocity. Under typical flotation conditions, however, these simplifications should not be accepted.

Sutherland (1948) accepted the assumptions of Gaudin (see p. 29) and recognised that it is implicitly assumed that the motion of bubble, particle, and fluid is independent. That is, momentum coupling between phases is

not considered. The neglect of momentum coupling is in fact one of the assumptions in the derivation of Houstoun (1925, p. 55), used by Gaudin (1932). To overcome this restriction, Sutherland (1948) used a streamline equation for potential flow of Ramsey (1935, p. 160), which would be valid for three-dimensional flow:

$$\sin^2\theta = \frac{Cr}{r^3 - r_b^3}, \tag{2.24}$$

where the notation relates to that in Fig. 2.2 on page 30, and where C is an integration constant. Note that Eq.(2.24) is of the same form as Eq.(2.21) when one replaces s_{min} by $\frac{r}{r_b}\sin^2\theta$, albeit for three-dimensional geometry. At the bubble's equator, that is at $\theta = \frac{\pi}{2}$, $r = r_b + r_p$, so that the constant of integration can be determined:

$$C = \frac{(r_b + r_p)^3 - r_b^3}{r_b + r_p} \tag{2.25}$$

Substitution of Eq.(2.25) into Eq.(2.24) and rearranging we obtain:

$$r\sin\theta = \sqrt{\frac{(r_b + r_p)^3 - r_b^3}{r_b + r_p}\frac{r^3}{r^3 - r_b^3}}, \tag{2.26}$$

where the same nomenclature is used as in Fig. 2.2. The separation distance of the streamline from the centre line throught the bubble is $r\sin\theta$. For large distance from the bubble, $r \to \infty$, Eq.(2.26) reduces to:

$$r\sin\theta = \sqrt{\frac{(r_b + r_p)^3 - r_b^3}{r_b + r_p}}. \tag{2.27}$$

Now, assuming that $r_p \ll r_b$ and replacing the LHS of Eq.(2.27) with the critical collision radius r_c, Sutherland (1948) obtained:

$$r_c = \sqrt{3r_p r_b} \tag{2.28}$$

The probability of particle-bubble collision is the ratio of the cross-sectional area of the stream tube with radius r_c to the cross-sectional area of the bubble (Dai et al., 2000), i.e.:

$$E_c = \frac{\pi r_c^2}{\pi r_b^2} = \frac{3d_p}{d_b} \tag{2.29}$$

Eq.(2.29) is the same result as Eq.(2.23) and has become known as the

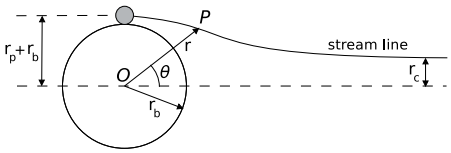

Figure 2.3. The critical streamline for particle-bubble collision (after Anfruns and Kitchener (1977)).

Sutherland equation. Eq.(2.29), has been derived for potential flow and is strictly not valid for "flotation size bubbles" (∼1 mm diameter), but only for larger ones (Yoon, 1993). Also, Sutherland (1948) deemed the neglect of inertia acceptable (Evans, 1954). Even though the applicability of Eq.(2.29) to real systems is very restricted, this geometric collision kernel forms the basis for most flotation models.

Yoon and Luttrell (1989) recognised that the key to an accurate geometric collision model is the derivation of the appropriate stream function. The correct stream function produces the correct critical stream tube radius r_c, as schematically depicted in Fig. 2.3. In the geometric family of collision models, Yoon and Luttrell (1989) defined the probability of collision as the ratio of particle cross-sectional area to bubble cross sectional area:

$$P_c = \frac{A_c}{A_b} = \left(\frac{r_c}{r_b}\right)^2, \tag{2.30}$$

For Stokes flow the stream function is (Lamb, 1932, art. 94, p. 125):

$$\Psi = U_b r_b^2 \sin^2\theta \left(\tfrac{1}{2}\tilde{r}^2 - \tfrac{3}{4}\tilde{r} + \frac{1}{4\tilde{r}}\right), \tag{2.31}$$

where $\tilde{r}$ is $\frac{r}{r_b}$. For $r \to \infty$, $\sin\theta \approx \frac{r_c}{r}$ can be substituted into Eq.(2.31) and Eq.(2.30) to yield (Gaudin, 1957, p. 345):

$$\begin{aligned} P_c &= \frac{2\Psi}{U_b r_b^2} \\ &= \sin^2\theta \left(\tilde{r}^2 - \tfrac{3}{2}\tilde{r} + \frac{1}{2\tilde{r}}\right) \end{aligned} \tag{2.32}$$

For the grazing limit, i.e. $r = r_p + r_b$ and $\theta = \frac{\pi}{2}$ (see Fig. 2.3), one obtains:

$$P_c = \frac{3}{2}\left(\frac{r_p}{r_b}\right)^2, \tag{2.33}$$

which is identical to Eq.(2.22), the model of Gaudin (1932). For potential flow, with stream function

$$\Psi = U_b r_b^2 \sin^2\theta \left(\tfrac{1}{2}\tilde{r}^2 - \frac{1}{2\tilde{r}} \right), \tag{2.34}$$

Yoon and Luttrell (1989) obtained the same result as Sutherland (1948), Eq.(2.29):

$$P_c = 3\left(\frac{r_p}{r_b}\right). \tag{2.35}$$

Under typical flotation conditions, however, the bubble Reynolds number lies between 0.2 and 100 (Yoon and Luttrell, 1989). Therefore, Yoon and Luttrell (1989) developed a new stream function, combining those for Stokes and potential flow:

$$\Psi = U_b r_b^2 \sin^2\theta \left(\tfrac{1}{2}\tilde{r}^2 - \tfrac{3}{4}\alpha\tilde{r} - \frac{1}{2\tilde{r}} + \frac{3\alpha}{4\tilde{r}} \right), \tag{2.36}$$

where α is a parameter to blend Eqs.(2.31) (α=1) and (2.34) (α =0). By fitting α as a function of Re versus $1-\frac{1}{\tilde{r}}$, for apparent experimental data[2], Yoon and Luttrell (1989) found the relationship:

$$\alpha = 1 - \frac{4\mathrm{Re}^{0.72}}{45}\left(1 - \frac{1}{\tilde{r}}\right) \tag{2.37}$$

According to Eq.(2.36), the collision efficiency increases with the square of particle-to-bubble size and also as a function of bubble Reynolds number (Dai et al., 2000). Dai et al. (2000) point out that although the Yoon-Luttrell model is more general than the Gaudin and Sutherland models, particle inertia is still ignored and the collisions are assumed to be uniform over the entire upstream half of the bubble, cf. Eq.(2.30). These assumptions have been shown to be unrealistic (Schulze, 1989; Dai et al., 1998). At this point, it is useful to summarise some of the above models, using a general form of the collision efficiency of Reay and Ratcliff (1975), as:

$$E_c = A\left(\frac{d_p}{d_b}\right)^n, \tag{2.38}$$

where constants A and n are summarised in Table 2.1 for different flow conditions.

[2]It was not clearly stated in Yoon and Luttrell (1989) how the data was obtained.

Flow regime	Reference	A	n
Stokes flow	Gaudin (1932)	$\frac{3}{2}$	2
Stokes flow	Reay and Ratcliff (1975)	3.6*	2.05*
Intermediate flow	Yoon and Luttrell (1989)	$\left[\frac{3}{2} + \frac{4Re^{0.72}}{15}\right]$	2
Intermediate flow	Weber and Paddock (1983)	$\left[\frac{3}{2} + \frac{\frac{9}{16}Re}{2+0.498Re^{0.56}}\right]$	2
Potential flow	Gaudin (1932) and Sutherland (1948)	3	1

* Measured for silica particles in water (Reay and Ratcliff, 1975).

Table 2.1. Values for parameters A and n in Eq.(2.38) (after Yoon and Luttrell (1989) and Reay and Ratcliff (1975)).

2.3.1.2 The effect of inertia

The first model that included inertial effects was reportedly (Viswanathan, 1999; Dai et al., 2000) that of Langmuir and Blodgett (1946) and Langmuir (1948). On the assumption that Stokes' law holds for all particle velocities, Langmuir (1948) defined a "particle range" λ_p which a particle can cross for a given initial velocity $U_{p,0}$. This idea is in essence similar to the "sphere of attraction" used by Smoluchowski (1917). The particle range λ_p is:

$$\lambda_p = \tau_p U_{p,0} = \frac{2\rho_p r_p^2 U_{p,0}}{9\mu}, \tag{2.39}$$

where τ_p is the particle relaxation time. In his two-dimensional analysis, Langmuir (1948) defined a "collection cylinder" of radius r_c and the geometric ratio K as:

$$K = \frac{\lambda_p}{r_c}. \tag{2.40}$$

It was found that a particle can reach the surface of the cylinder when $K \geqslant \frac{1}{12}$ and can hit the surface for $K \geqslant \frac{1}{8}$. In case of bubble-particle collision, the cylinder represents the bubble and K is a factor of the ratio of particle relaxation time and bubble relaxation time (see e.g. p. 24 of Crowe et al. (1997) and p. 630 of Roco (1993)). Langmuir (1948), then, formulated the collection efficiency of droplets by the collector cylinder as:

$$E_{c-LB} = \left(\frac{K}{K+0.2}\right)^2. \tag{2.41}$$

Langmuir and Blodgett (1946) and Langmuir (1948) derived Eq.(2.43) to predict the collection of rime on larger objects, e.g. outdoor electricity ca-

bles and aircraft wings. For large values of Ur_p Langmuir and Blodgett (1946) found strong deviation from the Stokes regime and found that the collection efficiency E_{c-LB} on a spherical object could be expressed as a function of the Reynolds number of the collision object and another dimensionless parameter φ:

$$\varphi = \frac{Re_p^2}{K} = \frac{18\rho_f^2 Ur_b}{\mu\rho_p}, \tag{2.42}$$

After more experimental data was collected Langmuir (1948) fitted an equation for collision efficiency to the data to cover both the Stokes and potential flow regimes:

$$E_{c-LB} = \left[1 + \frac{\frac{3}{4}\ln 2K}{K - 1.214}\right]^{-2}. \tag{2.43}$$

The model above has been developed for capture of fog droplets by larger solid objects such as cables. Fog droplets range in diameter between 1 and 15 μm (Podzimek, 1997) and the collision object size used of Langmuir (1948) is 2 to 50 mm. For particles smaller than approximately 50 μm, E_{c-LB} varies only with d_p^2 (Dai et al., 2000) and $C_{D,p}$ is assumed a function of particle radius alone. The Langmuir-Blodgett collision model is only valid for cases characterised by a high Stokes number (Dai et al., 2000).

In an attempt to come to a more generic collision model that includes particle inertia, Flint and Howarth (1971) derived expressions for collision efficiency in both the potential and Stokes flow limits. Flint and Howarth (1971) found that for small particle Stokes number the collision efficiency for potential and Stokes flow converges to:

$$E_c = \frac{G}{1+G}, \tag{2.44}$$

where G represents the non-dimensional particle settling velocity:

$$G = \frac{2\left(\rho_p - \rho_f\right) r_p^2 g}{9\mu U} \tag{2.45}$$

Flint and Howarth (1971) investigated the applicability of Eq.(2.44) by studying the trajectory of 6 μm galena particles near 50-100 μm air bubbles. The comparison gave fairly good results, but despite the fact that inertia is included in the model, the system studied is characterised by a Stokes number well below unity. Flint and Howarth (1971) mention this

and recognise that the model is likely to under-predict collision efficiency. The lack of momentum coupling was identified by Flint and Howarth (1971) as one of the key shortcomings of the model.

2.3.1.3 Non-ideal collisions

For particle trajectories "strongly deviating from the velocity streamline", Dukhin (1982) found an approximate solution for particle trajectory in potential flow:

$$\tilde{v} = \tilde{u} - K' \frac{d\tilde{V}}{dt} + K'' \frac{d\tilde{u}}{dt}, \tag{2.46}$$

where $\tilde{v}$ is the particle velocity normalised to bubble velocity, $\tilde{v} = \frac{U_p}{U_b}$, $\tilde{u}$ the liquid velocity normalised to bubble velocity, $\tilde{u} = \frac{U_l}{U_b}$. K' and K'' are functions of the Stokes number K $\left(\frac{\tau_p}{\tau_f} = \frac{2\rho_p r_p^2 U}{9\mu_f r_b}\right)$ to non-dimensionalise the equation:

$$K' = K\left(1 + \frac{\rho_p}{2\rho_f}\right) \tag{2.47}$$

$$K'' = \frac{3K\rho_p}{2\rho_f} \tag{2.48}$$

In Eq.(2.46), the particle trajectory is solved in a frame of reference relative to the bubble centre. Close to the bubble surface it is assumed that particle inertial only contributes in surface normal direction, i.e. $\tilde{v}_\theta \cong \tilde{u}_\theta$ (Dukhin, 1983).

Dukhin (1983) then proceeded with the numerical integration of Eq.(2.46), accepting a numerical error of up to 25% at the equator. The boundary conditions at $\frac{\theta}{2}$ are:

$$\tilde{r} - 1 = \frac{E_{c,0}}{3} \tag{2.49}$$

$$\left.\frac{d\tilde{r}}{d\theta}\right|_{\theta=\theta_t} = 0 \tag{2.50}$$

In Eq.(2.49), $E_{c,0}$ refers to the Sutherland collision efficiency $\frac{3d_p}{d_b}$ and $\tilde{r} = \frac{r}{r_b}$. In other words, Eqs.(2.49-2.50) make sure that at the equator the critical condition is that a particle exactly grazes the bubble and that, there, its tangential velocity vanishes. The latter relates to the condition of a completely immobile bubble surface. Assuming an immobile surface and potential flow directly at the surface, Dukhin (1983) made the approximation that $\frac{E_{c,0}}{3} \ll 1$ and thus $\tilde{r} - 1 \ll 1$, so that:

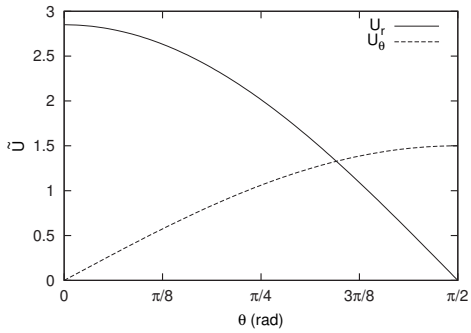

Figure 2.4. Values of Eqs.(2.51) and (2.52) as function of polar angle θ, with d_p= 50 μm and d_b = 1 mm.

$$\tilde{U}_r \cong -\left[1 - \frac{1}{\tilde{r}^3}\right]\cos\theta \cong -3\left(\tilde{r} - 1\right)\cos\theta \tag{2.51}$$

$$\tilde{U}_\theta \cong \left[1 - \frac{1}{2\tilde{r}^3}\right]\sin\theta \cong \tfrac{3}{2}\sin\theta \tag{2.52}$$

A key characteristic of this theory is that Dukhin (1982, 1983) decomposes the relative velocity between bubble surface and particle into a radial and a tangential component. The radial component is held responsible for the "pressing force" that can overcome the energy barrier of the balance between repulsive electric double layer forces and attractive Van der Waals forces. The tangential component is associated with centrifugal effects in the particle-bubble system. When the polar angle θ exceeds a certain critical value, called the angle of tangency θ_t, centrifugal forces on the particle exceed radial forces. The variation of $\tilde{U}_r$ and $\tilde{U}_\theta$ with θ is shown in Fig. 2.4. Using a parametrisation after results of Fuchs (Smirnov, 1949, p. 365) and Taylor expansion, Dukhin (1983) derived approximate expressions for the angle of tangency θ_t for $K' \rightarrow 0$, i.e. for very small particles with negligible inertia. Dai et al. (1998) wrote an extended version of the original balance equation between radial "pressing" forces and centrifugal outward forces of Dukhin (1982, 1983) as:

$$6\pi\mu r_p f + \tfrac{4}{3}\pi r_p^3\left(\rho_p - \rho_f\right)\frac{v_{p,\theta}}{r_p + r_b} = 0, \tag{2.53}$$

where f is a numerical factor of 2.034 to include short-range hydrodynamic interaction (Dukhin and Rulev, 1977). Now, substituting Eqs.(2.51) and (2.52) into Eq.(2.53) and solving for θ yields an expression for the angle of tangency θ_t as (Dai et al., 1998):

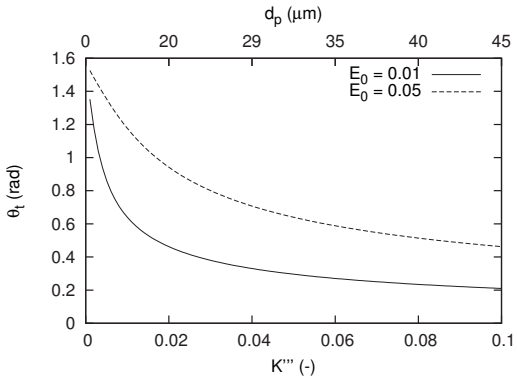

Figure 2.5. Angle of tangency θ_t versus parameter K''' for two values of $E_{c,0}$. The upper horizontal axis displays corresponding values for d_p, with ρ_p=3000 kg/m^3, ρ_f=1000 kg/m^3, d_b=1 mm, μ_f=0.001 Pa·s, and U_b=0.22 m/s.

$$\theta_t = \sin^{-1}\left(\left[2\beta\sqrt{1\beta^2} - \beta\right]^{\frac{1}{2}}\right), \tag{2.54}$$

where, for $E_{c,0} = \frac{3d_p}{d_b}$,

$$\beta = \frac{2E_{c,0}f}{9K'''} = \frac{2Ef}{9\left(K' - K''\right)}. \tag{2.55}$$

Provided that $K \ll K_c$ and considering only the centrifugal component of the inertial force (Dai et al., 2000), the collision efficiency is (usually expression normalised to $E_{c,0}$):

$$\frac{E_c}{E_{c,0}} = \sin^2\theta_t\left[1 - \frac{2\cos\theta_t}{\sin^2\theta_t}\left(1-\cos\theta_t\right)^2\left(2+\cos\theta_t\right)\right] \tag{2.56}$$

In honour of the contribution of Sutherland to the field of flotation modelling, Dai et al. (2000) named Eq.(2.56) the Generalised Sutherland Equation (GSE). Fig. 2.5 shows the variation of θ_t with K'''. K''' can also be expressed as $\frac{(\rho_p-\rho_f)}{\rho_f}K$ and can thus be seen as an "inertia-normalised" Stokes number and is a measure for particle inertia in terms of the centrifugal component of Eq.(2.46) (see Eq.(2.52) and Fig. 2.4) of particle motion along the surface of the bubble. One can see in Fig. 2.5 that larger particles are associated with a smaller angle of tangency. However, this effect may be an artifact of the approximations made, because Nguyen et al. (2006) report that θ_t first decreases, but later increases again with increasing d_p. Nguyen et al. (2006) conclude in their computational validation that Eq.(2.56), in fact, only seems to be valid for $d_p < 10$ μm.

Dai et al. (2000) investigated the GSE further and note that the evaluation of particle velocity at the point of tangency is strictly speaking not valid in general. Inertial forces are generally neglected in flotation models because it is assumed that the bubble surface is completely immobile (Dai et al., 1998). Dai et al. (1998) modified the Sutherland equation, Eq.(2.29), to include weak inertial forces. Dai et al. (1998) note that the GSE is valid for $K \approx K_c$, i.e. for the intermediate range in terms of particle inertia.

2.3.2 Probability of particle-bubble adhesion

Modelling of particle-bubble attachment has not received as much attention as the collision sub-process (Finch and Dobby, 1990, p. 43). This may be due to the fact that particle-bubble collision is governed by hydrodynamic processes, while particle-bubble attachment is more complex, entailing interfacial boundary layer flow as well as surface chemistry.

The first detailed cinematographic evidence of particle-bubble attachment was probably made by Bogdanov and Filanovski (1940) during the late 1930s. The work of Bogdanov and Filanovski (1940) showed that particles that collide with a bubble do not necessarily attach. First, the liquid film between particle and bubble must drain until a critical thickness. When this critical thickness has been reached, the film ruptures and three-phase contact is established. The time this attachment process takes is commonly referred to as the induction time t_i. When the sliding time[3] t_{sl} of the particle over the bubble surface exceeds the induction time, attachment can occur. In effect, the attachment of a particle to an interface can be viewed as the interplay between two important concepts: the forces involved in the formation of three-phase contact and the time available for these forces to act, i.e. $\frac{t_{sl}}{t_i}$. In the following two section the physico-chemical aspects of attachment and modelling of sliding time are discussed.

2.3.2.1 Attachment and sliding time

Bubble-particle attachment time can be divided into three distinct phases (Nguyen et al., 1998; Albijanic et al., 2010): the time of liquid film thinning t_f, the film rupture time t_r, and the time of three-phase contact formation t_{tpc}, respectively. The literature is inconsistent in notation and constitution of the induction. Schulze (1989), Nguyen et al. (1997a), Phan et al. (2003), and Albijanic et al. (2010) present similar ideas, but with different notations. Based on these publications, the induction time is defined as:

[3] In older literature sliding time is sometimes called contact time and attachment may be referred to as adhesion.

$$t_a \leqslant t_i = t_f + t_r + t_{tpc}, \tag{2.57}$$

where induction time becomes attachment time t_a once the induction period is exceeded during contact. First, the intervening liquid film between bubble and particle thins to a critical thickness h_c, after which rupture can occur. There are generally two limiting cases for the calculation of film thinning time t_f: Reynolds' equation for plane-parallel films and Taylor's equation[4] for a solid sphere approaching a rigid wall (Schulze, 1989, 1983, p. 124). These film thinning times are (Schulze, 1989):

$$t_{f,Reynolds} = \frac{3\mu_f r_f^2}{4h_c^2 F k} \tag{2.58}$$

$$t_{f,Taylor} = \frac{6\pi\mu_f r_p^2 \ln\left(\frac{r_p}{h_c}\right)}{F}, \tag{2.59}$$

where F is the approaching force, r_f the film radius (i.e. the radius of the thinning area), k a factor of 4 for a completely unretarded bubble and 1 for a completely retarded one. In Eqs.(2.58-2.59), h_c is the critical film thickness that can be modelled as (Schulze and Birzer, 1987):

$$h_c = 23.3\left[\gamma\left(1 - \cos\theta_{tpc,A}\right)\right]^{0.16}, \tag{2.60}$$

where γ is the surface tension, $\theta_{tpc,A}$ is the advancing contact angle, and h_c is expressed in nm.

Nguyen et al. (1997a) discuss different proposed mechanisms of film rupture. However, the film rupture time is in the order of 1 ms, much shorter than t_i and t_{tpc}, and commonly not taken into consideration in attachment time modelling (Albijanic et al., 2010).

Scheludko et al. (1976) was the first to consider three-phase contact line expansion in attachment kinetics (Nguyen et al., 1997a). Following the analysis of Schulze (1983, p. 169-177) and Scheludko et al. (1970), Nguyen et al. (1997c) wrote the balance of forces in non-dimensional form as:

[4]Eq.(2.59) is commonly attributed to G.I. Taylor (1925), although it was never published as such (Neto et al., 2005).

$$\frac{1}{A}\ln\left[\frac{d\alpha}{dt^*}+\sqrt{\left(\frac{d\alpha}{dt^*}\right)^2+1}\right]+\cos\theta_{tpc}-\cos\theta_Y-\overline{\kappa}\cot\alpha$$
$$-\,\mathrm{Bo}\left[1-\frac{rho_f}{\rho_p}f(\alpha)\right]=0 \tag{2.61}$$
$$\overline{\kappa}\sin\theta-\mathrm{Bo}\left[1-\frac{rho_f}{\rho_p}f(\alpha)\right]\cot\alpha=0, \tag{2.62}$$

where $\overline{\kappa}$ is the dimensionless line tension $\frac{\kappa}{r_p\gamma}$, A is the mobility of three-phase contact expansion a made dimensionless as $\frac{a\gamma}{2U_{tpc}}$, where U_{tpc} is the molecular three-phase contact line velocity at equilibrium. The dimensionless time t^* is $\frac{tr_p}{2U_{tpc}}$ and Bo is a modified Bond number $\frac{G}{2\pi r_p\gamma}$. The Young contact angle θ_Y is defined as $\cos^{-1}\left(\frac{\gamma_{sg}-\gamma_{sl}}{\gamma_{gl}}\right)$. In Eqs.(2.61-2.62), α is the wetting perimeter angle, as shown in Fig. 2.6, and the function $f(\alpha)=\frac{1}{4}\left(2+3\cos\alpha-\cos^2\alpha\right)$ is a measure for the particle volume submerged in water. A more detailed treatment of gas-liquid-solid contact line expansion is given by Stechemesser and Nguyen (1999), Yoon and Mao (1996), Boström et al. (2006), and Krasowska and Malysa (2007).

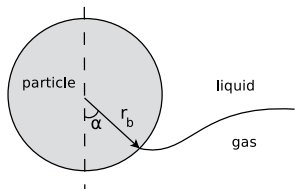

Figure 2.6. Wetting perimeter and the wetting perimeter angle α (after Nguyen et al. (1997c)).

The sliding time of a particle along the bubble surface can be modelled as (Dobby and Finch, 1986):

$$t_s=\int_{\theta_c}^{\theta_m}\frac{r_p+r_b}{U_{p,\theta}}d\theta \tag{2.63}$$

where the maximum angle of contact θ_m is $\frac{\pi}{2}$ in potential flow. The particle tangential velocity can be estimated from the stream function Ψ as (Flint and Howarth, 1971):

$$U_{p,\theta}=\frac{1}{r_b\sin\theta}\frac{d\Psi}{d\theta}, \tag{2.64}$$

where it is assumed that the particle velocity is that of the streamline at particle centre when the particle would not be present. Substituting Eq.(2.64) into Eq.(2.63), using Eq.(2.36) as the stream function for intermediate Reynolds number flow, Dobby and Finch (1986) derived the sliding time for potential flow as:

$$t_s = \frac{2r^*}{2\left(U_b + U_{p,t}\right) + \frac{U_b}{r^*}} \ln\left(\cot\frac{\theta_c}{2}\right), \tag{2.65}$$

where r^* is 1+$\frac{r_p}{r_b}$ and $U_{p,t}$ is the terminal settling velocity of the particle. Eq.(2.65) is very similar to the expression originally derived by Sutherland (1948); the difference is that the expression of Sutherland (1948) has a factor of 4 instead of 2 in the numerator, over-estimating sliding time by a factor of 2 (Schulze, 1989).

Scheludko et al. (1976) argued that the model for sliding or contact time should include deformation of the bubble surface. This idea was developed further by Schulze et al. (1989a), who accounted for a meniscus in two parts, separated by a transition point. Directly between the particle and bubble the meniscus is circular for a spherical particle (Nguyen et al., 1997b). This is where the intervening liquid film thins. The indentation in the bubble surface outside the thinning area is a non-spherical meniscus. The transition point divides these two areas and is defined by the transition angle α, as shown in Fig. 2.6. Based on experimental observation of coated glass spheres at a gas-liquid interface, Schulze et al. (1989a) deduced a semi-analytic expression for contact time (in the notation of Nguyen et al. (1997b)):

$$t_s = \frac{\pi}{f}\sqrt{\frac{d_p^3\left(\rho_p + 1.5\rho_f\right)}{24\gamma}}, \tag{2.66}$$

$$f = \frac{\sqrt{\left(\ln\left(\frac{L}{d_p\alpha_m}\right) + 0.25 - \gamma_e\right)}}{\left(\ln\left(\frac{L}{d_p\alpha_m}\right) + 0.5 - \gamma_e\right)\sqrt{2}}, \tag{2.67}$$

where α_m is the maximum transition angle, γ_e the Euler number 0.5772, γ surface surface tension, and L is the capillary length, defined as:

$$L = \sqrt{\frac{\gamma}{\left(\rho_f - \rho_g\right)g}} \tag{2.68}$$

For 0.036$\leqslant \frac{d_p}{L} \leqslant$0.4, Nguyen et al. (1997b) fitted an expression[5] to experimental data:

$$t_s = \frac{\pi \mathrm{We}}{\omega - \varepsilon\ln\omega + \varepsilon\ln\mathrm{We}}\frac{L}{U_{p,r}}, \tag{2.69}$$

[5]In the original paper of Nguyen et al. (1997b) for t_s t_s is called contact time t_c. Here, for consistent notation, it is written as t_s.

where We is the Weber number $\left(\frac{m_{p,eff}U_{p,r}^2}{4\pi\gamma L^2}\right)^{1/2}$, $U_{p,r}$ is the particle velocity relative to the interface, and fitting constants ω and ε are:

$$\omega - \varepsilon \ln \omega = 0.478 + 0.04 \ln \left(\frac{d_p}{L}\right), \tag{2.70}$$

$$\varepsilon = 0.020 + 0.03 \ln \left(\frac{d_p}{L}\right). \tag{2.71}$$

The above models for induction time require selection of the appropriate streamfunction and local flow conditions. In addition to this difficulty, the models are for a single bubble rising in quiescent liquid and an extrapolation to other flow regimes is questionable. Another method is to estimate the induction time from experimental data. Dai et al. (1999) correlated induction time with experimental data and proposed a relation of the form:

$$t_i = A d_p^B, \tag{2.72}$$

where constants A and B are fitting parameters. Koh and Schwarz (2006) assumed A and B to be functions of particle contact angle θ_{tpc} and not of d_p. Based on experimental data of Dai et al. (1999), Koh and Schwarz (2006) derived the following empirical expression for induction time:

$$t_i = \frac{75}{\theta_{tpc}} d_p^{0.6}. \tag{2.73}$$

Nguyen and Evans (2004) report a fair agreement between measured and predicted sliding time, with a slight under-prediction by the model.

2.3.2.2 Attachment models

Dobby-Finch

Dobby and Finch (1987) assumed that a particle collides with the bubble at a polar angle where the fluid stream line comes closest to the bubble. For $20 < Re_b < 400$, the angle θ_c is (Finch and Dobby, 1990, p. 41):

$$\theta_c = 78.1 - 7.37 \log \mathrm{Re}_b \tag{2.74}$$

The particle slides along the bubble surface between the angle θ_c and a maximum angle θ_m:

$$\theta_m = 9 + 8.1\rho_p + \theta_c\left(0.9 - 0.09\rho_p\right). \tag{2.75}$$

The sliding time of the particle along the surface of the bubble is modelled as:

$$t_s = \left(\theta_m - \theta'\right)\frac{d_p + d_b}{U_{p,\theta}}, \tag{2.76}$$

where θ' is the "sliding arc". Rearranging Eq.(2.76) and substituting t_i for t_s, gives the sliding arc θ':

$$\theta' = \theta_m - \frac{U_{b,\theta}t_i}{d_p + d_b}. \tag{2.77}$$

The attachment efficiency, thus, becomes (Finch and Dobby, 1990, p. 47):

$$E_a = \frac{\sin^2\theta'}{\sin^2\theta_c}. \tag{2.78}$$

For other bubble Reynolds number ranges, Ralston et al. (1999) suggest to use the expressions of Jowett (1980) for θ_c:

$$\theta_c = 78.1 - 7.37\log \mathrm{Re}_b, \quad \text{for } 20 < \mathrm{Re_b} < 400 \tag{2.79}$$

$$\theta_c = 85.5 - 12.49\log \mathrm{Re}_b, \quad \text{for } 1 < \mathrm{Re_b} < 20 \tag{2.80}$$

$$\theta_c = 85.0 - 2.50\log \mathrm{Re}_b, \quad \text{for } 0.1 < \mathrm{Re_b} < 1 \tag{2.81}$$

Nguyen

For bubbles with an intermediate Reynolds number, the flow is not fore and aft-symmetric (Nguyen, 1999). For this situation, Dobby and Finch (1987) and Finch and Dobby (1990) proposed Eq.(2.78). Dobby and Finch (1987) used the average sliding velocity in the derivation of their model. Nguyen (1999) took the same approach, but used an approximate numerical integration of the sliding trajectory. The resulting attachment efficiency for an immobile bubble surface is (Nguyen, 1999):

$$P_a = \frac{X + C + Y\cos\theta_a}{X + C + Y\cos\theta_c}\left(\frac{\sin\theta_a}{\sin\theta_c}\right)^2 \tag{2.82}$$

and for a mobile surface:

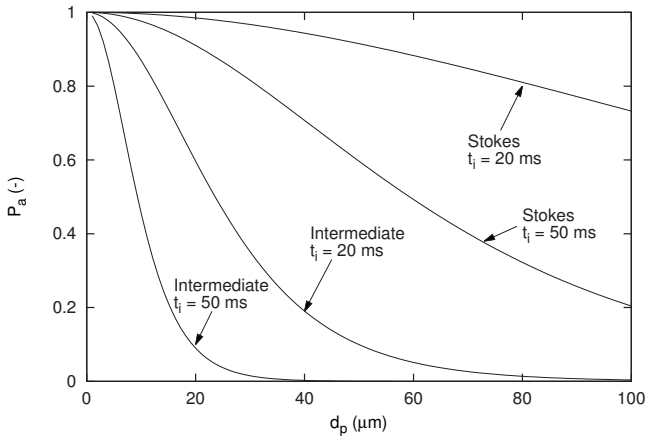

Figure 2.7. Probability of attachment for Stokes, Eq.(2.86), and intermediate flow, Eq.(2.87), for different induction times using the Yoon and Luttrell (1989) model.Here, d_b = 1 mm, ρ_f = 1000 kg/m^3, and μ_f = 0.001 Pa·s, and U_b = 0.105 m/s to fit the graph of Yoon and Luttrell (1989).

$$P_a = \frac{(X+C)\sin^2\theta_a - \frac{1}{3}C_1X^2\left(\cos^3\theta_a - 3\cos\theta_a + 2\right)}{(X+C)\sin^2\theta_c - \frac{1}{3}C_1X^2\left(\cos^3\theta_c - 3\cos\theta_c + 2\right)} \tag{2.83}$$

where the coefficients X, Y, C, and C_1 are listed in Table 2.2.

Parameter	Immobile surface	Mobile surface
X	$\frac{3}{2} + \frac{\frac{9}{32}\mathrm{Re}}{1+0.309\mathrm{Re}^{0.694}}$	$1 + \frac{0.0637\mathrm{Re}}{1+0.0438\mathrm{Re}^{0.976}}$
Y	$\frac{\frac{3}{8}\mathrm{Re}}{1+0.217\mathrm{Re}^{0.518}}$	$\frac{0.0537\mathrm{Re}}{1+0.0318\mathrm{Re}^{1.309}}$
C	$r_b^2 + \mathcal{O}\left(r_b^3\right)$	$r_b - r_b^2 + \mathcal{O}\left(r_b^3\right)$
C_1	$\frac{1}{2}K\left(1-\frac{\rho_f}{\rho_p}\right)\left(1+\mathcal{O}\left(r_b\right)\right)$	$\frac{1}{2}K\left(1-\frac{\rho_f}{\rho_p}\right)\left(\frac{1}{r_b}+\mathcal{O}\left(1\right)\right)$

Table 2.2. Parameters in Eq.(2.82) and Eq.(2.83).

Yoon-Luttrell

Yoon and Luttrell (1989) considered the probability of attachment for small particles as the ratio of the cross-sectional areas of particle and critical stream tube, as discussed in Section 2.3.1 (see Fig. 2.3). For the critical angle of collision θ_c, Yoon and Luttrell (1989) write:

$$P_a = \frac{r_c^2}{\left(r_b + r_p\right)^2} \equiv \sin^2\theta_c \tag{2.84}$$

Using formulations of Ψ for Stokes, intermediate, and potential flow, Yoon

and Luttrell (1989) used Eq.(2.63) to derive probabilities of attachment for the three flow conditions by substituting sliding time by induction time t_i to yield:

$$P_a = \sin^2\left[2\tan^{-1} e^{C_i}\right], \tag{2.85}$$

where C_i is an induction time coefficient:

$$C_i = \frac{-3U_b t_i}{2r_b\left(\frac{r_b}{r_p}+1\right)}, \qquad \text{for Stokes flow} \tag{2.86}$$

$$C_i = \frac{-\left(45+8\mathrm{Re}^{0.72}\right)U_b t_i}{30r_b\left(\frac{r_b}{r_p}+1\right)}, \qquad \text{for intermediate flow} \tag{2.87}$$

$$C_i = \frac{-3U_b t_i}{2\left(r_p+r_b\right)}, \qquad \text{for potential flow} \tag{2.88}$$

Fig. 2.7 shows values of P_a versus particle size for a given bubble size and two induction times. The graphs in Fig. 2.7 suggest that P_a increases for decreasing d_p (Yoon and Luttrell, 1989). Yoon and Luttrell (1989) attribute this effect to the lower tangential velocity of smaller particles compared to larger particles after collision has occurred. Luttrell and Yoon (1992) found good agreement between simplified theory and experimental data for coal particles between 11 and 40 μm in diameter.

2.3.3 Probability of aggregate stability

The third sub-process is that of the probability P_s of particle-bubble aggregate stability. This sub-process is probably the least understood and is often modelled as 1-P_d, where P_d is the probability of detachment. A metric commonly used in flotation engineering is the so-called "maximum flotability" (Schulze, 1983, p. 196), i.e. the largest particle that can be floated for a given bubble size and particle density. The aggregate stability is modelled after the balance of forces on a particle attached to the gas-liquid interface. An analysis of most of the forces involved can be found in (Schulze, 1983, p. 182-193) and in Schulze (1993). Fig. 2.8 shows a schematic view of a spherical particle at a planar gas-liquid interface.

The force balance for a particle, as shown in Fig. 2.8, can be described by (Schulze, 1993):

$$F_{ca} + F_{hyd} + F_b - F_g - F_d - F_\sigma = 0, \tag{2.89}$$

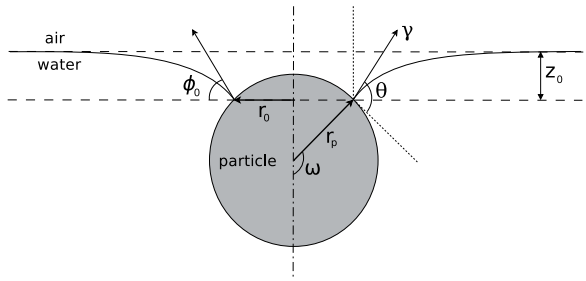

Figure 2.8. A spherical particle at a gas-liquid interface (after Schulze (1977)).

where the capillary force is:

$$F_{ca} = -2\pi r_p \gamma \sin\omega \sin(\omega + \theta), \tag{2.90}$$

the hydrostatic pressure force is:

$$F_{hyd} = \pi r_0^2 \rho_f g z_0 = \pi r_p^2 \sin^2(\omega) \rho_f g z_0, \tag{2.91}$$

where angles ω and θ are shown in Fig. 2.8. The buoyancy force is:

$$F_b = \tfrac{\pi}{3} r_p^3 \rho_f g \left[(1 - \cos\omega)^2 (2 + \cos\omega) \right], \tag{2.92}$$

the gravity force is:

$$F_g = \tfrac{4}{3}\pi r_p^3 \rho_p g, \tag{2.93}$$

the drag force is:

$$F_d = \tfrac{4}{3}\pi r_p^3 \rho_p a, \tag{2.94}$$

where a is acceleration. Finally, the capillary pressure force is:

$$F_\sigma = \pi r_0^2 p_\sigma \approx \pi r_p^2 \left(\sin^2\omega\right) \left(\frac{2\gamma}{r_b} - 2 r_b \rho_f g \right). \tag{2.95}$$

Under real flotation conditions, i.e. $d_p < 300\ \mu m$ and a contact angle θ smaller than about 90°, the hydrostatic term can typically be ignored and the angle ω is approximated by $\omega \approx \pi - \frac{\theta}{2}$ (Schulze, 1983, p. 182). The ratio of attachment and detachment forces can be modelled using a modified Bond number (Schulze, 1982):

$$Bo' = \frac{F_{det}}{F_{att}} = \frac{F_g - F_b + F_d - F_\sigma}{F_{ca} + F_{hyd}}, \tag{2.96}$$

or (Schulze, 1982, 1993):

$$Bo' = \frac{d_p^2 \left[(\rho_p - \rho_f) g + \rho_p a \right] + \left(\frac{\gamma}{6} - \frac{3}{2} d_p^2 \rho_f \right) \sin^2 \omega}{|6\gamma \sin \omega \sin (\omega + \theta)|}. \tag{2.97}$$

The acceleration a is commonly associated with the centrifugal acceleration of turbulent eddies. It is assumed that the dominant eddies that interact with the bubble-particle aggregate and the aggregate itself are of the same size (Liepe, 1977). This acceleration is called "machine acceleration" b_m and can be obtained from the radius r_v and RMS velocity $\overline{\Delta w^2}$ of the turbulent eddies (Schulze et al., 1989b). Assuming isotropic turbulence, one obtains (Schulze, 1983, p. 39):

$$b_m \approx \frac{\overline{\Delta w^2}}{r_v} \approx \frac{\left(1.38 \left(\varepsilon r_v \right)^{1/3} \right)^2}{r_v} \approx 1.9 \frac{\varepsilon^{2/3}}{r_v^{1/3}}, \tag{2.98}$$

where ε is the turbulent kinetic energy dissipation rate. The eddy radius r_v can be replaced by the aggregate radius $r_p + r_b$. The probability, or efficiency, of bubble-particle aggregate stability P_s is (Bloom and Heindel, 1997) (after Plate and Schulze (1991)):

$$P_s = 1 - e^{\left(1 - \frac{1}{Bo'}\right)} \tag{2.99}$$

The approach above can also be used for a slightly different formulation, called the tenacity of attachment (Nguyen, 2003; Phan et al., 2003). Writing out the balance of forces for an attached particle, Nguyen (2003) found for the tenacity T:

$$T = \frac{\pi}{2} d_p \gamma \left(1 - \cos \theta \right) \left[1 + 0.016 \frac{d_p}{2L} \right]. \tag{2.100}$$

Now, assuming that the detachment forces are mainly gravitational and centrifugal, in nature, one can write the detachment force as (Phan et al., 2003):

$$F_{det} = \tfrac{4}{3} \pi r_p^3 \left(\rho_p - \rho_f \right) \left(g + b_m \right) \tag{2.101}$$

The stability of the aggregate is defined by $T \leqslant F_{det}$. Substituting the LHS of Eq.(2.100) with the RHS of Eq.(2.101) and writing particle radius as the

maximum floatable particle radius $r_{p,max}$ one obtains (Nguyen, 2003):

$$r_{p,max} = \sqrt{\frac{3\gamma\left(1-\cos\theta\right)L^2}{4\left(\rho_p-\rho_f\right)\left(g+b_m\right)}} \tag{2.102}$$

Crawford and Ralston (1988) and Nishkov and Pugh (1991) have presented experimental work on maximum floatable particle size.

2.4 Particle-bubble interaction frequency

The approaches discussed in Section 2.3.1 are mechanistic and deterministic in nature. That is, most models are derived for the interaction between a single bubble and a single particle in an unbound medium. Mechanistic-deterministic modelling can yield valuable insight in the mechanisms that govern flotation. However, for modelling of the entire flotation process it is often useful to take a kinetic approach. One common approach is to choose a method based on kinetics and population balance modelling. Much of this work is rooted in the coagulation theory proposed by Smoluchowski (1917). Although there are hybrid approaches, such as by Seppälä et al. (2008) and Wierink et al. (2009), most kinetic population balance approaches rely on the work of Smoluchowski (1917), Saffman and Turner (1956), and Abrahamson (1975).

The basic idea behind the coagulation theory of Smoluchowski (1917) is that there exist two particles, 1 and 2, within an interaction volume V_{int}, that interact according to an interaction function f_{int}. The interaction volume, upon collision, is assumed to be of the order of the new aggregate size. That is, $r_{int} = \mathcal{O}\left(r_1 + r_2\right)$ and thus:

$$V_{int} = \mathcal{O}\left(r_{int}^3\right) \equiv \left(r_1 + r_2\right)^3, \tag{2.103}$$

where r_1 and r_2 are the radii of particle 1 and particle 2, respectively. Scaling up the interaction volume, so that e.g. a rain drop can grow by colliding with smaller drops, leads to the form containing the number concentrations N_1 and N_2 of particle type 1 and type 2, respectively. The general form of the collision rate equation is:

$$Z = \tfrac{4}{3}\pi\left(r_1 + r_2\right)^3 N_1 N_2 f_{int}, \tag{2.104}$$

where the interaction function f_{int} is typically called the collision kernel. In the work of Smoluchowski (1917) the interaction function is a function

of absolute temperature, viscosity, and the velocity gradient normal to the direction of travel of the colloidal particle.

Smoluchowski (1917) assumed uniform shear and particles that follow streamlines exactly, which was a reasonable assumption for colloidal particle motion in laminar fluid. Smoluchowski (1917) also assumed that all collisions between particles lead to coalescence. Saffman and Turner (1956) extended Smoluchowski (1917)'s theory to turbulent flow conditions (Mei and Hu, 1999). Assuming Gaussian, isotropic turbulence Saffman and Turner (1956) formulated the collision frequency as:

$$Z \approx \tfrac{1}{2} N_1 N_2 \int_A -\langle |w_r| \rangle dA, \tag{2.105}$$

where the integral index A refers to the surface of the sphere of interaction and U_r is the relative velocity between particles. Note that the ensemble average should be taken over the entire integral. However, because Saffman and Turner (1956) assumed isotropic turbulence the ensemble average may be moved inside the integral as an approximation (Mei and Hu, 1999). For particles smaller than the Kolmogorov length scale one can make the approximation of:

$$\langle |w_r| \rangle \approx R \left\langle |\frac{\partial U_r}{\partial r}| \right\rangle. \tag{2.106}$$

Saffman and Turner (1956) then used a relation of Taylor (1935) to relate the average velocity gradient to the turbulent dissipation rate ε as:

$$\left\langle \frac{\partial U_r}{\partial r} \right\rangle = \frac{\varepsilon}{15\nu}. \tag{2.107}$$

Assuming a normal distribution, Saffman and Turner (1956) obtained:

$$\left\langle |\frac{\partial U_r}{\partial r}| \right\rangle = \left(\frac{2\varepsilon}{15\nu} \right)^{1/2}. \tag{2.108}$$

Finally, Saffman and Turner (1956) substituted Eqs.(2.106) and(2.108) into Eq.(2.105) and used $\int_A dA = 4\pi R^2$ to obtain:

$$Z = \left(\frac{8\pi}{15} \right)^{1/2} N_1 N_2 d_{12}^3 \left(\frac{\varepsilon}{\nu} \right)^{1/2}. \tag{2.109}$$

where d_{12} is the aggregate diameter.

Abrahamson (1975) noted that Eq.(2.109) is only valid for d_{12} smaller than the Kolmogorov length scale and only for particles that follow fluid streamlines exactly. Assuming independent and normal distributions of particle velocities and that the particle-fluid relative motion is in the Stokes range, Abrahamson (1975) obtained:

$$\begin{aligned} Z &= (8\pi)^{1/2} N_1 N_2 d_{12}^2 \sqrt{\left(\overline{U}_1^2 + \overline{U}_2^2\right)} \\ &\approx 5.0 N_1 N_2 d_{12}^2 \sqrt{\left(\overline{U}_1^2 + \overline{U}_2^2\right)} \end{aligned} \tag{2.110}$$

Using the collision frequency Z, the total flotation rate constant for the pulp phase can calculated using Eq.(2.12). In turn, the rate constant can be used to describe global flotation kinetics by e.g. Eq.(2.1). Eq.(2.110) has been applied successfully to mineral froth flotation by Koh et al. (2000); Koh and Schwarz (2003, 2006, 2007); Liu and Schwarz (2009a,b) and to deinking flotation by Bloom and Heindel (1997, 2002, 2003). It must be noted here that the use of orthokinetic and independent collision models, such as those based on Smoluchowski (1917), Camp and Stein (1943), and Abrahamson (1975), for flotation systems is questions in the literature (Pedocchi and Piedra-Cueva, 2005; Meyer and Deglon, 2011). However, the focus of this thesis is a modelling framework for coupled bubble-particle interaction, including surfactant dynamics. Detailed simulation of the behaviour of bubbles and particle can give valuable insight in the critical mechanisms of the system and provide input for semi-statistical methods to model the entire flotation cell.

3. Model structure

3.1 Introduction

The discussion in Chapter 2 brings forward two main points to be addressed in further development of models for bubble-particle interaction. The first point of attention is kinematic coupling, in terms of physical momentum coupling as well as coupling between hydrodynamics and physicochemistry. Clearly, methods that use higher order momentum coupling are a better representation of experimental observations than methods where inertia and momentum are neglected. The second major point to address is the bridging of temporal and spatial scales. Empirical observations from industry tell a great deal about the macroscopic behaviour of three-phase systems. Equally important are the advancements of knowledge about processes at (sub-)molecular scale. The union of knowledge on the micro- and macro-scales is one of the main reasons simplification and probabilistic interpretation of processes are necessary. However, with reference to Fig. 1.1 on p. 18, it is the intermediate meso-scale where macroscopic hydrodynamics and microscopic physico-chemistry meet. Integral modelling at the meso-scale can provide a valuable test harness for theory and validation bridging the gap between the micro- and macro-scales.

In this chapter a modelling framework for integral meso-scale modelling of bubble-particle interaction is discussed. In Section 3.2 momentum coupling between dispersed and carrier phases is examined in the light of mineral froth flotation. Section 3.3 treats the main architectural aspects of the modelling framework. The coupling between solid particles and the fluid phases is made possible by a coupled CFD-DEM code, which is outlined in Section 3.4. The choice of modelling approach for the liquid and gas phases is discussed in Section 3.5, followed by three sections on forces and transport phenomena that are specific to bubble-particle interaction with soluble surfactants. These sections are Section 3.6 on the convective-diffusive transport of soluble surfactant within the finite volume method, Section 3.7 on particle motion in liquid and particle-particle forces, and finally Section 3.8 on the forces that occur when a solid particle approaches

the gas-liquid interface closely.

3.2 Momentum coupling

From the discussion in the previous chapter it has come clear that current flotation models can predict flotation process behaviour only in certain cases and that the governing principles are not yet understood deeply enough. Most successful models lean heavily on empirical knowledge and may fit, but have limited predictive power. Two major assumptions behind classic models are that the motion of the mixture and the momentum of the individual phases can be decoupled and that physical momentum and chemical potential can be decoupled as well. Under certain conditions these are valid assumptions, for example for dilute body force driven flows. However, in the case where the small scale interaction between dispersed phases is the very reason the process is used, detailed three-phase interaction requires attention in modelling and experimental research.

Elghobashi (1991) mapped the interaction between dispersed phases in terms of level of momentum coupling. One-way momentum coupling refers to the situation where momentum is only transferred from the carrier phase to the dispersed phase. With two-way momentum coupling the momentum of the dispersed phase interacts with the momentum of the carrier phase. When bubbles and particles find themselves closer to each other than about 10 times their own diameter, the system is characterised by so-called four-way coupling. Under such conditions the equations of motion of the different phases need strong coupling to describe the system accurately. In industrial processes such as mineral froth flotation, the distance between dispersed bubbles is typically in the order of one bubble diameter or less. Suspended solid particles are in many cases separated by less than the particle diameter. Mineral froth flotation therefore lies in the very right hand side of Fig. 3.1. (Wierink and Heiskanen, 2008) In addition, at the scales that are important in mineral froth flotation, physico-chemical forces play a key role in the momentum exchange within the system. For these reasons the further development of mineral froth flotation models benefits from a modelling approach with natural implementation of higher order momentum coupling. The two central themes around which further development of flotation models evolves are:

1. physical momentum coupling between phases, and
2. coupling between chemical potential and physical momentum.

The next section describes the architecture of the implementation of these two aspects of momentum coupling.

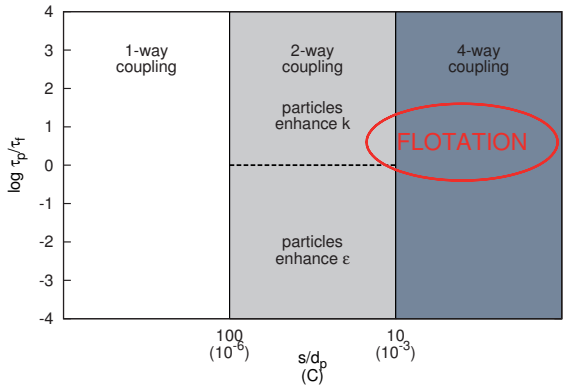

Figure 3.1. Momentum coupling regimes for the log of the ratio of particle response time τ_p and fluid response time τ_f (log Stokes number)versus particle-particle distance s, normalised by particle diameter d_p (after Elghobashi (1991)). Approximate volumetric concentration C of the dispersed phase is indicated in brackets..

3.3 A coupled modelling framework

After the discussion in Chapter 2 and Section 3.2 it is clear that by including momentum coupling and coupling with physico-chemical phenomena bubble-particle models can achieve more accurate results. The method of implementation of these couplings is however of the same magnitude of importance as the phenomena themselves. From the perspective of model architecture, the reason is that the various aspects of physics and chemistry involved are understood at different levels. For example, the motion of a spherical particle through a fluid is better understood than film rupture in the presence of surface active components. Nevertheless, both of these aspects are important and need to be included in the model. Key architectural features of the modelling framework are therefore modularity and flexibility.

In classical flotation models bubbles are assumed spherical particles that are separate from the fluid domain. Consequently, bubble break-up and coalescence can only be handled by PBM or a similar approach, where bubble size and number density is computed according to a population kernel. In some cases this approach has proven effective, but important phenomena such as dynamic adsorption of surfactants and Marangoni stresses are difficult to include in a consistent way. One of the central challenges is how rapid adsorption dynamics interact with topological change of the adsorption surface, i.e. during bubble break-up and coalescence. Topological change of the gas-liquid interface has been identified as an important phenomenon by several authors (Omelka et al. (2009), Ata (2009), Clift et al. (1978, p. 339-347)) in bubble-particle interaction

and bubble dynamics. Integral and consistent simulation of multi-phase multi-species systems requires the ability to handle topological changes of the interfaces.

In the model presented in this thesis the discrete phases are treated differently than in typical flotation modelling. Air bubbles are not treated as discrete entities as such, but rather as an interface between liquid and gas that can form distinct topological sets according to local stresses. The motion of particles is computed by the DEM in its own frame of reference, while coupled to forces interacting with the fluid domain. These solid particles are modelled as Lagrangian points that are in fact dynamic lists of properties, such as diameter, location, and contact angle. Depending on the characteristics of the system the list of particle properties can be changed and extended. This feature allows ready implementation of particle surface mineralogy and the effects of activators, depressants, and other surfactants at the particle surface. For example, interfacial properties such as zeta potential can be made dependent on surfactant concentration on a near gas-liquid surface.

The two main values of this modelling framework are:

1. that complex, coupled modelling of bubble-particle interaction is made computationally feasible in a modular and extensible way and
2. further research needs are identified.

The author is aware that the various constituents of an integral bubble-particle interaction model are characterised by different levels of understanding of the key phenomena. In many cases the reason is the great difficulty in deriving conclusive results from complex and dynamic systems such as those with multiple phases and species. The modelling elements described in the following sections reflect this variation in understanding. Inclusion of even the simplest sub-model in the framework brings with it two important features. Firstly, the value of the sub-model itself can be assessed in the context of a dynamic system and, secondly, the interaction with other sub-models can be investigated. The dynamic nature of the coupled system of sub-models creates an additional degree of freedom, which the modelling framework presented can help to understand. Rather than omitting sub-models, the current modelling structure serves as a test harness for integral model development. The most urgent areas of further development readily crystallise and the relative influence of various physical and physico-chemical phenomena are brought forward. For example, one area of interest may be adsorption and desorption of soluble surfactants near a moving gas-liquid interface in the presence of fine solids. The following sections detail the modelling elements currently implemented in the framework and the work is intended as a stepping stone

to more integral modelling of multi-phase multi-species systems.

3.4 CFD-DEM coupling

The modelling of particulate and dispersed flows can be approached by two main strategies, the continuum and discrete approaches (Goniva et al., 2010). In the continuum approach the dispersed phase is thought of as an artificial continuum to which conservation equations are applied (Gidaspow et al., 1992). In discrete modelling of particulate flow, however, the dynamics of individual particles and particle-particle collisions are treated with a specific collision kernel (Goniva et al., 2010; Wierink et al., 2011). One of the most important discrete models is the so-called Discrete Element Method (DEM) (Cundall and Strack, 1979). The DEM accurately captures all granular physical phenomena, provided that models for these phenomena are included.

The aims and necessary model features considered in Sections 3.1 and 3.2 require an integral and modular framework to simulate three-phase interaction. The combination of CFD and DEM appears a natural choice and the CFDEM project[1] (Goniva et al., 2011; Kloss et al., 2011) fulfils this requirement. The CFDEM package consists of the coupling of the open source CFD code OpenFOAM® and the open source DEM solver LIGGGHTS. The dynamics of fluids and particles are computed on their own respective meshes and momentum and void fraction are transferred between the two codes through an MPI message passing library. The coupling between OpenFOAM and LIGGGHTS can be summarised as follows (Goniva et al., 2010):

1. particle positions and velocities are calculated by the DEM solver;
2. these particle positions and velocities are transferred to the CFD solver;
3. for each corresponding computational cell, the particle volume fraction as well as a mean particle velocity is determined;
4. based on the particle volume fraction, the momentum exchange between particles and carrier phases is calculated within the CFD solver;
5. the forces acting on each particle are sent to the DEM code and used for the next time step;
6. the local fluid velocity is calculated by CFD solver, taking into account the local volume fraction and momentum exchange;
7. the routine is repeated from (1).

[1] CFDEM - Open Source CFD, DEM, and CFD-DEM: `http://www.cfdem.com`, accessed October 2011.

3.5 Modelling approach

The detailed simulation of gas-liquid flows can be divided into two main categories; interface tracking methods (cf. Mclaughlin (1996); Cuenot et al. (1997); Palaparthi et al. (2006); Tuković (2005); Tuković and Jasak (2008, 2012)) and interface capturing methods (cf. James and Lowengrub (2004); Drumright-Clarke and Renardy (2004); Xu et al. (2006); Lakshmanan and Ehrhard (2008, 2010)). In interface tracking the gas-liquid interface is formed by the boundary between two separate computational domains. Interface tracking is more accurate than interface capturing, but interface break-up and coalescence is challenging. Break-up and coalescence can be modelled using interface tracking (cf. Menon et al. (2008)), but the topological changes are complex and computationally intensive. In the interface capturing method, the interface is formed of the gradual change of a phase fraction function and the interface is smeared to some extent. The interface sharpness can be improved by combining a level-set based method with the Volume Of Fluid (VOF) method (Hirt and Nichols, 1981) (cf. Lakshmanan and Ehrhard (2008, 2010)), for example as developed by Olsson and Kreiss (2005). In practise, however, this type of hybrid model can be unstable and lead to unphysical results (Weller, 2010). The VOF method is mass conservative and topological changes of the interface are readily captured. Since mass conservation and bubble-bubble interaction are important aspects in the motivation of this work, the VOF method is a natural choice and forms a good basis for the consistent implementation of the physico-chemical models needed to simulate bubble-particle interaction with variable surface tension.

In the VOF model, motion of the gas-liquid interface is captured by computing the motion of a phase fraction, or colour function, α through the computational domain. The governing equations are the continuity equation:

$$\nabla \cdot \mathbf{U} = 0, \tag{3.1}$$

the phase transport equation:

$$\frac{\partial \alpha}{\partial t} + \nabla \cdot (\alpha \mathbf{U}) = 0, \tag{3.2}$$

and the momentum equation:

$$\frac{\partial (\rho \mathbf{U})}{\partial t} + \nabla \cdot (\rho \mathbf{U}\mathbf{U}) = -\nabla \cdot \overleftrightarrow{\sigma} + \mathbf{g}, \tag{3.3}$$

where $\overleftrightarrow{\sigma}$ is the total stress tensor and $\mathbf{g}$ gravitational acceleration. The total stress tensor is composed of contributions by pressure, shear, and interfacial tension forces as:

$$\overleftrightarrow{\sigma} = \overleftrightarrow{\sigma}_p + \overleftrightarrow{\sigma}_\tau + \overleftrightarrow{\sigma}_\sigma. \tag{3.4}$$

The standard VOF method is rather dispersive due to numerical diffusion (Weller, 2008), but the diffuse interface is also a characteristic of the VOF method itself. Weller (2008) recognised this property and implemented a counter-gradient transport equation (Weller, 1993) in the VOF solver in the OpenFOAM (OpenCFD Ltd., 2011a) CFD package. This equation takes the form of:

$$\frac{\partial \alpha}{\partial t} + \nabla \cdot (\alpha \mathbf{U}) + \nabla \cdot [\mathbf{U}_c \alpha (1 - \alpha)] = 0, \tag{3.5}$$

where the interface compression velocity $\mathbf{U}_c$ is defined as:

$$\mathbf{U}_c = \min (c_\alpha |\mathbf{U}|, \max (|\mathbf{U}|)) \frac{\nabla \alpha}{|\nabla \alpha|}. \tag{3.6}$$

In Eq.(3.6), c_α is a parameter to set the magnitude of the interface compression. In the work presented here, c_α is set to 1. From Eq.(3.5) it can readily be seen that through the term $\alpha (1 - \alpha)$ an interface-normal flux, proportional to $\mathbf{U}_c$, is generated at the interface only. This additional flux results in compression and sharpening of the gas-liquid interface.

3.6 Transport and sorption of soluble of surfactant

The transport of surfactant on the surface of the bubble follows essentially Fick's law, however, some care is needed with regard to the formulation. During adsorption of surfactant from the bulk onto the bubble surface a scalar field, surfactant concentration, is mapped from a volumetric space onto a surface. That is:

$$\mathbf{S}_C : C \mapsto \Gamma, \tag{3.7}$$

where $\mathbf{S}_C$ is a source-sink term, C surfactant concentration in the liquid, and Γ surfactant concentration on the bubble surface.

During desorption the opposite of Eq.(3.7) takes place. Hence, $\mathbf{S}_C$ couples the bulk and surface transport equations for surfactant. In the pure VOF method, however, the gas-liquid interface is not clearly defined. Rather, the interface is a diffuse region across which the integral of the colour function is unity. In this approach we assign a region in space that is characterised by a non-zero gradient of the colour function. This region is depicted in Fig. 3.2, moving across the gas-liquid interface located at $x = 0$.

The approach of an interfacial region that is diffuse, rather than a sharp

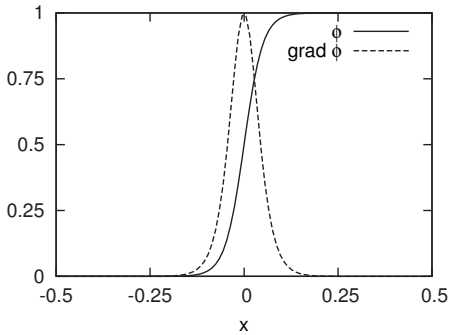

Figure 3.2. Value of the colour function ϕ and its normalised gradient$\nabla\phi$ across the gas-liquid interface. The distance is shownon the horizontal axis, with the centre of the interface located at $x = 0$.

interface, calls for a volumetric surface transport equation for surfactant concentration. Special care need be taken in the formulation of this equation, in particular the definitions of the surface gradient and surface Laplacian operators in a volumetric context. The formulation of the volumetric surface transport equation is elaborated below.

The general transport equation for any field ϕ is of the form:

$$\frac{\partial \phi}{\partial t} + \nabla \cdot \mathbf{J}_\phi = \mathbf{S}_\phi, \tag{3.8}$$

where $\mathbf{S}_\phi$ is the source-sink term for ϕ and the total flux $\mathbf{J}_\phi$ is defined as:

$$\mathbf{J}_\phi = \mathbf{U}\phi - \mathcal{D}\nabla\phi \tag{3.9}$$

Substitution of Eq.(3.9) into Eq.(3.8) and replacing field ϕ with surfactant concentration C yields:

$$\frac{\partial C}{\partial t} + \nabla \cdot (\mathbf{U}C) = \nabla \cdot (\mathcal{D}\nabla C) + \mathbf{S}_C \tag{3.10}$$

The diffusion coefficient $\mathcal{D}$ in the diffusive term on the right-hand side of Eq.(3.10) is, in fact, a tensor and should remain within the divergence operator. Only under very dilute conditions can we treat the diffusion tensor as a scalar coefficient and take it out of the divergence operator. Dilute surfactant transport may be an appropriate assumption in the bulk liquid in most process applications, but is unlikely to be valid on the surface of a bubble contaminated by surfactants. For now, however, we accept this shortcoming in the light of mathematical convenience and treat the diffusion tensor as a scalar coefficient.

In Eq.(3.10), $\mathbf{S}_C$ is governed by the adsorption-desorption dynamics of bulk liquid and gas-liquid interface and is modelled as (Levich, 1952):

$$\mathbf{S}_C = k_a C_\Gamma \left(1 - \frac{\Gamma}{\Gamma_\infty}\right) - k_d \Gamma, \tag{3.11}$$

where k_a and k_d are the adsorption and desorption coefficients, respectively, Γ_∞ is the maximum concentration of surfactant at the interface, and C_Γ is the surfactant concentration in the boundary layer of the bubble. It is important to note that C_Γ follows the bulk surfactant transport equation for C and represents C in the interfacial region of the gas-liquid transition, i.e. the bubble boundary layer. Surface concentration Γ can only exchange mass with C_Γ and not with C directly. This exchange mechanism is schematically shown in Fig. 3.3 and is needed because Γ is modelled as a volumetric concentration stored in the interface region of the bubble.

The vector fields in Eq.(3.10), i.e. velocity and surfactant gradient, can be decomposed in interface-normal and interface-tangential components as:

$$\begin{aligned} &\frac{\partial C}{\partial t} + \nabla \cdot (\mathbf{U}_n C + \mathbf{U}_s C) \\ &\quad = \mathcal{D} \nabla_s^2 C + \mathcal{D} \nabla \cdot ([\nabla C \cdot \mathbf{n}]\, \mathbf{n}) + \mathbf{S}_C \end{aligned} \tag{3.12}$$

Now, splitting the term $\nabla \cdot (\mathbf{U}_n C + \mathbf{U}_s C)$ and expressing $\mathbf{U}_n$ as $(\mathbf{U} \cdot \mathbf{n})\, \mathbf{n}$, Eq.(3.12) becomes:

$$\begin{aligned} &\frac{\partial C}{\partial t} + \nabla \cdot [C\, (\mathbf{U} \cdot \mathbf{n})\, \mathbf{n}] + \nabla \cdot (\mathbf{U}_s C) \\ &\quad = \mathcal{D} \nabla_s^2 C + \mathcal{D} \nabla \cdot ([\nabla C \cdot \mathbf{n}]\, \mathbf{n}) + \mathbf{S}_C, \end{aligned} \tag{3.13}$$

or

$$\begin{aligned} &\frac{\partial C}{\partial t} + C\, (\mathbf{U} \cdot \mathbf{n})\, \nabla \cdot \mathbf{n} + \mathbf{n} \cdot \nabla\, [C\, (\mathbf{U} \cdot \mathbf{n})] + \nabla_s \cdot (\mathbf{U} C) \\ &\quad = \mathcal{D} \nabla_s^2 C + \mathcal{D} \nabla \cdot (|\nabla C| \mathbf{n}) + \mathbf{S}_C \end{aligned} \tag{3.14}$$

Diffusion in the interface normal direction is accounted for by the sorption isotherm in the sink-source term $\mathbf{S}_C$. Therefore, we we can eliminate interface normal diffusion by setting term $\mathcal{D} \nabla \cdot (|\nabla C| \mathbf{n})$ in Eq.(3.14) to zero. Also, the surfactant concentration C in Eq.(3.14) is now the surface concentration, although in volumetric form, since transport takes place within the interfacial region rather than on a surface. Eq.(3.14) thus takes the form:

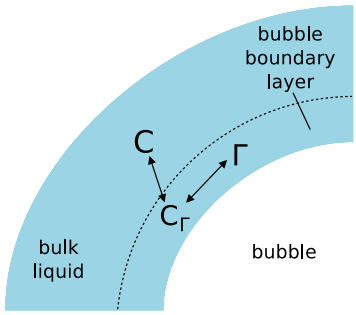

Figure 3.3. Schematic representation of the exchange of surfactant betweenconcentrations C in the bulk liquid, C_Γ in the bubble's boundary, and subsequently, betweenC_Γ and the volumetric surface concentration Γ.

$$\frac{\partial \Gamma}{\partial t} + \Gamma\left(\mathbf{U}\cdot\mathbf{n}\right)\nabla\cdot\mathbf{n} + \mathbf{n}\cdot\nabla\left[\Gamma\left(\mathbf{U}\cdot\mathbf{n}\right)\right] + \nabla_s\cdot\left(\mathbf{U}\Gamma\right) = \mathcal{D}\nabla_s^2\Gamma + k_a C_\Gamma\left(1-\frac{\Gamma}{\Gamma_\infty}\right) - k_d\Gamma \tag{3.15}$$

The surface gradient operator ∇_s is defined as $(\mathbf{I}-\mathbf{n}\otimes\mathbf{n})\nabla$. The Laplacian operator of field ϕ can be decomposed as:

$$\nabla^2\phi = \nabla\cdot\left(\left[\nabla\phi\cdot\mathbf{n}\right]\mathbf{n}\right) + \nabla\cdot\left(\left[\nabla\phi\cdot\mathbf{t}_1\right]\mathbf{t}_1\right) + \nabla\cdot\left(\left[\nabla\phi\cdot\mathbf{t}_2\right]\mathbf{t}_2\right), \tag{3.16}$$

where $\mathbf{t}_1$ and $\mathbf{t}_2$ are the two tangential surface vectors. The first term on the right-hand side of Eq.(3.16) represents the surface normal contribution to the Laplacian while the second and third terms represent the surface contribution. Therefore, the surface Laplacian can be obtained by rewriting Eq.(3.16) as:

$$\nabla_s^2\phi = \nabla\cdot\left(\left[\nabla\phi\cdot\mathbf{t}_1\right]\mathbf{t}_1\right) + \nabla\cdot\left(\left[\nabla\phi\cdot\mathbf{t}_2\right]\mathbf{t}_2\right) = \nabla^2\phi - \nabla\cdot\left(\left[\nabla\phi\cdot\mathbf{n}\right]\mathbf{n}\right) \tag{3.17}$$

3.7 Particle motion

The motion of particles is modelled in a Lagrangian frame of reference. The governing equation is:

$$m_p\frac{d\mathbf{U}_p}{dt} = \sum\mathbf{F}, \tag{3.18}$$

where $\mathbf{F}$ contains the relevant forces acting on the particle. Commonly

these are the drag force, the buoyancy force, and a driving force due to pressure gradient. Interfacial, electrostatic, and other forces can be added in Eq.(3.18) to accommodate the physics specific to the system at hand. The particle forces described in the current and next section are models found in literature and are surely incomplete. However, the structure of the current modelling framework allows to continuously update the particle model according to experimental and theoretical findings.

To account for particle-particle collisions in more dense dispersed flows a soft-sphere collision model Bertrand et al. (2005) and Cundall and Strack (1979) was implemented. Particles are represented by spheres with a centre point and a radius. During particle-particle collision the particles are allowed a small overlap δ_p, as shown in Fig. 3.4. The normal force $\mathbf{F}_{cn,i,j}$ between particles i and j is the calculated as (Bertrand et al., 2005):

$$\mathbf{F}_{cn,i,j} = k_n \delta_{n,i,j}^{\beta_1} + C_n \frac{\partial \delta_{n,i,j}}{\partial \tau} \tag{3.19}$$

and the tangential force as:

$$\mathbf{F}_{tn,i,j} = k_t \delta_{t,i,j}^{\beta_2} + C_t \frac{\partial \delta_{t,i,j}}{\partial \tau}, \tag{3.20}$$

where k_n and k_t are the stiffness coefficients and C_n and C_t are the damping coefficients, in the normal direction n and tangential direction t, respectively. In this work a linear collision model is used so that the coefficients β_1 and β_2 are both set to 1. The forces in Eqs.(3.19) and (3.20) are then added to the right hand side of Eq.(3.18). In the results presented here, k is 0.9 kg/s^2 and C is 800 kg/s. The values for k and C are not based on physical particle properties, but rather to ensure that particles do not overlap and collide with reasonable restitution and to provide a proof of concept. At a later stage physical parameters are to be tested, such as those reported by Malone and Xu (2008).

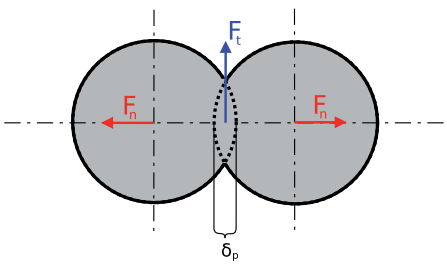

Figure 3.4. Particles colliding using the soft-sphere collision model. The particles overlap by distance δ_p, $\mathbf{F}_n$ is the normal force and $\mathbf{F}_n$ the tangential force.

3.8 Forces between bubbles and particles

Particles that find themselves at short distance from the gas-liquid interface experience not only hydrodynamic forces, but also forces due to chemical interactions. The range at which these chemical forces become important is thought to be around 10 nm (Israelachvili, 1992, p. 247), slightly varying for different systems. This range corresponds to zone 3 in Fig. 2.1 on p. 26. The forces acting on particles at such close range have been investigated in the context of Brownian motion since the late eighteenth century. The introduction of the concept of the ζ-potential to describe the electrostatic state of a surface by von Helmholtz (1879) and the extension of this theory to charge mobility and electrophoresis by Smoluchowski (1903), made it possible for colloidal interaction to be measured (Russel et al., 2001, p. 9). Von Helmholtz treated the solid surface as planar, with linear decay of the electrostatic field away from the surface. In order to accommodate more general conditions with a diffuse surface charge distribution, Gouy (1910) and Chapman (1913) proposed a model where some ions can diffuse into the bulk and the field strength decays exponentially (Rosen, 2004, p. 36). Surface charge and its heterogeneous distribution manifests as a region close to the surface, called the electric double-layer. The force resulting from this surface charge is referred to as the electric double-layer repulsion force.

During the late 1930s, Verwey and de Boer (1938) investigated characteristics of colloid suspensions, in particular the relation between (surface) electro-chemical and mechanical properties. They recognised that the effect of interactions between the electric double layers of small quartz particles ($d_p \sim 1$ μm) caused dilatancy of the suspension. However important, electric double-layer interaction cannot be the only significant force with regard to the stability of colloidal suspensions. Several phenomena suggest the presence of a long-range attractive force as well (Verwey and Overbeek, 1948, p. 19). This long-range attractive force was attributed to non-ideal Van der Waals forces, where fluctuations in the charge distribution of one atom can polarise another. This theory was postulated by London (1930, 1937) and is therefore referred to as the Van der Waals-London attraction force. Verwey and Overbeek (1948, p. 104-105) point out that for distances larger than about 10^{-8} m, the seventh power law breaks down and a relativistic correction is needed, leading to the London-Van der Waals attraction force.

In simultaneous but separate work, Derjaguin and Landau (1941) and Verwey and Overbeek (1948) assumed additivity of the electric double-layer and Van der Waals forces and proposed that the total interaction between charged surfaces is the sum of these two forces. The classical

theory by Derjaguin and Landau (1941) and Verwey and Overbeek (1948) has become known as the DLVO theory and is the subject of the next section.

3.8.1 DLVO forces

The classical DLVO theory, in the context of bubble-particle interaction, predicts that the total energy of interaction can be described by the summation of the London-Van der Waals and electric double-layer forces. The total potential energy of interaction V_{tot} is:

$$V_{tot} = V_e + V_{vdW}, \tag{3.21}$$

where V_e is the electrostatic interaction energy and V_{vdW} is the London-Van der Waals energy. Fig. 3.5 shows schematically the change of interaction energy as a function of distance from surface. As two surfaces approach one another, the sum between attractive and repulsive forces first reaches a minimum; point *a* in Fig. 3.5. Commonly this point is referred to as the secondary minimum. At even shorter separation distance the total interaction energy shows a peak at point *b* in Fig. 3.5, closer than which the total energy of interaction is strongly attractive, towards the primary minimum at point *c*. When applied to bubble-particle interaction, it is a commonly accepted view that the energy peak at point *b* in Fig. 3.5 forms an energy barrier for the particle-bubble pair to overcome before adhesion can occur. (Israelachvili, 1992, p. 247) Fig. 3.5 schematically depicts the current view of classical DLVO and has been redrawn after Israelachvili (1992, Fig. 12.12, p. 248)), although Derjaguin and Kusakov (1936) already published practically the same diagram. Derjaguin and Kusakov (1936) drew the interaction forces versus distance.

For two hard spheres with different charge densities or different potentials, Hogg et al. (1966) derived the following expression for the electrostatic interaction energy:

$$V_e = \frac{\varepsilon r_1 r_2 \left(\Psi_1^2 + \Psi_2^2\right)}{4\left(r_1 + r_2\right)} \left\{ \frac{2\Psi_1\Psi_2}{\left(\Psi_1^2 + \Psi_2^2\right)} \ln\left[\frac{1 + e^{-\kappa H}}{1 - e^{-\kappa H}}\right] + \ln\left(1 - e^{-2\kappa H}\right) \right\}, \tag{3.22}$$

where ε is the dielectric constant $\varepsilon_r \varepsilon_0$, r_1 and r_2 are the radii of the two spheres, Ψ_1 and Ψ_2 their respective potentials, and H is the separation distance between the spheres. κ is the inverse Debye screening length. The screening length occurs in an electrolyte solution containing free charges. In such an environment, all electrostatic fields are "screened" due to charge

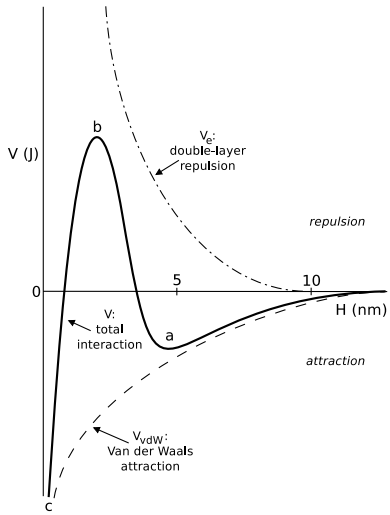

Figure 3.5. Schematic interaction energy as function of separation distance H according to DLVO theory (after Israelachvili (1992, Fig. 12.12, p. 248)).

polarisation and the field decays exponentially, roughly according to $e^{-\kappa x}$ (Israelachvili, 1992, p. 199). The Debye, or Thomas-Fermi, screening length characterises the thickness of the diffuse charge atmosphere close to a charged surface and is expressed as (Israelachvili, 1992, p. 238):

$$\kappa = \sqrt{\frac{\sum_i \rho^e_{\infty i} z_i^2}{\varepsilon k T}}, \tag{3.23}$$

where $\rho^e_{\infty i}$ is the charge density, z_i the electrovalence, k the Boltzmann constant, and T absolute temperature. Israelachvili (1992, p. 245) also points out that the potential interaction energy between surfaces usually has a maximum at roughly $\frac{1}{\kappa}$. In Eq.(3.22) the characteristic length scale of interaction has been replaced by $\frac{r_1 r_2}{(r_1+r_2)}$ to represent the interaction between cylinders or spheres (Israelachvili and Pashley, 1982). In the expressions to follow the same substitution is made.

For different types of electrovalences Israelachvili (1992, p. 238) further states that the magnitude of κ solely depends on properties of the liquid and not on surface properties, and that κ scales with $\sqrt{C_b}$. For a monovalent electrolyte Israelachvili (1992, p. 238) writes the following approximate expression:

$$\kappa = \frac{\sqrt{C_b}}{0.304} \tag{3.24}$$

When we note that $\rho^e_{\infty i}$ in Eq.(3.23) is in fact the ion number density in the bulk, we can express $\rho^e_{\infty i}$ as $N_A C_b$, where N_A is the Avogadro number.

Comparison Eq.(3.23) and Eq.(3.24) shows that both expressions do not yield the same result. Fig. 3.6 shows results for V_e, Eq.(3.22), for different particle diameters $2r_1$, a bubble diameter $2r_2$ of 1 mm, a temperature of 298 K, and a bulk surfactant concentration C_b of $4.0 \cdot 10^{-4}$ mol/m^3. The results on the left in Fig. 3.6 have been calculated using Eq.(3.23) for κ and the results on the right using Eq.(3.24) in Eq.(3.22). The shape of the curves in Fig. 3.6 are nearly the same, but the effective range of the field differs by about an order of magnitude between using Eq.(3.23) or Eq.(3.24) in Eq.(3.22).

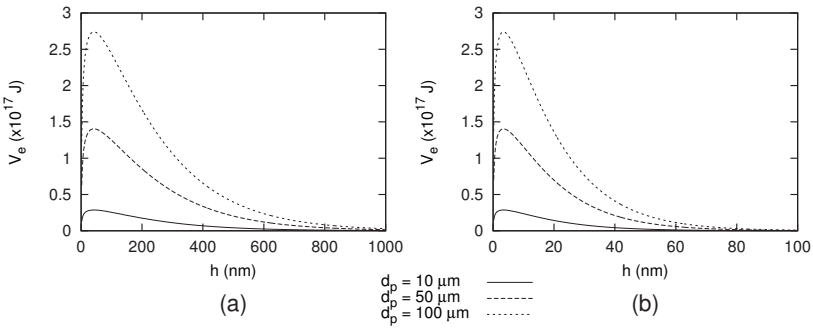

Figure 3.6. DLVO electric interaction potential V_e for different particle diameters. V_e is computed using Eq.(3.22) using Eq.(3.23) for κ (left) and using Eq.(3.24) (right). The bubble diameter is 1 mm, the temperature 298 K, and the bulk concentration C_b is $4.0 \cdot 10^{-4}$ mol/m^3. Note the different scales on the horizontal axes.

The second contribution in Eq.(3.21) is the dispersion energy that arises due to Van der Waals forces between non-polar molecules (Mao, 1998). The London-Van der Waals (dispersion) energy V_{vdW} can be written as (Rabinovich and Churaev, 1979):

$$V_{vdW} = -\frac{A_{132} r_1 r_2}{6H\left(r_1 + r_2\right)} \left[1 - \frac{1 + 2bl}{1 + \frac{bc}{H}}\right], \tag{3.25}$$

where $b = 3 \cdot 10^{-17}$ s, $l = 3.3 \cdot 10^{15}$ s^{-1}, and $c = 3 \cdot 10^{8}$ m/s. The term between square brackets is a correction factor for the retardation effect (Mao, 1998). In Eq.(3.25), A_{132} is the complex Hamaker constant for solid-gas-liquid interaction and is defined as (Hamaker, 1937):

$$A_{132} = \left(\sqrt{A_{11}} - \sqrt{A_{33}}\right)\left(\sqrt{A_{22}} - \sqrt{A_{33}}\right), \tag{3.26}$$

where A_{11}, A_{22}, and A_{33} are the Hamaker constants of air in vacuum, of solid in vacuum, and of water in vacuum, respectively. For a bubble with low surface surfactant concentration, A_{11} is about zero, while $A_{22} > A_{33}$ in most flotation systems. Therefore, A_{132} becomes negative and V_{vdW}

becomes positive. This means that in a typical flotation system the attractive Van der Waals force is in fact a repulsive dispersion force (Yoon, 1991; Yoon and Mao, 1996). It has been recognised that, under typical flotation conditions, the only significant driving force behind particle-bubble attachment is the (non-DLVO) hydrophobic force (Yoon, 1991; Yoon and Mao, 1996; Mao, 1998).

3.8.2 Non-DLVO forces

Experimental evidence of Laskowski and Kitchener (1969) showed that for a repulsive electrostatic energy and repulsive Van der Waals energy, the net interaction energy was still negative and thus attractive for methylated quartz particles. This finding suggested the presence of a third force, the so-called hydrophobic force (Yoon, 1991). The attractive hydrophobic force is larger than the Van der Waals force and probably cannot be determined using continuum calculations alone (Rabinovich and Yoon, 1994). About a decade after Laskowski and Kitchener (1969), Pashley and Israelachvili (1981) measured the effect of the hydrophobic force directly. Israelachvili and Pashley (1982) measured the interaction force between two crossed quartz cylinders rendered hydrophobic by a CTAB solution[2]. By subtracting the measured force from the sum of theoretical electrostatic and Van der Waals forces, they measured directly an additional force with exponential decay:

$$\frac{F}{r} = Ce^{\frac{-H}{D_0}}, \tag{3.27}$$

where r is the cylinder radius, C a constant ($\sim$0.14), and D_0 the decay length ($\sim$1 nm). It is important to note that Israelachvili and Pashley (1982) arrive at Eq.(3.27) by subtracting DLVO forces from the force measured experimentally. The rest term is then associated with the hydrophobic force, although it is not guaranteed at all that this excess term is general, nor that its origin is a single physico-chemical phenomenon. Nevertheless, the existence of the hydrophobic force has been widely accepted, although its origin is still not understood and formulations depend strongly on empirical fitting parameters (Mao, 1998; Butt et al., 2003, p. 107).

Xu and Yoon (1989, 1990) used Eq.(3.27) to extend the DLVO theory with an additional hydrophobic term. To fit data presented by Pashley et al. (1985), Eq.(3.27) was adjusted and fitted to experimental evidence (Pashley et al., 1985; Claesson et al., 1986; Tsao et al., 1991) of stronger hy-

[2]CetylTrimethylAmmonium Bromide (CTAB) is a cationic surfactant that is used to control the ζ-potential.

drophobic forces (Rabinovich and Yoon, 1994; Yoon and Ravishankar, 1996):

$$\frac{F}{r} = C_1 e^{\frac{-H}{D_1}} + C_2 e^{\frac{-H}{D_2}}, \tag{3.28}$$

where decay lengths D_1 and D_2 are ~1 nm and ~3-24 nm, respectively, and C_1 (≈10-40 mN/m) and C_2 (≈0.1-1.2 mN/m) are fitting parameters. Yoon and Ravishankar (1996) showed that Eq.(3.27) is valid for an advancing contact angle smaller than 90°, while Eq.(3.28) is suitable for advancing contact angles that exceed 90°. Yet another expression for the hydrophobic force is the so-called power law expression (Rabinovich and Yoon, 1994):

$$\frac{F}{r} = -\frac{K}{6H^2}, \tag{3.29}$$

where K is a fitting parameter. Experimental data rarely fits well with a quadratic decay, but Eq.(3.29) is mathematically much more convenient since it is simple and has only one parameter (Rabinovich and Yoon, 1994).

To write the total interaction potential, Eq.(3.21) in the form (Yotsumoto and Yoon, 1993):

$$V_{tot} = V_e + V_{vdW} + V_h, \tag{3.30}$$

where V_h is the hydrophobic interaction potential, one must integrate one of the Eqs.(3.27-3.29) as (Yoon and Mao, 1996):

$$V_h = -\tfrac{1}{2}\int_{\infty}^{H} F_h dH, \tag{3.31}$$

to yield (using Eq.(3.29):

$$V_h = -\frac{r_p r_b}{6\left(r_p + r_b\right)}\frac{K_{132}}{H}, \tag{3.32}$$

where K_{132} represents the kinetic interaction constant. Yoon and Mao (1996) compare K_{132} to A_{132} since Eq.(3.29) is of the same form as the non-retarded Van der Waals equation. It is furthermore instructive to point out that for the valid use of the integration in Eq.(3.31), one has to make at least the following assumptions:

1. the Derjaguin approximation holds,
2. the charge and field strength distribution with the boundary layer of

the bubble is uniform and constant,

3. the electrolyte concentration near the interface must be so low that the Poisson-Boltzmann equation can be linearised around the interface.

Assumption 1 was postulated by Derjaguin and Kusakov (1936), who assumed that the characteristic length of interaction is much smaller than the radius of the particles interacting. In essence, this is a flat plate approximation for the interacting surfaces. The Derjaguin approximation has of course its limitations, but it does allow for a first order approximation of the interaction (White, 1983) and to use the integration limit of infinity (White, 1983; Russel et al., 2001, p. 150), so that only the term in Eq.(3.31) remains after integration. In the interaction between flat plates, each point on one plate interacts with the entire other plate (Bhattacharjee and Elimelech, 1997; Bhattacharjee et al., 1998). The Derjaguin approximation, however, assumes that a unit surface area element only interacts with the corresponding unit surface area element on the opposite plate in surface perpendicular direction (Glendinning and Russel, 1983; White, 1983; Israelachvili, 1992, p. 161-164). The advantage of Derjaguin's approximation is that it allows us to split the interaction energy into a geometric parameter, R or $\frac{r_1 r_2}{(r_1+r_2)}$, and a set of parameters that reflect the material properties and distance (Butt et al., 2003, p. 95). The latter is derived from the thermodynamic properties of the intervening liquid film (Schulze, 1983, p. 78). The topic of the next section is therefore the thermodynamics of liquid films, in particular in relation to the so-called disjoining pressure.

3.8.3 Thermodynamic aspects of particle-interface forces

In an investigation of the adhesion of colloidal particles to interfaces, Derjaguin (1934) proposed that between particles and between particles and gas in liquid a thin layer of liquid existed. Due to the curvature of the interface, the pressure inside the liquid is higher than outside the liquid. Derjaguin (1934) referred to this effect as the "pressure defect". This result follows from Laplace's equation for pressure and is schematically depicted in Fig. 3.7a. Two years later, Derjaguin and Kusakov (1936) extrapolated this idea from capillarity between particles to a an excess pressure that exists within a thin liquid film between two interacting surface, schematically depicted in Fig. 3.7b.

Paulsen et al. (1996) derived an expression for the disjoining pressure as a function of separation distance h, surface surfactant concentration Γ, surface tension γ, Hamaker constant A, and hydrophobic force constant

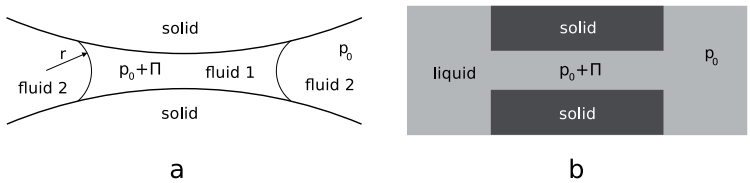

Figure 3.7. Schematic diagram of "pressure defect" between particle in a three-phase system (a) (after Derjaguin (1934)) and the disjoining pressure between solids in liquid (b) (Derjaguin and Kusakov, 1936) (after Butt et al. (2003, p. 96)).

K_s as:

$$P^* = -\frac{\partial^2 h^*}{\partial^2 x^{*2}}\left(1 + \frac{M\Gamma_0}{\gamma_0}\Gamma^*\right) - \frac{A^*}{h^{*3}} + K_s^* e^{-\frac{h^*}{d^*}}, \tag{3.33}$$

where:

$$P^* = \frac{P}{P_0} \tag{3.34}$$

$$P_0 = \frac{4\pi^2\gamma h_0}{\lambda^2} \tag{3.35}$$

$$h^* = \frac{h}{h_0} \tag{3.36}$$

$$x^* = \frac{x}{x_0} \tag{3.37}$$

$$d^* = \frac{d}{h_0} \tag{3.38}$$

$$M = \frac{\partial\gamma}{\partial\Gamma} \tag{3.39}$$

$$\Gamma^* = \frac{\Gamma}{\Gamma_0} \tag{3.40}$$

$$A^* = \frac{A\lambda^2}{\gamma k^2 h_0^2} \tag{3.41}$$

$$k = \frac{2\pi h_0}{\lambda} \tag{3.42}$$

$$K_s^* = \frac{K_s x_0^2}{\gamma h_0} \tag{3.43}$$

In Eqs.(3.35) and (3.42) λ is a characteristic length related to the wavelength of the perturbation. Derjaguin and Kusakov (1936) write the force to overcome the energy barrier and make attachment occur as the integral of disjoining pressure from infinity to the separation distance h:

$$F(h) = \int_h^\infty P(h)\, dh \tag{3.44}$$

Now, using a more complete formulation of the disjoining pressure, such as Eq.(3.33), we can integrate pressure to force. This force may be an

estimate for the attachment force between bubble and particle. To use Eq.(3.33) in Eq.(3.44), the disjoining pressure needs to be rewritten in a form that suits Eq.(3.44). Now, using the expression of Paulsen et al. (1996) for h^*:

$$h^* = \frac{h}{h_0} = 1 + \epsilon \cos x^*, \tag{3.45}$$

and working term by term in Eq.(3.33), $\frac{\partial^2 h^*}{\partial^2 x^{*2}}$ can be written as:

$$\begin{aligned} \frac{\partial^2 h^*}{\partial^2 x^{*2}} &= \frac{\partial^2}{\partial^2 x^{*2}} \left(1 + \epsilon \cos x^*\right) \\ &= -\epsilon \cos x^* \\ &= 1 - \frac{h}{h_0} \end{aligned} \tag{3.46}$$

$$\tag{3.47}$$

Using Eqs.(3.34-3.43) and (3.46), we can rewrite Eq.(3.33) as:

$$P\left(h, \lambda\right) = \left(1 - \frac{h}{h_0}\right)\left(1 - \frac{RT\Gamma_\infty}{\left(\Gamma_\infty - \Gamma\right)}\frac{\Gamma}{\gamma_0}\right) - \frac{A\lambda^2}{4\pi^2\gamma h_0 h^3} + \frac{K_s\lambda^2}{4\pi^2\gamma d}e^{-\frac{h}{d}}, \tag{3.48}$$

where Langmuir's equation of state:

$$\gamma = \gamma_0 + RT\Gamma_\infty \ln\left(1 - \frac{\Gamma}{\Gamma_\infty}\right) \tag{3.49}$$

was used to determine M in Eq.(3.39). Eq.(3.48) can be integrated in accordance with Eq.(3.44) as:

$$\begin{aligned} F\left(h, \lambda\right) &= \int_h^\infty P\left(h, \lambda\right) dh \\ &= \left[\left(h - \frac{h^2}{2h_0}\right)\left(1 - \frac{RT\Gamma_\infty}{\left(\Gamma_\infty - \Gamma\right)}\frac{\Gamma}{\gamma_0}\right) - \frac{A\lambda^2}{8\pi^2\gamma h_0 h^2} + \frac{K_s\lambda^2}{4\pi^2\gamma d^2}e^{-\frac{h}{d}}\right]_h^\infty \end{aligned} \tag{3.50}$$

The difficulty with Eq.(3.50) lies in the fact that the upper limit for integration is divergent in this formulation. The reason is the term $1 - \frac{h}{h_0}$ from Eq.(3.45), where film rupture is artificially triggered by perturbing the thinning film. The use of Eq.(3.45) and the physical consequences for Eq.(3.50) need further study. In this work, let us use a modified version of Eq.(3.30), outlined in Nguyen and Schulze (2004, Ch. 16). The interaction between spheres is often modelled using a linearisation of the Poisson-Boltzmann equation, the analytical solution of which is cumbersome to use (Adamczyk and Weroński, 1999). An approximate solution to

the problem by McCartney and Levine (1969) was extended by Bell et al. (1970) and Sader et al. (1995) for dissimilar spheres. Following the non-linear superposition approximation of Sader et al. (1995) one can write the electrostatic interaction force as (Nguyen and Schulze, 2004, p. 340):

$$\begin{aligned} F_e\left(h\right) =& 64\pi\tilde{R}\varepsilon\varepsilon_0\kappa\left(\frac{k_BT}{ez}\right) \\ & \tanh^{-1}\left[e^{-\kappa h/2}\tanh\left(\frac{ez\Psi_p}{4k_BT}\right)\right] \\ & \tanh^{-1}\left[e^{-\kappa h/2}\tanh\left(\frac{ez\Psi_b}{4k_BT}\right)\right], \end{aligned} \tag{3.51}$$

where

$$\tilde{R} = \frac{r_p r_b}{r_p + r_b}. \tag{3.52}$$

Now, by dividing Eqs.(3.25) and (3.32) by $\tilde{R}$, Eq.(3.52), the Van der Waals and hydrophobic forces are recovered from the respective potentials:

$$F_{vdW}\left(h\right) = \frac{V_{vdW}}{\tilde{R}} = -\frac{A_{132}}{6H}\left[1 - \frac{1+2bl}{1+\frac{bc}{H}}\right] \tag{3.53}$$

and

$$F_h\left(h\right) = \frac{V_h}{\tilde{R}} = -\frac{K_{132}}{6h}. \tag{3.54}$$

The total force between a particle and a bubble surface is the sum of Eqs.(3.51-3.54).

The forces in Eqs.(3.51-3.54) are dependent on the distance between particle and bubble surface. To implement Eqs.(3.51-3.54) as particle forces within the VOF framework, the particle-interface force can be modelled as (Wierink et al., 2011):

$$\mathbf{F}_a \propto -\hat{\mathbf{n}} f\left(\alpha\right) F_a, \tag{3.55}$$

where

$$\hat{\mathbf{n}} = \frac{\nabla\alpha}{|\nabla\alpha|}, \tag{3.56}$$

and

$$F_a = F_e + F_{vdW} + F_h. \tag{3.57}$$

Function $f(\alpha)$ determines the correct sign of $\mathbf{F}_a$ on each side of the gas-liquid interface. For $f(\alpha)$ it is convenient to use a hyperbolic tangent, since this function is smooth and switches signs on each side of a centred value. In addition, many electrostatic problem are also hyperbolic in nature. When a quadratic hyperbolic tangent is used Eq.(3.57) can be distributed smoothly around the gas-liquid interface and the particle experiences a weak equilibrium when captured in the centre of the interface. Therefore, $f(\alpha)$ is chosen to be of the form:

$$f(\alpha) = \left(\tanh^2\left[\lambda_\alpha(\alpha - \tilde{\alpha})\right] - \tanh^4\left[\lambda_\alpha(\alpha - \tilde{\alpha})\right]\right), \tag{3.58}$$

where $\tilde{\alpha}$ is the centre value of the interface, chosen to be α = 0.5, and λ_α is a parameter to control the decay of the force away from the interface.

Eq.(3.57) only applies when a particle approaches a gas-liquid interface closely. Upon film rupture wetting forces come into play. For a silica particle approaching an air bubble in water, Englert et al. (2009) found a force maximum of around 1 mN/m just before film rupture. Choosing λ_α = 25 mimics this behaviour, albeit artificially. At film rupture, however, Eq.(3.57) breaks down. The critical distance at which rupture likely occurs is the critical film thickness. In this work a formulation of Scheludko (1962) is used for the critical film thickness h_{crit}:

$$h_{crit} = \left(\frac{A\lambda^2}{128\pi\gamma}\right)^{1/4} \tag{3.59}$$

An important assumption behind Eq.(3.59) is that the bubble surface is not strongly retarded (Manev and Nguyen, 2005). However, even under condition with high surfactant concentrations, Eq.(3.59) is considered a fairly good approximation (Schulze, 1983, p. 113). Scaling the valid interval of Eq.(3.57) by Eq.(3.59) is physically artificial, but it does allow for coupling of Eq.(3.57) with the equation of state, e.g. Eq.(3.49), and a non-uniform distribution of surfactant concentration in time and space.

Before F_a can be computed by Eq.(3.57), physico-chemical properties that describe the state of the system must be provided. Fielden et al. (1996) and Englert et al. (2009) investigated particle-bubble forces experimentally and found the quantities presented in Table 3.1 in good agreement with their observations. Englert et al. (2009) also provide a value for

the bubble surface potential Ψ_b, but using this static value would defeat the purpose of including non-uniform surfactant distribution and dynamic surface tension. Dukhin et al. (2002, p. 248) provide an approximation for the bubble surface potential as:

$$\Psi_b(\Gamma) \approx -\frac{k_B T}{e}\frac{2}{z^+}\ln\left(\frac{z\kappa\Gamma}{2z^+C_0^+}\right), \tag{3.60}$$

where e is the unit electron charge, z and z^+ are the valence of the dissociated species, and C_0^+ is the surfactant concentration in the bulk directly at the bubble surface, equivalent to C_Γ in Eq.(3.15). With Eq.(3.60) it is assumed that there is an equilibrium between surface adsorption and bulk concentration immediately next to the surface and that the surface surfactant layer is an infinitely thin mono-layer ($\kappa\delta_D \ll 1$, with δ_D the diffusion layer thickness) (Dukhin et al., 2002, p. 243). A more serious limitation to the use of Eq.(3.60) is that it must be assumed that surface charge obeys a Boltzmann distribution (see e.g. Masliyah and Bhattacharjee (2006, Ch. 6)) and is smeared out over the entire bubble surface (Dukhin et al., 2002, p. 243). Despite these severe limitations, Eq.(3.60) seems a better option than a static value for Ψ_b so that also F_e of Eq.(3.51) varies with Γ. Fig. 3.8 shows the magnitude of the force according to Eq.(3.57) when using Eq.(3.58) as scaling factor.

Table 3.1. Physical properties needed in Eqs.(3.51) and (3.53), as found by Fielden et al. (1996) and Englert et al. (2009) for the air-water-silica system in $5.8\cdot10^{-5}$ M KCl solution.

Property	Value	Description
Ψ_p	$-100\cdot10^{-3}$ V	Particle surface potential
Ψ_b	$-34\cdot10^{-3}$ V	Particle surface potential
A	$-1\cdot10^{-20}$ J	Hamaker constant
κ^{-1}	$40\cdot10^{-9}$ m	Inverse Debye length
ε	78.4	Dielectric constant of liquid

3.9 Numerical solution method

3.9.1 Pressure-velocity coupling

Solution of the momentum equation, Eq.(3.3), is challenging because of two reasons. The first difficulty lies in the fact that the convective term in Eq.(3.3) is non-linear and needs to be solved by iteration. The second and greater difficulty is that the pressure field, which is one of the source

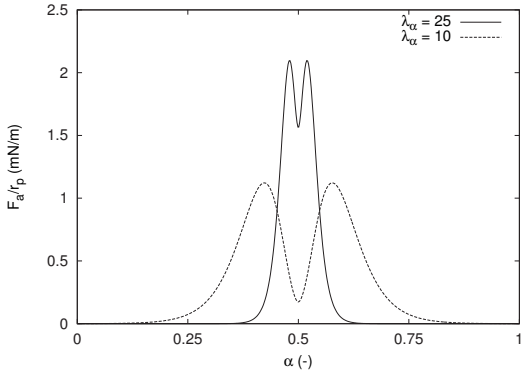

Figure 3.8. Magnitude of the particle-interface force, Eq.(3.55). The gas-liquid interface is assumed to be at α = 0.5 for two values of λ_α. In this study λ_α is chosen to be 25.

terms in the Navier-Stokes equation, is not known a priori. The pressure field is indirectly included when the continuity equation, Eq.(3.1) is satisfied. This, however, is only useful when using an simultaneous solution method. (Patankar (1980, p. 113-114); Ferziger and Peric (2002, p. 167)) Simultaneous solution of the inter-linked pressure-velocity system of equations is possible, but expensive in terms of computer memory (Ubbink, 1997). As CFD is a memory intensive type of simulation already, it is in many cases more efficient to choose an iterative solution procedure. There are several iterative techniques available, of which the Pressure Implicit with Splitting of Operators (PISO) (Issa, 1986) and the Semi-Implicit Method for Pressure-Linked Equations (SIMPLE) (Patankar and Spalding, 1972) are typically used in OpenFOAM® solvers (OpenCFD Ltd., 2011c, p. U-125). The SIMPLE algorithm is commonly used for steady-state problems, while the PISO algorithm is more appropriate for transient cases. In the VOF solver used in this work, the PISO algorithm was already implemented. The following is a short outline of the PISO algorithm as implemented in OpenFOAM®.

Discretisation of the momentum equation, Eq.(3.3), results in the following linear system (Weller, 2007):

$$[\![\mathcal{M}\,[\mathbf{U}]]\!] = -\nabla p, \tag{3.61}$$

where $[\![\mathcal{M}\,[\mathbf{U}]]\!]$ contains diagonal and off-diagonal coefficients, implicit source terms, and time derivatives. The momentum matrix, the LHS of Eq.(3.61), can be decomposed into diagonal and off-diagonal components. Eq.(3.61) is the momentum predictor equation and is solved for $\mathbf{U}$. The decomposed matrix equation is of the form:

$$[\![\mathcal{M}[\mathbf{U}]]\!] \rightarrow A\mathbf{U} - \mathbf{H}(\mathbf{U}), \tag{3.62}$$

where A is a matrix of diagonal components and $\mathbf{H}$ the so-called H-operator, containing the off-diagonal components. Combining Eqs.(3.61) and (3.62) and rearranging gives:

$$A\mathbf{U} = \mathbf{H}(\mathbf{U}) - \nabla p, \tag{3.63}$$

or,

$$\mathbf{U} = \frac{\mathbf{H}}{A} - \frac{1}{A}\nabla p. \tag{3.64}$$

By interpolating Eq.(3.64) onto cell faces the face flux ϕ is obtained as:

$$\phi = \left(\frac{\mathbf{H}}{A}\right)_f \cdot \mathbf{S}_f - \left(\frac{1}{A}\right)_f \nabla_f p, \tag{3.65}$$

where $\mathbf{S}_f$ is the face area vector. Mass continuity can now be enforced by setting the divergence of the face flux to zero, i.e. a face based continuity equation. After rearranging we obtain (Weller, 2007):

$$[\![\nabla \cdot \left(\frac{1}{A}\right)_f \nabla_f p]\!] = \nabla \cdot \left[\left(\frac{\mathbf{H}}{A}\right)_f \cdot \mathbf{S}_f\right], \tag{3.66}$$

which is called the pressure correction equation (Versteeg and Malalasekra, 2007, p. 188). The corrected pressure is fed back to the flux corrector equation, Eq.(3.65), and the momentum corrector equation, Eq.(3.64), until convergence is reached (Weller, 2007).

3.9.2 Discretisation

The OpenFOAM (OpenCFD Ltd., 2011a) code uses finite volume discretisation (OpenCFD Ltd., 2011c) on a co-located grid. Fig. 3.9 shows an example of two polyhedral cells with cell centres P and N. Fluxes between cell centres are calculated across the cell faces, where two cell centres only share a single face. In Fig. 3.9, $\mathbf{S}_f$ is the face area vector and its magnitude is proportional to the area of the face.

In the finite volume (FV) method, the discretised differential equations are integrated over each control volume (Patankar, 1980, p. 30). For values of quantity ϕ in a computational cell with centre P the volume integral

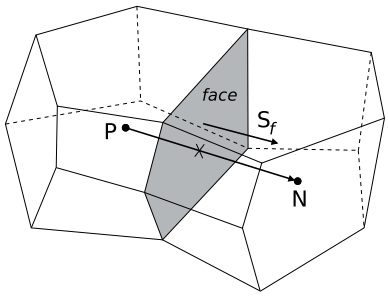

Figure 3.9. Spatial discretisation showing two control volumes with cell centres N and P. $\mathbf{S}_f$ is the face area vector (drawn after (OpenCFD Ltd., 2011b, p. 30)).

can be written as (Versteeg and Malalasekra, 2007, p. 244):

$$\int_V \phi dV = \phi_P V_P \tag{3.67}$$

The volume integrals of spatial derivatives can be approximated by a surface integral over the cell faces, according to Gauss' theorem (OpenCFD Ltd., 2011b, p. 36):

$$\int_V \nabla \star \phi dV = \int_S d\mathbf{S} \star \phi, \tag{3.68}$$

where $\star$ represents the inner, outer, or cross product of tensor field ϕ, and $\mathbf{S}$ is the surface area vector. The surface integral on the RHS of Eq.(3.68) is integrated and linearised by the sum of face integral fluxes as (OpenCFD Ltd., 2011b, p. 38):

$$\begin{aligned} \int_V \nabla \star \phi dV &= \int_S d\mathbf{S} \star \phi \\ &\approx \sum_f \mathbf{S}_f \star \phi_f \\ &= \sum_f |\mathbf{S}_f| \cdot \mathbf{n}_f \star \phi_f, \end{aligned} \tag{3.69}$$

where f refers to cell face values. All spatial derivatives are discretised according to Eq.(3.69).

For FV discretisation of transient flow problem the PDEs need not only be integrated over volume, but also over time (Versteeg and Malalasekra, 2007, p. 244). That is, the discretised equations in the form of Eq.(3.69) are also integrated over discrete time. In the work presented here the standard Euler time discretisation scheme available in OpenFOAM® was used. The first time derivative is discretised as (OpenCFD Ltd., 2011b,

p. 42):

$$\frac{\partial}{\partial t}\int_V \rho\phi_P dV = \frac{(\rho_P\phi_P V)^n - (\rho_P\phi_P V)^o}{\Delta t}, \tag{3.70}$$

where index P denotes the cell centre value, as depicted in Fig. 3.9, and superscripts n and o denote new and old values, respectively. A transient PDE in discretised form can be written as:

$$\int_t^{t+\Delta t}\left[\frac{\partial}{\partial t}\int_V \rho\phi dV + \int_V \nabla \star \rho\phi dV\right] dt = 0 \tag{3.71}$$

The temporal derivative in Eq.(3.71) can be discretised using the explicit Eulerian, implicit Eulerian, or a blended method, such as Crank-Nicholson. In the work presented here the implicit Euler scheme is used and the temporal and spatial discretised derivatives are respectively:

$$\begin{aligned}\int_t^{t+\Delta t}\left[\frac{\partial}{\partial t}\int_V \rho\phi dV\right] dt &= \int_t^{t+\Delta t}\frac{(\rho_P\phi_P V)^n - (\rho_P\phi_P V)^o}{\Delta t} dt \\ &= \frac{(\rho_P\phi_P V)^n - (\rho_P\phi_P V)^o}{\Delta t}\Delta t\end{aligned} \tag{3.72}$$

and

$$\begin{aligned}\int_t^{t+\Delta t}\left[\int_V \nabla \star \rho\phi dV\right] dt &= \int_t^{t+\Delta t}(\nabla \star \rho\phi dV)^* \, dt \\ &= (\nabla \star \rho\phi^n dV)^* \, \Delta t,\end{aligned} \tag{3.73}$$

where superscript * denotes the spatially discretised form. The Eulerian discretisation scheme presented above is implicit, first order accurate in time, and guarantees boundedness. (OpenCFD Ltd., 2011b, p. 39-42)

4. Simulation of bubble-particle interaction

This chapter is an overview of a test case for coupled CFD-DEM simulation of bubble-particle interaction. The aim of this case is to demonstrate the capabilities of the method presented in this work and to show that fully coupled simulation is feasible and can generate useful data for model development and validation.

4.1 Case setup

The test case featured in this Section consists of a cubical domain where an air bubble is initialised in the lower half and a cloud of particles in the upper half of the domain. Fig. 4.1 shows a frontal view of the computational domain. As a rule of thumb the bubble-wall distance is commonly set as 6 or more bubble diameters, i.e. the domain is minimum 13 bubble diameters wide. Lakshmanan and Ehrhard (2010) and Lakshmanan et al. (2011), however, showed in a comparable study of bubble rise velocity that for a domain width larger than 5 bubble diameters the bubble dynamics are similar. Wall effects were only observed for a domain smaller than 5 bubble diameters. Therefore, in the work presented here, a domain of $5\times5\times5$ bubble diameters was chosen. It is however not clear whether the presence of solid particles can enhance wall effects. The effects of bubble-particle dynamics and particle volume displacement needs further study.

This test case consists of a cubical of $5\times5\times5$ mm filled with water and a 1 mm air bubble, as shown in Fig. 4.1. The bubble centre is 1 mm above the bottom of the domain. A cloud of 1000 randomly placed particles is initialised within a cylinder between 1.5 and 3 mm above the bottom of the domain. The cylindrical particle injection area is aligned with the z-axis and has a diameter of 2 mm. The liquid density is 1000 kg/m^3, gas density is 1 kg/m^3, and the solid particles have a density of 3000 kg/m^3. The gravitational field points in the negative z-direction.

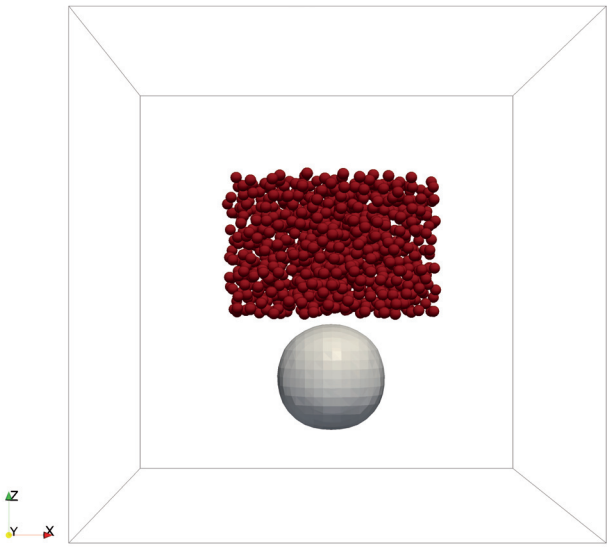

Figure 4.1. View of the case setup. The computational domain is $5\times5\times5$ bubble diameters with a static orthogonal mesh of $100\times100\times100$ cells. A single bubble of 1 mm in diameter interacts with 1000 particles of 50 μm in diameter. The material densities for water, gas, and solid are 1000, 1, and 3000 kg/m^3, respectively. The direction of the gravitational field is in the negative z-direction.

The boundary conditions for the case are summarised in Table 4.1. At the bottom patch, a Dirichlet boundary condition is imposed on pressure and a boundary condition of Neumann type on the velocity. For the sides and top of the domain a Dirichlet boundary condition is imposed on velocity, while for pressure the so-called "buoyantPressure" boundary condition is used. The buoyantPressure boundary condition is a condition of Neumann type, where the face normal gradient is fixed at hydrostatic pressure. The boundary conditions for the phase fraction α are mixed Dirichlet-Neumann conditions, named "inletOutlet" in OpenFOAM®, at the bottom and "outletInlet" at the other patches. These boundary conditions switch between Dirichlet and Neumann type depending on the sign of the flux ϕ. In the summary in Table 4.1, a positive flux refers to a flux into the domain.

The fixed time step in the simulation is $1\cdot10^{-5}$ s and the maximum Courant number around 0.4. The CFD-DEM coupled simulation was performed on a 1 million cell orthogonal mesh. The simulation time was approximately 1332 hrs of wall clock time per second of simulated time on an Intel Quad-Core Q9550 2.83 GHz CPU with 8 Gb of DIMM on a 64 bit system. The software versions used are OpenFOAM-2.0.x and CFDEM 2.1.0.

Table 4.1. Summary of boundary conditions. "Bottom patch" refers to the bottom of the domain in Fig. 4.1, while "Other patches" refers to the sides and top of the domain. Here, flux ϕ is positive when pointing into the domain.

Field	Bottom patch	Other patches
U	$\nabla_n \mathbf{U} = 0$	U = (0 0 0)
p	p = 0	$\nabla_n p = \rho\,(\mathbf{n} \cdot \mathbf{g})$
α	$\phi \geqslant 0 \rightarrow \alpha = 1$	$\phi \geqslant 0 \rightarrow \nabla_n \alpha = 0$
	$\phi < 0 \rightarrow \nabla_n \alpha = 0$	$\phi < 0 \rightarrow \alpha = 1$

Table 4.2. Physical properties and their values used in the bubble-particle interaction simulation.

Property	Value	Unit	Description
$\mathcal{D}_b$	$2.7 \cdot 10^{-10}$	m^2/s	Bulk surfactant diffusivity
$\mathcal{D}_s$	$1 \cdot 10^{-9}$	m^2/s	Surface surfactant diffusivity
k_a	$5 \cdot 10^{-5}$	m/s	Surfactant adsorption coefficient
k_d	$5 \cdot 10^{-5}$	s^{-1}	Surfactant desorption coefficient
Γ_∞	$5 \cdot 10^{-5}$	mol m^{-2}	Maximum surface surfactant concentration
$C_{b,max}$	$5 \cdot 10^{-3}$	mol m^{-3}	Maximum surfactant bulk concentration
ρ_p	3000	kg m^{-3}	Particle density
d_p	$50 \cdot 10^{-6}$	m	Particle diameter
T	293.15	K	Temperature
σ_0	0.072	kg s^{-2}	Clean water-air surface tension

4.2 Discussion of results

4.2.1 Estimate of model accuracy

The accuracy of the method used to capture the gas-liquid interface can be assessed by comparing the pressure jump across the interface with an analytical solution. Brackbill et al. (1992) compared the pressure jump across the interface of a droplet with the result of the Young-Laplace equation for an incompressible system in zero gravity. In their numerical experiment surface tension is kept constant. Under these conditions the surface stress boundary condition reduces to the Young-Laplace equation (Landau and Lifshitz, 1987, p. 106-108) for "surface pressure" p_s as:

$$p_s \equiv p_2 - p_1 = \gamma\kappa, \tag{4.1}$$

where κ is the interface curvature and p_1 and p_2 are the pressure outside and inside the drop, respectively. The comparison of the numerical calculation of surface pressure to the analytical value of Eq.(4.1), is proportional to the accuracy of the interfacial curvature calculation (Brackbill

et al., 1992). As a test case Brackbill et al. (1992) used a two-dimensional drop of 4 cm in diameter, centred in a square numerical domain of 6 by 6 cm. The mesh resolution is 60 by 60 cells, drop density is 1000 kg/m^3, background density is 500 kg/m^3, and surface tension is constant at 0.02361 N/m.

Under these conditions the pressure jump condition can be estimated by:

$$p_s = \gamma\kappa \equiv \frac{\gamma}{r_d}, \tag{4.2}$$

where r_d is the drop radius in 2D. In 3D the RHS of Eq.(4.2) is $\frac{\sigma}{r_{d,1}+r_{d,2}}$, with $r_{d,1}$ and $r_{d,2}$ the primary and secondary radii of curvature. Using the above material properties, the pressure jump across the droplet is 1.1805 Pa for the 2D case and 2.3610 Pa for the 3D case. Brackbill et al. (1992) computed the mean drop pressure by:

$$\langle p \rangle = \frac{1}{N_d} \sum_{i,j=1}^{N_d} p_{i,j}, \tag{4.3}$$

for computational cells (i,j). The number of "drop cells" N_d is defined as the number of cells for which $\rho \geqslant 990$ kg/m^3. Fig 4.2 shows $\langle p \rangle / p_s$ for the 2D Brackbill et al. (1992) test case, a 3D version, and results of the same test for a 1 mm air bubble in water. For all three cases the accuracy is between 0.75 and 0.8. This accuracy is not particularly high, however, Brackbill et al. (1992) and Ubbink (1997) reported similar results for curvature. The inaccuracy is likely related to the principle drawback of the VOF method for surface tension dominated flows. High local curvature can result in so-called parasitic currents (Lafaurie et al., 1994), which are shown in Fig. 4.3 for the 2D Brackbill test case. Parasitic currents are caused by an error in the continuous surface force model, giving rise to unphysical fluctuations in the pressure and velocity fields (Vincent and Caltagirone, 2003; Harvie et al., 2008). Parasitic currents increase in magnitude with increasing surface tension and with decreasing viscosity (Ubbink, 1997). For a Morton number lower than about 10^{-7} parasitic currents become significant and thus great care must be taken in the modelling of small bubbles (Tomiyama et al., 1993). For such small Morton number the interfacial force balance becomes independent of viscous effects (White and Beardmore, 1962) and surface tension dominates. Therefore, reduction of the discretisation error of the gradient operator associated with grid anisotropy is key in an accurate surface tension and curvature calculation. Preliminary tests of a numerical scheme that reduces the effect of grid anisotropy have shown promising results, but this is beyond the scope of this thesis. However, accurate calculation of curvature can reduce the influence of parasitic currents in the VOF method and improve accuracy for the type of modelling presented here.

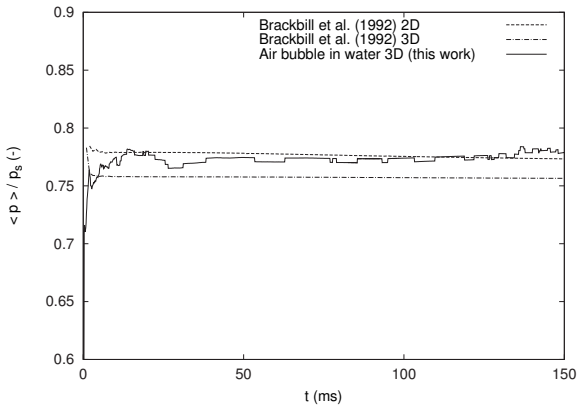

Figure 4.2. Result of the droplet surface pressure test Brackbill et al. (1992) for computed mean drop pressure $\langle p \rangle$ in Eq.(4.3) and analytical surface pressure p_s according to the Young-Laplace equation.

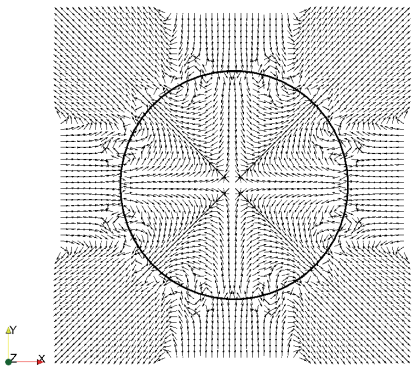

Figure 4.3. Parasitic currents in and around the drop of the 2D test case of Brackbill et al. (1992) using the VOF method. The drop density is 1000 kg/m^3, the background density is 500 kg/m^3, the surface tension is 0.02361 N/m, the drop diameter is 4 cm, the domain diameter is 6 cm squared, and computational mesh consists of 60×60 cells.

4.2.2 Surfactant adsorption-desorption dynamics

Recent experimental results (Javór et al., 2010; Omelka et al., 2010) show the importance of including adsorption-desorption dynamics in the modelling of bubble-particle interaction. As mentioned in Section 4.2.1, the dynamics of small bubbles with low Morton number are surface tension dominated. In systems characterised by a heterogeneous distribution of surfactants it is therefore important to include adsorption and desorption of surfactant and the resulting Marangoni stress terms in the momentum equation. Alke and Bothe (2009), Lakshmanan and Ehrhard (2008), Lakshmanan and Ehrhard (2010), and Lakshmanan et al. (2011) studied the adsorption and desorption of surfactants on a gas-liquid interface, using the VOF method. Lakshmanan and Ehrhard (2010) validated their adsorption-desorption model against an analytical solution of the surfactant transport equation. For vanishing surface diffusivity, Lakshmanan and Ehrhard (2010) write their equivalent of Eq.(3.15) in a non-dimensional form as:

$$\Gamma' = \frac{k'_a}{k'_a + k'_d}\left[1 - e^{-\left((k'_a + k'_d)t'\right)}\right], \tag{4.4}$$

where

$$k'_a = \frac{2k_a C_\Gamma}{\kappa \Gamma_\infty U_0}, \tag{4.5}$$

$$k'_d = \frac{k_d}{\kappa \Gamma_\infty U_0}, \tag{4.6}$$

$$t' = \frac{t\kappa}{U_0}, \tag{4.7}$$

$$U_0 = \sqrt{\frac{g}{\kappa}}. \tag{4.8}$$

In Eqs.(4.5-4.8) the bubble diameter used by Lakshmanan and Ehrhard (2010) is replaced by $\frac{2}{\kappa}$ to include bubble shape deformation due to Marangoni stress. Fig. 4.4 shows the non-dimensional surface surfactant concentration Γ' over non-dimensional time for the analytical solution and simulation results. The numerical solution fluctuates strongly around the analytical solution. The reason may be that the analytical solution does not take the motion of the interface into account. In addition, parasitic cur-

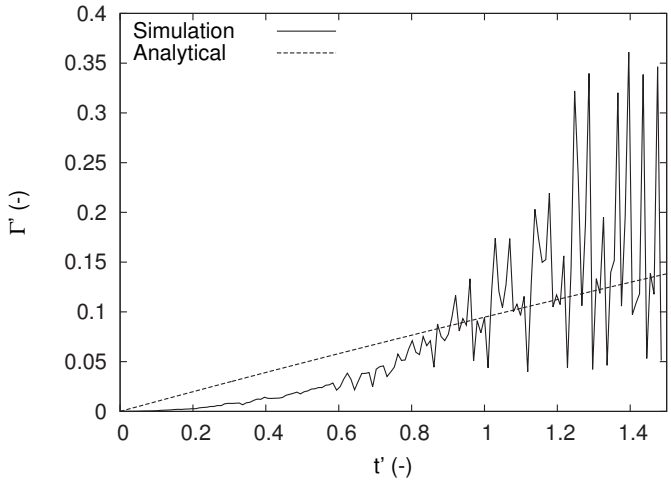

Figure 4.4. Dimensionless surface surfactant concentration versus dimensionless time. Comparison of simulation results and analytical solution of Lakshmanan and Ehrhard (2010).

rents likely cause an unphysical convective transport of surfactant near and at the interface.

The effect of surfactant dynamics on a system with buoyancy can be evaluated by comparing the rise velocity of a bubble. The computational domain is not large enough for the bubble to reach a steady-state terminal velocity, but a difference in rise velocity between a system with and without surfactants can be observed. There are many models to compute the terminal rise velocity of bubbles in pure systems and systems with various surfactants. These models however usually assume homogeneous distribution of surfactant and a static surface tension. The model presented in this work captures more dynamics and it is inevitable that values for rise velocity differ from steady-state models. However, the current models should arrive at the same order of magnitude and also display lower rise velocity for a system containing surfactants. One model including surface tension and liquid viscosity, fitted to experimental data, is that of Grace et al. (1976) (see also (Clift et al., 1978, p. 175-176)). Valid for Morton number $M < 10^{-3}$, Eötvös number $Eo < 40$, and $Re > 0.1$, Grace et al. (1976) write for the terminal rise velocity of bubbles coated by surfactant:

$$U_T = \frac{\mu_l}{\rho_l d_b} M^{-0.149} \left(J - 0.587\right), \tag{4.9}$$

where fitting parameter J is defined as[1]:

[1]Note that the original factor of $\left(\frac{4}{3}\right)^{0.757}$ is included in the prefactor 0.94 of Grace et al. (1976) and (Clift et al., 1978, p. 176), resulting in a prefactor of 1.17.

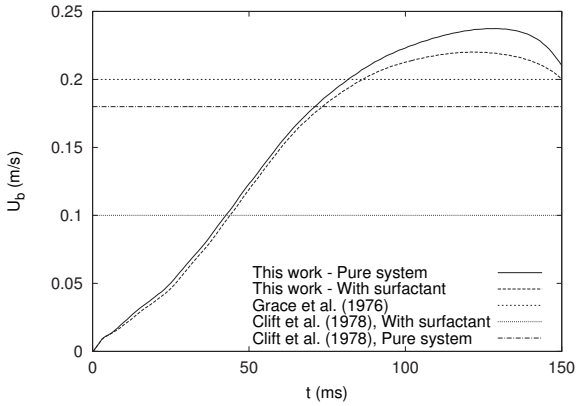

Figure 4.5. Bubble rise velocity versus time for a pure system and a system with surfactant, as computed using the model presented in this work. The results correlate well with the result of Eq.(4.9) of Grace et al. (1976). For reference the rise velocity of a 1 mm air bubble in water for a pure and contaminated system are also drawn, after Clift et al. (1978, Fig. 7.3, p. 172).

$$J = 1.17 \left[EoM^{-0.149} \left(\frac{\mu_g}{\mu_l} \right)^{-0.14} \right]^{0.757} . \tag{4.10}$$

In Eq.(4.10), Eo and M are defined as (Clift et al., 1978, p. 360-362):

$$Eo = \frac{g\left(\rho_l - \rho_g\right) d_b^2}{\sigma} \tag{4.11}$$

and

$$M = \frac{g\mu_l^4 \left(\rho_l - \rho_g\right)}{\rho_l^2 \sigma^3}. \tag{4.12}$$

Fig. 4.5 shows the bubble rise velocity as simulated using the model in this work, as well as values computed by Eq.(4.9) and the lower and upper limits of the experimental values summarised in Clift et al. (1978, Fig. 7.3, p. 172). The current model shows a bubble rise velocity in the same order of magnitude as experimental observations and also a lower rise velocity for a system with surfactants, compared to a pure system. The domain however is not large enough for the bubble to reach steady-state velocity. A thorough comparison with experimental work is needed for more conclusive validation.

The surface surfactant concentration Γ and the normalised surface surfactant concentration $X = \Gamma/\Gamma_\infty$ are shown in Fig. 4.6. The maximum surface surfactant concentration, after 15 ms, was $8.4 \cdot 10^{-6}$ mol·m^{-2}, or a

normalised surface concentration X of 0.16. The results shown in Fig. 4.6 are similar to those of Alke and Bothe (2009). The high adsorption rate cause a relatively high surface concentration of surfactant at the beginning of the simulation. When the bubble starts to rise up, convective transport of surfactant becomes more important and surfactant is swept to the downstream section of the bubble. These dynamics cause a slight change in rise velocity and bubble shape compared to the pure system. Between the left-most and right-most images in Fig. 4.6 a shift from a wider lower half of the bubble to a more spherical and stiffer bubble can be observed. Experimental data detailed enough for thorough quantitative comparison between model and experiment is to the knowledge of the author not yet available. The experimental work of Omelka et al. (2010) and Javór et al. (2010) focus on this area and may produce the data needed for a validation study.

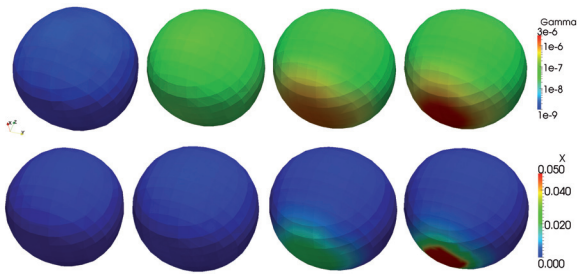

Figure 4.6. Surface surfactant concentration Γ in mol·m^{-2} (upper row) and normalised surface surfactant concentration $X = \Gamma/\Gamma_\infty$ (lower row) after 0, 5, 10, and 15 ms, respectively.

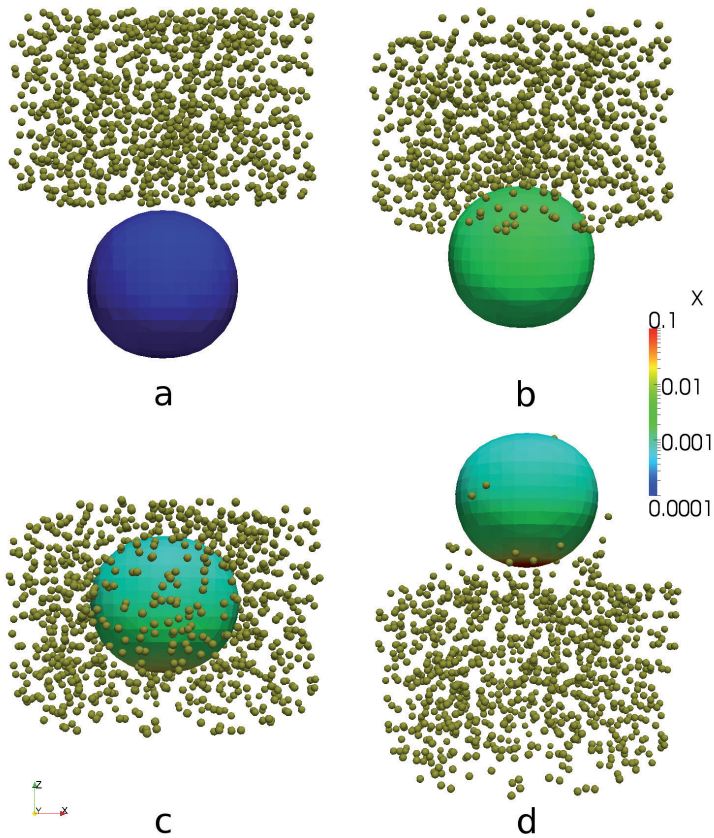

Figure 4.7. A 1 mm air bubble rising through a cloud of settling solid particles. The bubble is depicted by the 0.5 phase fraction contour (α=0.5). The colour on the surface of the bubble represents normalised surface surfactant concentration $X = \Gamma/\Gamma_\infty$. The snapshots are taken after 0 (a), 5 (b), 10 (c), 15 (d) ms.

4.2.3 Bubble-particle interaction

The result of a coupled CFD-DEM simulation of bubble-particle interaction is shown in Fig. 4.7. The material properties are discussed in Section 4.1 and Eq.(3.55) is used to compute the particle-interface force. The gas-liquid interface is shown as the α = 0.5 volume fraction contour and the contour is coloured by normalised surface surfactant concentration $X = \Gamma/\Gamma_\infty$. From top left to bottom right the 1 mm bubble adsorbs surfactant and rises through a cloud of settling particles.

Upon contact with the bubble surface, particles slide along the bubble surface, or rather through the interfacial layer. Some particles attach and detach from the surface, others just slide. Several particles remain attached to the bubble and rise to the free surface at the top of the domain. One would expect the bubble to capture more particles. However, the influence of particles within the interfacial layer likely changes the local surface

surfactant concentration and therefore the bubble surface potential and surface tension. Bubble capture behaviour in such a dynamic system is hard to predict. The effect of particle momentum on convective transport of surfactant on the surface of the particle is a phenomena of particular interest that is highlighted by this example simulation. In the current model rheological and non-Newtonian effects in the boundary layer of the surfactant-laden bubble are not included. However, it is evident that further development of the model in terms of interface rheology would be an interesting next step. Furthermore, it must be noted that the parameters listed in Table 4.2 are taken from literature and are somewhat arbitrary. A thorough validation study is needed to verify the results. Nevertheless, these results do show that modelling of bubble-particle interaction with full momentum coupling and physico-chemical coupling is feasible and can yield at least qualitatively promising results.

5. Summary and conclusions

This chapter concludes this thesis and consists of four sections. A concise summary of the chapters is followed by a statement on the significance of the work and an outlook on further development. Finally, conclusions are discussed.

5.1 Summary

Following an introduction to the topic in Chapter 1, current models of mineral froth flotation are reviewed in Chapter 2. There are reviews available in the literature, in particular on modelling of bubble-particle collision. However, rarely the assumptions behind the model and the original derivations are discussed. This has lead to a gradual stretching and extrapolation of flotation models to areas where many important modelling elements break down. Two key assumptions relate to the level of momentum coupling between phases and to the coupling of chemical potential and physical momentum.

Mineral froth flotation is a complex multiphase process where a wide range of spatial and temporal scales are important. The need to model the entire process has lead to a modelling strategy of an ideally mixed tank reactor where a reaction rate equation determines the outcome of the process. Commonly a first order rate constant is used and fit to experimental data. This is an effective way to model the wide range of scales involved, but important information is lost and flotation models typically apply to only one specific unit process. The development of the rate equation, applied to flotation modelling, flotation kinetics, and basic physicochemical aspects are discussed in Sections 2.1 and 2.2. If one accepts the approximation of an ideally mixed vessel that obeys a reaction rate equation of some kind, the challenge then is to formulate the flotation rate constant. In literature the flotation rate constant is typically constructed from a probability of flotation, which itself consists of the product of the probabilities of bubble-particle collision, attachment, and aggregate sta-

bility. Due to the complex interactions between dispersed bubble, particles, surfactants, and a typically turbulent flow field, simplified models for collision, attachment, and aggregate stability have been developed. The origin of these equations can be found in the modelling of a single hard sphere in laminar flow and modelling of other complex phenomena, such as rain droplet aggregation in clouds. Assumptions such as potential flow, fore and aft symmetry, and one-way momentum coupling may have been valid choices for the modelling of icing on cables, droplets in clouds, or a sphere in creeping flow. Extrapolation of these modelling elements to the field of three-phase, multi-component flow with high void fraction, however, requires great care. The assumptions and choices in original model development and their consequences for application to modelling of flotation are discussed in Chapter 2. A summary of the key assumptions, with regard to flotation modelling, is as follows:

- An air bubble is stiff and the flow around it is fore and aft symmetric, i.e. creeping flow around a hard sphere in an infinite domain.
- The exchange of momentum between phases is characterised by so-called one-way coupling. That is, the motion of the carrier phase influences the motion of the dispersed phases, but not vice versa.
- Particles are small enough to be described by massless points without volume displacement.
- The system is so dilute that the interaction between a single bubble and a single particle captures the key system dynamics. Particle-particle and bubble-bubble interaction are excluded.
- The stability of a bubble-particle aggregate can be described by the balance of forces in a mechanistic centrifugal system with the bubble at the centre of rotation. Turbulent eddies of the same size as the aggregate provide the centrifugal force field.
- The kinetic time scale of motion is so much shorter than the characteristic time scale of surfactant dynamics, that surface tension and contact angle can be assumed static in the model.
- There is no coupling between physical momentum and chemical potential. For example, coupling between transport of surfactants and surface potential is neglected.
- The chemical potential at the bubble surface is such that the Stern layer is thin, static, and symmetric, and surface charge distribution obeys a Boltzmann or Gouy-Chapman type distribution.
- Mineral froth flotation is an ideally mixed process that is described by a rate equation with a single, lumped rate constant.

The vast range of spatial and temporal scales involved in the flotation

process typically makes the above assumptions necessary for modelling of the process. For re-design of flotation equipment and significant changes in operating parameters, however, many of the assumptions listed remove important information from the model. For this reason it is instructive to develop a model that allows higher order coupling between the momenta of the different phases as well as the physico-chemical potential. The development of such a coupled model is the topic of Chapter 3.

The modelling method discussed in Chapter 3 allows for coupled simulation of three-phase systems in the presence of a soluble surfactant. The Volume Of Fluid (VOF) method is used to compute the motion of a bubble in a liquid domain using the finite volume (FV) approach. The motion of suspended solid particles is solved for in a separate model, using the Discrete Element Method (DEM). Particle and fluid motion are coupled through the exchange of a void fraction parameter and momentum between the FV and DEM codes. The CFD-DEM coupled code is part of an open source project named CFDEM, where the open source CFD code OpenFOAM and the DEM code LIGGGHTS are coupled through an MPI library. Particle-interface force is solved for as a function of gas-liquid phase fraction, chemical potential of the bubble surface, and the effect of adsorption-desorption dynamics of a soluble surfactant. Surface tension is computed from the surface surfactant concentration using Langmuir's equation of state.

Chapter 4 features an example of bubble-particle interaction as simulated by the model presented in this thesis. A 1 mm air bubble rises through a cloud of settling mineral particles. A basic adsorption-desorption model solves for the concentration of soluble surfactant at the bubble surface. The surface surfactant concentration changes local surface tension and contributes to the gas-liquid momentum equation via a Marangoni stress term. The VOF based modelling method also allows for topological changes, such as bubble break-up and coalescence and can be applied to a larger domain containing multiple bubbles and in the order of 10^4 particles.

5.2 Contribution and significance

The body of literature on modelling of bubble-particle interaction in mineral froth flotation is extensive. Significant progress has been made since the early insights gained around the middle of the previous century, but the fundamental background has not changed very much since then. To fully exploit current understanding of molecular dynamics, adsorption, hydrodynamics, as well as macroscopic process behaviour and computational power, a paradigm shift is needed in flotation modelling. The mod-

elling method presented in this thesis is the first of a new generation of models to study bubble-particle interaction with soluble surfactants. In this thesis three important features are addressed that are not found in flotation modelling in current literature. These features are full kinetic momentum coupling between phases, physico-chemical momentum coupling, and the ability to study dynamics of many sub-models combined. It is the first time that these three features are combined and can be used for a reasonable computational effort.

Modelling bubble-particle interaction with full momentum coupling means that results are valid over the entire range of surface-to-surface distance and Stokes numbers depicted in Fig. 3.1 on p. 55. Simulation results can therefore be generated reliably for many different flow regimes and void fractions. This capability is of key importance for consistent modelling of mineral froth flotation, in particular when applied to mechanically agitated flotation cells. The model in this thesis provides the possibility to study bubble-particle interaction in different zones of a flotation cell, both in the strongly turbulent rotor-stator area as well as in more laminar zones near to the froth.

The second feature of momentum coupling relates to the coupling between hydrodynamics and physico-chemistry. Hydrodynamics at the scale of a bubble swarm drives global convective transport of surfactant, while diffusion and the effects of sorption occur at macro-molecular scale. Nevertheless, hydrodynamics and physico-chemistry occupy the same space and time and are strongly coupled. Dynamic adsorption-desorption at a moving gas-liquid interface and the Marangoni effect are marked examples of such coupling. In addition to kinetic momentum coupling the model in this thesis also includes coupling between physico-chemistry and the momentum equation. This coupling is achieved by a simple but complete adsorption-desorption model, use of the equation of state to couple surfactant concentration and surface tension, and finally the addition of the Marangoni stress term to the two-phase momentum equations for the gas-liquid system. In this way adsorption-desorption of surfactant, bubble surface motion, liquid motion, and the motion of solid particles interact. For example, a solid particle can change the flow field near a bubble, in turn changing transport of soluble surfactant near and on the bubble surface. Change in surfactant concentration can lead to a Marangoni stress, which directly influences the local flow field and the motion of the particle. This example also illustrates the next key feature that make the model in this thesis unique in the field of flotation modelling.

The third important feature of the current model is the ability to combine several sub-models into a coupled simulation. The division of bubble-

particle interaction into sub-models has lead to separate development efforts and validation. From an experimental as well as theoretical point of view it is helpful to reduce and control the amount of variable studied and validated. However, the division into sub-models brings about an new degree of freedom in modelling. This additional degree of freedom is caused by the dynamic interaction between sub-models. The model in this thesis can be used to study the behaviour of sub-models, such as bubble-particle collision and attachment, in the context of the entire framework. Combinations of sub-models and sub-model reaction rates may have characteristic modes that may significantly change the dynamics of the system.

Finally, from a perspective of continued development the modelling framework possesses several useful features for modular and concurrent research. The framework uses the CFDEM modelling tool, where the CFD code OpenFOAM and the DEM code LIGGGHTS are coupled (see Section 3.4). OpenFOAM, LIGGGHTS, and CFDEM are open source codes using object orientated programming and MPI. The current modelling framework is modular and highly flexible. Advanced computational techniques and large scale parallel simulation make CFDEM a unique platform for concurrent and integral model development. The combination of kinetic momentum coupling, physico-chemical coupling, and a dynamic modelling platform can aid fast and efficient development in a feasible computational effort.

5.3 Outlook and recommendations

The model presented in this thesis can benefit from further development in several areas. The current model does not include a consistent implementation of a model for film rupture and induction time of three-phase contact line expansion. The consistent implementation of wetting forces and film rupture within the VOF framework needs to be considered for further development.

A major assumption is made with regard to rheology. Inherently it is assumed that the surfactant is inert, the solution is dilute, and diffusion is governed by a diffusion constant rather than an anisotropic tensor. In many practical cases there is more than one surfactant present, an effect that requires attention as well. In particular in flotation the interaction between surfactants, frothers, and fine solids is an interesting effect to incorporate. For higher concentration of surfactants and fine solids the diffusion tensor is likely to be anisotropic and surface viscosity may be non-Newtonian.

In the current model momentum between phases is coupled. However, at high void fraction also volume displacement of solids should be taken into account. Simulation on a more dense computational mesh allows for flow around particles to be resolved to some extent as well. This type of simulations can help to understand the thinning of the liquid film between bubble and particle. Finally, the DEM code used here can also be used to compute molecular dynamics (MD). Molecular dynamics simulation of a domain of the size presented in this thesis is not practical. However, the MD capabilities of the DEM code may be put to use by resolving MD locally during film rupture or other important processes at molecular scale.

The results presented in this thesis have been generated for a laminar system. Turbulence is an important factor in probabilistic collision kernels and aggregate stability models. Therefore, it would be useful to study bubble-particle dynamics under influence of an induced turbulence field. The computational domain is likely too large and the physics too complex to perform Direct Numerical Simulation (DNS). Reynolds-Averaged Navier-Stokes (RANS) simulation of the system would smear out some of the key dynamics and therefore Large Eddy Simulation (LES), possibly with partially resolved DEM, would be the most promising method to include the effect of turbulence.

5.4 Conclusions

This study should be regarded as a step towards coupled modelling of bubble-particle interaction. Physical and chemical momentum coupling are key elements of an integral model that can be used to further understand the fundamentals of bubble-particle interaction. The background for this work is the modelling of mineral froth flotation. However, it is not the main aim to develop a flotation model. Rather, it is the modelling framework in which the physical and physico-chemical aspects of bubble-particle interaction can be explored. The models discussed in Chapter 2 can often produce a good fit to experimental data. However, the range of validity of these models is typically narrow and extrapolation is not without risk. The modular and generic structure of the modelling framework presented in this thesis removes this rigidity and makes generalisation to some extent possible. For example, the Lagrangian particles are in fact dynamic lists that contain properties such as position, current time, and radius as attributes. Particle attributes can change over time and space, as well as interact with other fields. This flexible and modular property makes the framework a unique and powerful development platform. For example, the effects of activation, depression, and oxidation of mineral surfaces can be implemented in a fully coupled and consistent way. The

modelling framework shows promising first results. It is the hope of the author that the current modelling framework provides a test harness for theory and validation of both micro- and macro-scale processes. Bridging scales by meso-scale model development and validation can increase the value of fundamental knowledge for industrial practise and vice versa.

References

Abrahamson, J. (1975). Collision rates of small particles in a vigorously turbulent fluid. *Chem Eng Sci*, 30(11):1371–1379.

Adamczyk, Z. and Weroński, P. (1999). Application of the DLVO theory for particle deposition problems. *Adv Colloid Interf Sci*, 83(1-3):137–226.

Albijanic, B., Ozdemir, O., Nguyen, A. V., and Bradshaw, D. (2010). A review of induction and attachment times of wetting thin films between air bubbles and particles and its relevance in the separation of particles by flotation. *Adv Colloid Interf Sci*, 159(1):1–21.

Alke, A. and Bothe, D. (2009). 3D numerical modeling of soluble surfactant at fluidic interfaces based on the volume-of-fluid method. *Fluid Dynamics & Materials Processing*, 5(4):345–372.

Anfruns, J. P. and Kitchener, J. A. (1977). Rate of capture of small particles in flotation. *Trans IMM, Section C: Mineral Process Extract Metall*, 86:C9–C15.

Asimov, I. (1982). *Asimov's Biographical Encyclopedia of Science and Technology*. Doubleday, MI, USA, second rev edition.

Ata, S. (2009). The detachment of particles from coalescing bubble pairs. *J Colloid Interf Sci*, 338(2):558–565.

Bascur, O. A. (1982). *Modeling and computer control of a flotation cell*. PhD thesis, Univ Utah, Salt Lake City, Utah, USA.

Bell, G. M., Levine, S., and McCartney, L. N. (1970). Approximate methods of determining the double-layer free energy of interaction between two charged colloidal spheres. *J Colloid Interf Sci*, 33(3):335–359.

Bertrand, F., Leclaire, L.-A., and Levecque, G. (2005). DEM-based models for the mixing of granular materials. *Chem Eng Sci*, 60(8-9):2517–2531.

Bhattacharjee, S. and Elimelech, M. (1997). Surface element integration: A novel technique for evaluation of DLVO interaction between a particle and a flat plate. *J Colloid Interf Sci*, 193(2):273–285.

Bhattacharjee, S., Elimelech, M., and Borkovec, M. (1998). DLVO interaction between colloidal particles: Beyond Derjaguin's approximation. *Croatica Chemica Acta*, 71(4):883–903.

Bloom, F. and Heindel, T. J. (1997). Mathematical modelling of the flotation deinking process. *Mathl Comput Modelling*, 25(5):13–58.

Bloom, F. and Heindel, T. J. (2002). On the structure of collision and detachment frequencies in flotation models. *Chem Eng Sci*, 57(13):2467–2473.

Bloom, F. and Heindel, T. J. (2003). Modeling flotation separation in a semi-batch process. *Chem Eng Sci*, 58(2):353–365.

Bogdanov, O. S. and Filanovski, M. S. (1940). On the question of attachment of mineral particles to air bubbles (in Russian). *J Phys Chem*, 14(2):243–247.

Boström, M., Deniz, V., Franks, G. V., and Ninham, B. W. (2006). Extended DLVO theory: Electrostatic and non-electrostatic forces in oxide suspensions. *Adv Colloid Interf Sci*, 123-126:5–15.

Brackbill, J. U., Kothe, D. B., and Zemach, C. (1992). A continuum method for modelling surface tension. *J Comput Phys*, 100(2):335–354.

Butt, H.-J., Graf, K., and Kappl, M. (2003). *Physics and chemistry of interfaces*. Wiley-VCH, Weinheim, Germany.

Camp, T. R. and Stein, P. C. (1943). Velocity gradients and internal work in fluid motion. *J Boston Soc Civil Engrs*, 30(4):219–237.

Chanson, H. (2007). Le potentiel de vitesse pour les écoulements de fluides réels: La contribution de Joseph-Louis Lagrange. *La Houille Blanche*, 5:127–131.

Chapman, D. L. (1913). A contribution to the theory of electrocapillarity. *Philos Mag Series 6*, 25(148):475–481.

Claesson, P. M., Blom, C. E., Herder, P. C., and Ninham, B. W. (1986). Interactions between water-stable hydrophobic Langmuir-Blodgett monolayers on mica. *J Colloid Interf Sci*, 114(1):234–242.

Clift, R., Grace, J., and Weber, M. E. (1978). *Bubbles, drops, and particles*. Academic Press, New York.

Crawford, R. and Ralston, J. (1988). The influence of particle size and contact angle in mineral flotation. *Int J Miner Process*, 23(1-2):1–24.

Crowe, C., Sommerfeld, M., and Tsuji, Y. (1997). *Multiphase flows with droplets and particles*. CRC Press, New York.

Cuenot, B., Magnaudet, J., and Spennato, B. (1997). The effects of slightly soluble surfactants on the flow around a spherical bubble. *J Fluid Mech*, 339:25–53.

Cundall, P. A. and Strack, O. D. L. (1979). A discrete numerical model for granular assemblies. *Géotechnique*, 29(1):47–65.

Dai, Z., Dukhin, S., Fornasiero, D., and Ralston, J. (1998). The inertial hydrodynamic interaction of particles and rising bubbles with mobile surfaces. *J Colloid Interf Sci*, 197(2):275–292.

Dai, Z., Fornasiero, D., and Ralston, J. (1999). Particle-bubble attachment in mineral flotation. *J Colloid Interf Sci*, 217(1):70–76.

Dai, Z., Fornasiero, D., and Ralston, J. (2000). Particle-bubble collision models – a review. *Adv Colloid Interf Sci*, 85(2-3):231–256.

Derjaguin, B. (1934). Untersuchungen über die Reibung und Adhäsion, IV. Theorie des Anhaftens kleiner Teilchen. *Kolloid Z*, 69(2):155–164.

Derjaguin, B. V. and Dukhin, S. S. (1961). Theory of flotation of small and medium-size particles. *Trans Inst Min Metall*, 70:221–246.

Derjaguin, B. V. and Kusakov, M. M. (1936). Properties of thin layers of liquids and their effect on the interaction of solid surfaces (in Russian). *Proc USSR Acad Sci*, 5:741–753.

Derjaguin, B. V. and Landau, L. (1941). Theory of the stability of strongly charged lyophobic sols and of the adhesion of strongly charged particles in solutions of electrolytes. *Acta Phys Chim USSR*, 14:633–662.

Dobby, G. S. and Finch, J. A. (1986). A model of particle sliding time for flotation size bubbles. *J Colloid Interf Sci*, 109(2):493–498.

Dobby, G. S. and Finch, J. A. (1987). Particle size dependence in flotation derived from a fundamental model of the capture process. *Int J Miner Process*, 21(3-4):241–260.

Drumright-Clarke, M. A. and Renardy, Y. (2004). The effect of insoluble surfactant at dilute concentration on drop breakup under shear with inertia. *Phys Fluids*, 16(1):14–21.

Dukhin, S. (1982). The role of inertial forces in the flotation of small particles (in Russian). *Colloid J*, 44(3):431–441.

Dukhin, S. (1983). On the critical value of the Stokes number and the Sutherland formula (in Russian). *Colloid J*, 45(2):207–217.

Dukhin, S. S., Kretzschmar, G., and Miller, R. (2002). *Dynamics of adsorption at liquid interfaces: Theory, experiment, application*, volume 1 of *Studies in Interface Science*. Elsevier, Amsterdam.

Dukhin, S. S. and Rulev, N. N. (1977). Hydrodynamic interaction of a solid spherical particle bubble in a unit flotation act (in Russian). *Colloid J*, 39(2):270–275.

Elghobashi, S. (1991). Particle-laden turbulent flows: Direct simulation and closure models. *Appl Sci Res*, 48(3–4):301–314.

Englert, A. H., Krasowska, M., Fornasiero, D., Ralston, J., and Rubio, J. (2009). Interaction force between an air bubble and a hydrophilic spherical particle in water, measured by the colloid probe technique. *Int J Mineral Process*, 92(3–4):121–127.

Evans, L. F. (1954). Bubble-mineral attachment in flotation. *Ind Eng Chem*, 46(11):2420–2424.

Ferziger, J. H. and Peric, M. (2002). *Computational Methods for Fluid Mechanics*. Springer, Berlin, third rev. edition.

Fielden, M. L., Hayes, R. A., and Ralston, J. (1996). Surface and capillary forces affecting air bubble-particle interactions in aqueous electrolyte. *Langmuir*, 12(15):3721–3727.

Finch, J. A. and Dobby, G. S. (1990). *Column Flotation*. Pergamon Press, Oxford, UK.

Flint, L. R. and Howarth, W. J. (1971). The collision efficiency of small particles with spherical air bubbles. *Chem Eng Sci*, 26(8):155–1168.

Fuks, N. A. (1955). *Aerosol Mechanics (in Russian)*. Akad Nauk CCCP, Moscow.

Garcia Zuñiga, H. (1935). Flotation recovery is an exponential function of time (in Spanish). *Bol Minero Soc Nacl Min (Santiago)*, 47:83–86.

Gaudin, A. M. (1932). *Flotation*. McGraw-Hill, New York.

Gaudin, A. M. (1957). *Flotation*. McGraw-Hill, New York, 2nd edition.

Gidaspow, D., Bezburuah, R., and Ding, J. (1992). Hydrodynamics of Circulating Fluidized Beds, Kinetic Theory Approach. In *Proc. Fluidization VII, Proceedings of the 7th Engineering Foundation Conference on Fluidization*, pages 75–82.

Glembotskii, V. A., Klassen, V. I., and Plaksin, I. N. (1963). *Flotation*. Primary Sources, New York.

Glendinning, A. B. and Russel, W. B. (1983). The electrostatic repulsion between charged spheres from exact solutions to the linearized Poisson-Poltzmann equation. *J Colloid Interf Sci*, 93(1):95–104.

Goniva, C., Kloss, C., Hager, A., and Pirker, S. (2010). An Open Source CFD-DEM Perspective. In *Proc. 5th OpenFOAM workshop*, Chalmers University, Gothenburg, Sweden, June 21-24 2010.

Goniva, C., Kloss, C., Hager, A., Wierink, G., and Pirker, S. (2011). A multi-purpose open source CFD-DEM approach. In *Proc. 8th Int Conf CFD in the Oil & Gas, Metallurgical and Process Industries (CFD 2011)*, SINTEF/NTNU, Trondheim, Norway, 21-23 June 2011.

Gorain, B. K., Franzidis, J.-P., and Manlapig, E. V. (1995a). Studies on impeller type, impeller speed and air flow rate in an industrial scale flotation cell. Part 1. Effect on bubble size distribution. *Min Eng*, 8(6):615–635.

Gorain, B. K., Franzidis, J.-P., and Manlapig, E. V. (1995b). Studies on impeller type, impeller speed and air flow rate in an industrial scale flotation cell. Part 2. Effect on gas holdup. *Min Eng*, 8(12):1557–1570.

Gorain, B. K., Franzidis, J.-P., and Manlapig, E. V. (1996). Studies on impeller type, impeller speed and air flow rate in an industrial scale flotation cell. Part 3. Effect on superficial gas velocity. *Min Eng*, 9(6):639–654.

Gorain, B. K., Franzidis, J.-P., and Manlapig, E. V. (1999). The empirical prediction of bubble surface area flux in mechanical flotation cells from cell design and operating data. *Min Eng*, 12(3):309–322.

Gorain, B. K., Napier-Munn, T. J., Franzidis, J.-P., and Manlapig, E. V. (1998). Studies on impeller type, impeller speed and air flow rate in an industrial scale flotation cell. Part 5: Validation of $k - S_b$ relationship and effect of froth depth. *Min Eng*, 11(7):615–626.

Gouy, G. (1910). Sur la constitution de la charge á la surface d'un électrolyte. *J Phys*, 9:457–468.

Grace, J. R., Wairegi, T., and Nguyen, T. H. (1976). Shapes and velocities of single drops and bubbles moving freely through immiscible liquids. *Trans Inst Chem Eng*, 54:167–173.

Hadamard, J. S. (1911). Mouvement permanent lent d'une sphere liquide et visqueuse dans un liquide visqueux. *C R Acad Sci*, 152:1725–1738.

Hamaker, H. C. (1937). The London-Van der Waals attraction between spherical particles. *Physica*, 4(10):1058–1072.

Harvie, D. J. E., Rudman, M., and Davidson, M. R. (2008). Parasitic current generation in Combined Level Set and Volume of Fluid immiscible fluid simulations. In Read, W., Larson, J. W., and Roberts, A. J., editors, *Proc 13th Biennial Computational Techniques and Applications Conference, CTAC-2006*, volume 48 of *ANZIAM J*, pages C868–C884.

Herbst, J., Rajamani, R. K., Mular, A., and Flintoff, B. (2002). *Mineral processing plant/circuit simualtions: An overview*, volume 1 of *Mineral Processing Plant Design, Practice, and Control*, chapter 4 Models and simulations for selection, sizing, and design, pages 383–403. SME, Littleton, Colorado, USA.

Hirt, C. W. and Nichols, B. D. (1981). Volume of fluid (VOF) method for the dynamics of free boundaries. *J Comp Phys*, 39(1):201–225.

Hogg, R., Healy, T. W., and Fuerstenau, D. W. (1966). Mutual coagulation of colloidal dispersions. *Trans Faraday Soc*, 62:1638–1651.

Houstoun, R. (1925). *An introduction to mathematical physics*. Longmans Green, London.

Israelachvili, J. and Pashley, R. (1982). The hydrophobic interaction is long range, decaying exponentially with distance. *Nature*, 300(5890):341–342.

Israelachvili, J. N. (1992). *Intermolecular and surface forces*. Academic Press, London, second edition.

Issa, R. I. (1986). Solution of the implicitly discretised fluid flow equations by operator-splitting. *J Comp Phys*, 62(1):40–65.

James, A. J. and Lowengrub, J. (2004). A surfactant-conserving volume-of-fluid method for interfacial flows with insoluble surfactant. 201(2):685–722.

Jameson, G. J., Nam, S., and Young, M. M. (1977). Physical factors affecting recovery rates in flotation. *Min Sci Eng*, 9(3):103–118.

Javór, Z., Schreithofer, N., and Heiskanen, K. (2010). Fast adsorption phenomena at air/liquid interfaces. In *Proc. XXV Int Miner Process Congr (IMPC)*, Brisbane, Australia, September 6-10, 2010.

Jowett, A. (1980). Formation and disruption of particle-bubble aggregates in flotation. In Somasundaran, P., editor, *Proc Int Symp Fine Particle Processing*, pages 720–754, Vol. 1, Ch. 37, Las Vegas, USA, February 24-28.

Kloss, C., Goniva, C., Amberger, S., and Pirker, S. (2011). LIGGGHTS open source DEM: Models, features, parallelism and quality assurance. In *Proc. 8th Int Conf CFD in the Oil & Gas, Metallurgical and Process Industries (CFD 2011)*, SINTEF/NTNU, Trondheim, Norway, 21-23 June 2011.

Koh, P. T. L., Manickam, M., and Schwarz, M. P. (2000). CFD simulation of bubble-particle collisions in mineral flotation cells. *Min Eng*, 13(14-15):1455–1463.

Koh, P. T. L. and Schwarz, M. P. (2003). CFD modelling of bubble-particle collision rates and efficiencies in a flotation cell. *Min Eng*, 16(11):1055–1059.

Koh, P. T. L. and Schwarz, M. P. (2006). CFD modelling of bubble-particle attachments in flotation cells. *Min Eng*, 19(6-8):619–626.

Koh, P. T. L. and Schwarz, M. P. (2007). CFD model of a self-aerating flotation cell. *Int J Miner Process*, 85(1-3):16–24.

Krasowska, M. and Malysa, K. (2007). Wetting films in attachment of the colliding bubble. *Adv Colloid Interf Sci*, 134-135:138–150.

Lafaurie, B., Nardone, C., Scardovelli, R., Zaleski, S., and Zanetti, G. (1994). Modelling merging and fragmentation in multiphase flows with SURFER. *J Comp Phys*, 113(1):134–147.

Lakshmanan, P. and Ehrhard, P. (2008). Direct numerical simulation of single gas bubbles in pure and contaminated liquids. *Proc Appl Math Mech*, 8(1):10625–10626.

Lakshmanan, P. and Ehrhard, P. (2010). Marangoni effects caused by contaminants adsorbed on bubble surfaces. *J Fluid Mech*, 647(1):143–161.

Lakshmanan, P., Peters, F., Fries, N., and Ehrhard, P. (2011). Gas bubbles in simulation and experiment. *J Colloid Interface Sci*, 354(1):364–372.

Lamb, H. (1932). *Hydrodynamics*. Cambridge University Press, New York, 6th edition.

Landau, L. and Lifshitz, E. (1987). *Fluid Mechanics*, volume 6 of *Course of Theoretical Physics*. Pergamon Press, New York, second edition.

Langmuir, I. (1948). The production of rain by a chain reaction in cumulus clouds at temperatures above freezing. *J Meteorology*, 5(5):175–192.

Langmuir, I. and Blodgett, K. B. (1946). A mathematical investigation of water droplet trajectories. Technical Report 5418, US Army Air Forces Technical report.

Laskowski, J. S. and Kitchener, J. A. (1969). The hydrophylic-hydrophobic transition on silica. *J Colloid Interf Sci*, 29(4):670–679.

Levich, V. G. (1952). *Physicochemical hydrodynamics (in Russian)*. Acad Nauk CCCP, Moscow, Russia.

Liepe, F. (1977). *In: Mechanische Verfahrenstechnik I*, pages 65–79. VEB Deutscher Verlag für Grundstoffindustrie, Leipzig, Germany.

Liu, T. Y. and Schwarz, M. P. (2009a). CFD-based modelling of bubble-particle collision efficiency with mobile bubble surface in a turbulent environment. *Int J Miner Process*, 90(1-4):45–55.

Liu, T. Y. and Schwarz, M. P. (2009b). CFD-based multiscale modelling of bubble-particle collision efficiency in a turbulent flotation cell. *Chem Eng Sci*, 64(24):5287–5301.

London, F. (1930). Zur Theorie und Systematik der Molekularkräfte. *Z Physik*, 63(3-4):245–279.

London, F. (1937). The general theory of molecular forces. *Trans Faraday Soc*, 33:8–26.

Luttrell, G. H. and Yoon, R.-H. (1992). A hydrodynamic model for bubble-particle attachment. *J Colloid Interf Sci*, 154(1):129–137.

Malone, K. F. and Xu, B. H. (2008). Determination of contact parameters for discrete element method. *Particuology*, 6(6):521–528.

Manev, E. D. and Nguyen, A. V. (2005). Effects of surfactant adsorption and surface forces on thinning and rupture of foam liquid films. *Int J Mineral Process*, 77(1):1–45.

Mao, L. (1998). *Application of extended DLVO theory: Modeling of flotation and hydrophobicity of dodecane*. PhD thesis, Virginia Polytechnic Institute and State University, Blacksburg, Virginia, USA.

Masliyah, J. H. and Bhattacharjee, S. (2006). *Electrokinetic and Colloid Transport Phenomena*. Wiley-Interscience.

McCartney, L. N. and Levine, S. (1969). An improvement on Derjaguin's expression at small potentials for the double layer interaction energy of two spherical colloidal particles. *J Colloid Interf Sci*, 30(3):345–354.

Mclaughlin, J. B. (1996). Numerical simulation of bubble motion in water. *J Colloid Interf Sci*, 184(2):614–625.

Mei, R. and Hu, K. C. (1999). On the collision rate of small particles in turbulent flows. *J Fluid Mech*, 391:67–89.

Menon, S., Rothstein, J., Schmidt, D. P., and Ž. Tuković (2008). Simulating non-newtonian droplet formation with a moving-mesh method. In *Proc. ILASS Americas, 21st Annual Conference on Liquid Atomization and Spray Systems*, Orlando, Florida, USA.

Meyer, C. J. and Deglon, D. A. (2011). Particle collision modeling - A review. *Min Eng*, 24(8):719–730.

Neto, C., Evans, D. R., Bonaccurso, E., Butt, H.-J., and Craig, V. S. J. (2005). Boundary slip in newtonian liquids: a review of experimental studies. *Rep Prog Phys*, 68(12):2859–2897.

Nguyen, A. V. (1999). Hydrodynamics of liquid flows around air bubbles in flotation: a review. *Int J Miner Process*, 56(1-4):165–205.

Nguyen, A. V. (2003). New method and equations for determining attachment tenacity and particle size limit in flotation. *Int J Miner Process*, 68(1-4):167–182.

Nguyen, A. V. and Evans, G. M. (2004). Attachment interaction between air bubbles and particles in froth flotation. *Exp Thermal Fluid Sci*, 28(5):381–385.

Nguyen, A. V., Ralston, J., and Schulze, H. J. (1998). On modelling of bubble-particle attachment probability in flotation. *Int J Miner Process*, 53(4):225–249.

Nguyen, A. V. and Schulze, H. J. (2004). *Colloidal science of flotation*, volume 118 of *Surfactant Series*. Marcel Dekker, New York.

Nguyen, A. V., Schulze, H. J., and Ralston, J. (1997a). Elementary steps in particle-bubble attachment. *Int J Miner Process*, 51(1-4):183–195.

Nguyen, A. V., Schulze, H. J., Stechemesser, H., and Zobel, G. (1997b). Contact time during impact of a spherical particle against a plane gas-liquid interface: Theory. *Int J Miner Process*, 50(1-2):97–111.

Nguyen, A. V., Stechemesser, H., Zobel, G., and Schulze, H. J. (1997c). Order of three-phase (solid-liquid-gas) contact line tension probed by simulation of three-phase contact line expansion on small hydrophobic spheres. *J Colloid Interf Sci*, 187(2):547–550.

Nguyen, C. M., Nguyen, A. V., and Miller, J. D. (2006). Computational validation of the Generalized Sutherland Equation for bubble-particle encounter efficiency in flotation. *Int J Miner Process*, 81(3):141–148.

Nishkov, I. and Pugh, R. J. (1991). Studies on the bubble-particle detachment forces in relationship to mineral flotation. In *Proc. XVII Int Miner Process Congr (IMPC)*, pages 339–351, Vol. II, Dresden, Germany, September 23-28 1991.

Olsson, E. and Kreiss, G. (2005). A conservative level set method for two phase flow. *J Comput Phys*, 210(1):225–246.

Omelka, B., Schreithofer, N., and Heiskanen, K. (2010). Effect of hydropobicity and frother concentration on bubble-particle aggregate behaviour in turbulent flow. In *Proc. XXV Int Miner Process Congr (IMPC)*, Brisbane, Australia, September 6-10, 2010.

Omelka, B., Schreithofer, N., Wierink, G., and Heiskanen, K. (2009). Particle detachment in flotation. In *Proc. Procemin 2009*, pages 257–263, Santiago, Chile, December 4-5 2009. Gecamin.

OpenCFD Ltd. (2011a). OpenFOAM - The open source CFD toolbox, http://www.openfoam.com.

OpenCFD Ltd. (2011b). OpenFOAM Programmer's Guide Version 2.0.0, 16th June 2011.

OpenCFD Ltd. (2011c). OpenFOAM User Guide Version 2.0.0, 16th June 2011.

Palaparthi, R., Papageorgiou, D. T., and Maldarelli, C. (2006). Theory and experiments on the stagnant cap regime in the motion of spherical surfactant-laden bubbles. *J Fluid Mech*, 559:1–44.

Pashley, R. M. and Israelachvili, J. N. (1981). A comparison of surface forces and interfacial properties of mica in purified surfactant solutions. *Colloids Surf*, 2(2):169–187.

Pashley, R. M., McGuiggan, P. M., Ninham, B. W., and Evans, D. F. (1985). Attractive forces between uncharged hydrophobic surfaces: direct measurements in aqueous solution. *Science*, 229(4718):1088–1089.

Patankar, S. V. (1980). *Numerical Heat Transfer and Fluid Flow*. Taylor & Francis, New York, first edition.

Patankar, S. V. and Spalding, D. B. (1972). A calculation procedure for heat, mass and momentum transfer in three-dimensional parabolic flows. *Int J Heat Mass Transfer*, 15(10):1787–1806.

Paulsen, F. G., Pan, R., Bousfield, D. W., and Thompson, E. V. (1996). The dynamics of bubble/particle attachment and the application of two disjoining film rupture models to flotation.: I. Nondraining model. *J Colloid Interf Sci*, 178(2):400–410.

Pedocchi, F. and Piedra-Cueva, I. (2005). Camp and Stein's velocity gradient formalization. *J Envir Eng*, 131:1369–1376.

Phan, C. M., Nguyen, A. V., Miller, J. D., Evans, G. M., and Jameson, G. J. (2003). Investigations of bubble-particle interactions. *Int J Miner Process*, 72(1-4):239–254.

Plate, H. and Schulze, H. J. (1991). Modelling of the overall flotation process based on physico-chemical micro-processes – Techniques and application. In *Proc. XVII Int Miner Process Congres (IMPC)*, pages 365–377, Vol. III, Dresden, Germany, 23-28 September.

Plimpton, S. (1995). Fast parallel algorithms for short-range molecular dynamics. *J Comp Phys*, 117(1):1–19.

Podzimek, J. (1997). Droplet concentration and size distribution in haze and fog. *Studia Geophysica et Geodaetica*, 41(3):277–296.

Pyke, B. (2004). *Bubble-particle capture in turbulent flotation sytems*. PhD thesis, University of South Australia, Adelaide.

Rabinovich, Y. I. and Churaev, N. V. (1979). Effect of electromagnetic lag on forces of molecular attraction between solids. *Colloid J*, 41:392–397.

Rabinovich, Y. I. and Yoon, R.-H. (1994). Use of atomic force microscope for the measurements of hydrophobic forces between silanated silica plate and glass sphere. *Langmuir*, 10(6):1903–1909.

Ralston, J., Fornasiero, D., and Hayes, R. (1999). Bubble-particle attachment and detachment in flotation. *Int J Miner Process*, 56(1-4):133–164.

Ramsey, A. S. (1935). *A treatise on hydrodynamics. Part II. Hydrodynamics*. G. Bell and Sons, London.

Reay, D. and Ratcliff, G. A. (1975). Experimental testing of the hydrodynamic collision model of fine particle flotation. *Canadian J Chem Eng*, 53(5):481–486.

Rehbinder, P. A. (1940). Wetting and flotation in connection with the problem of the transition layer. *Trans Faraday Soc*, 35:295–305.

Roco, M. C. (1993). *Particulate Two-Phase Flow*. Butterworth-Heinemann, Boston.

Rosen, M. J. (2004). *Surfactants and Interfacial Phenomena*. Wiley, Hoboken, NJ, USA.

Russel, W. B., Saville, D. A., and Schowalter, W. R. (2001). *Colloidal dispersions*. Cambridge University Press, Cambridge, UK, 1995 reprint edition.

Rybczynski, W. (1911). Über die fortschreitende Bewegung einer flüssigen Kugel in einem zähen Medium. *Bull Acad Pol Sci Lett, Cl Sci Math Nat, A*, pages 40–46.

Sader, J. E., Carnie, S. L., and Chan, D. Y. C. (1995). Accurate analytic formulas for the double-layer interaction between spheres. *J Colloid Interf Sci*, 171(1):46–54.

Saffman, P. G. and Turner, J. S. (1956). On the collision of drops in turbulent clouds. *J Fluid Mech*, 1(1):16–30.

Scheludko, A. (1962). Sur certaines particularités des lames mousseuses. III. Nature et épaisseur des lames noires et durée des mousses. In *Proc Koninkl Nederl Akad Wet B*, pages 97–108, Amsterdam.

Scheludko, A., Toshev, B. V., and Bojadjiev, D. T. (1976). Attachment of particles to a liquid surface (Capillary theory of flotation). *J Chem Soc, Faraday Trans I*, 72:2815–2828.

Scheludko, A., Tschaljowska, S., and Fabrikant, A. (1970). Contact between a gas bubble and a solid surface and froth flotation. *Spec Discuss Faraday Soc*, 1:112–117.

Schuhmann, R. (1942). Flotation kinetics. I. Methods for steady-state study of flotation problems. *J Phys Chem*, 46(8):891–902.

Schulze, H. J. (1977). New theoretical and experimental investigations on stability of bubble/particle aggregates in flotation: A theory on the upper particle size of floatability. *Int J Miner Process*, 4(3):241–259.

Schulze, H. J. (1982). Dimensionless number and approximate calculation of the upper particle size of floatability in flotation machines. *Int J Miner Process*, 9(4):321–328.

Schulze, H. J. (1983). *Physico-chemical elementary processes in flotation*, volume 4 of *Developments in Mineral Processing*. Elsevier, Amsterdam, The Netherlands.

Schulze, H. J. (1989). Hydrodynamics of bubble-mineral particle collisions. *Min Process Extr Metall Rev*, 5(1&4):43–76.

Schulze, H. J. (1993). *In: Coagulation and flocculation: Theory and applications*, chapter 7. Flotation as a heterocoagulation process: Possibilities of calculating the probability of flotation, pages 321–353. Surfactant Science Series nr. 47. Dekker, New York.

Schulze, H. J. and Birzer, J. O. (1987). Stability of thin liquid films on Langmuir-Blodgett layers on silica surfaces. *Colloids Surf*, 24(2-3):209–224.

Schulze, H. J., Radoev, B., Geidel, T., Stechemesser, H., and Töpfer, E. (1989a). Investigations of the collision process between particles and gas bubbles in flotation – A theoretical analysis. *Int J Miner Process*, 27(3-4):263–278.

Schulze, H. J., Wahl, B., and Gottschalk, G. (1989b). Determination of adhesive strength of particles within the liquid/gas interface in flotation by means of centrifuge method. *J Colloid Interf Sci*, 128(1):57–65.

Scriven, L. E. and Sternling, C. V. (1960). The Marangoni effects. *Nature*, 187:186–188.

Seppälä, M., Laakkonen, M., Manninen, M., Alopaeus, V., and Aittamaa, J. (2008). Development of automatic zoning algorithm for combining CFD and multibloc modelling and application to flotation cell. In *Proc. 6th Int Conf CFD in Oil & Gas, Metallurgical and Process Industries*, SINTEF/NTNU, Trondheim, Norway, June 10-12.

Shurman, J. (2010). *Multivariable calculus*. Reed College, Portland, OR, USA.

Smirnov, V. I. (1949). *A Course in Higher Mathematics (in Russian)*, volume 3, part 2. Moscow.

Smoluchowski, M. (1903). Contribution à la théorie de l'endosmose électrique et de quelques phenomènes corrélatifs. *Bull Int Acad Sci Cracovie*, 8:182–200.

Smoluchowski, M. (1917). Versuch einer mathematische Theorie der Koagulationskinetik kolloider Lösungen. *Z Phys Chem*, 92:129–168.

Stechemesser, H. and Nguyen, A. V. (1999). Time of gas-solid-liquid three-phase contact expansion in flotation. *Int J Miner Process*, 56(1-4):117–132.

Sutherland, K. L. (1948). Physical chemistry of flotation. XI. Kinetics of the flotation process. *J Phys Chem*, 52(2):394–425.

Taylor, G. I. (1935). Statistical theory of turbulence. *Proc R Soc London A*, 151:421–444.

Tomiyama, A., Zun, I., Sou, A., and Sakaguchi, T. (1993). Numerical analysis of bubble motion with the VOF method. *Nuclear Eng Design*, 141(1-2):69–82.

Tsao, Y., Yang, S. X., and Evans, D. F. (1991). Interactions between hydrophobic surfaces. Dependence on temperature and alkyl chain length. *Langmuir*, 7(12):3154–3159.

Tuković, Ž. (2005). *The finite volume method on a domain of variable shape (in Croatian)*. PhD thesis, University of Zagreb, Croatia.

Tuković, Ž. and Jasak, H. (2008). Simulation of free-rising bubble with soluble surfactant using moving mesh finite volume/area method. In *Proc. 6th Int Conf CFD in Oil & Gas, Metallurgical and Process Industries*, SINTEF/NTNU, Trondheim, Norway.

Tuković, Ž. and Jasak, H. (2012). A moving mesh finite volume interface tracking method for surface tension dominated interfacial fluid flow. *Computers & Fluids*, 55:70–84.

Tuteja, R. K., Spottiswood, D. J., and Misra, V. N. (1994). Mathematical models of the column flotation process a review. *Min Eng*, 7(12):1459–1472.

Ubbink, O. (1997). *Numerical prediction of two fluid systems with sharp interfaces*. PhD thesis, Imperial College London.

Versteeg, H. and Malalasekra, W. (2007). *An Introduction to Computational Fluid Dynamics: The Finite Volume Method*. Prentice Hall, second rev. edition.

Verwey, E. J. W. and de Boer, J. H. (1938). Dilatancy. *Rec Trav Chim*, 57(4):345–458.

Verwey, E. J. W. and Overbeek, J. T. G. (1948). *Theory of the stability of lyophobic colloids: The interaction of sol particles having an electric double layer*. Elsevier, Amsterdam.

Vincent, S. and Caltagirone, J.-P. (2003). Parasitic currents induced by surface tension. *Test-cases for interface tracking methods*, http://test.interface.free.fr.

Viswanathan, S. (1999). Numerical study of particle collection by single water droplets. *Ind Eng Chem Res*, 38(11):4433–4442.

von Helmholtz, H. L. F. (1879). Studien über elektrische Grenzschichten. *Ann Phys*, 7:337–382.

Weber, M. E. and Paddock, D. (1983). Interceptional and gravitational collision efficiencies for single collectors at intermediate Reynolds numbers. *J Colloid Interf Sci*, 94(2):328–335.

Weller, H. (2007). Pressure-velocity solution algorithms for transient flows. Technical Report TR/HGW/05, OpenCFD Ltd.

Weller, H. (2008). A New Approach to VOF-based Interface Capturing Methods for Incompressible and Compressible Flow. Technical Report TR/HGW/04, OpenCFD Ltd.

Weller, H. (2010). Personal communication.

Weller, H. G. (1993). The development of a new flame area combustion model using conditional averaging. Technical Report TF 9307, Imperial College of Science, Technology and Medicine.

White, E. T. and Beardmore, R. H. (1962). The velocity of rise of single cylindrical air bubbles through liquids contained in vertical tubes. *Chem Eng Sci*, 17(5):351–361.

White, L. R. (1983). On the Deryaguin approximation for the interaction of macrobodies. *J Colloid Interf Sci*, 95(1):286–288.

Wierink, G., Tiitinen, J., and Heiskanen, K. (2009). Mapping of collision regimes in flotation modelling. In *Proc. 7th Int Conf CFD in Oil & Gas, Metallurgical and Process Industries*, CSIRO, Melbourne, Australia, December 9-11.

Wierink, G. A., Goniva, C., Ničeno, B., and Heiskanen, K. (2011). Mechanistic modelling of particle-interface interaction in three-phase flows. In *Proc. 8th Int Conf CFD in the Oil & Gas, Metallurgical and Process Industries (CFD 2011)*, SINTEF/NTNU, Trondheim, Norway, 21-23 June 2011.

Wierink, G. A. and Heiskanen, K. (2008). Momentum coupling in flotation modelling. In *Proc. Computational Modelling '08*, Cape Town, South Africa.

Xu, J.-J., Li, Z., Lowengrub, J., and Zhao, H. (2006). A level-set method for interfacial flows with surfactant. *J Comp Phys*, 212(2):590–616.

Xu, Z. and Yoon, R.-H. (1989). The role of hydrophobic interactions in coagulation. *J Colloid Interf Sci*, 132(2):532–541.

Xu, Z. and Yoon, R.-H. (1990). A study of hydrophobic coagulation. *J Colloid Interf Sci*, 134(2):427–434.

Yoon, R.-H. (1991). Hydrodynamics and surface forces in bubble-particle interactions. In *Proc. XVII Int Miner Process Congr (IMPC)*, pages 17–31, Vol. II, Dresden, Germany, September 23-28 1991.

Yoon, R.-H. (1993). Microbubble flotation. *Min Eng*, 6(6):619–630.

Yoon, R.-H. and Luttrell, G. H. (1989). The effect of bubble size on fine particle flotation. *Min Process Extr Metall Rev*, 5(1&4):101–122.

Yoon, R.-H. and Mao, L. (1996). Application of extended DLVO theory, IV: Derivation of flotation rate equation from first principles. *J Colloid Interf Sci*, 181(2):613–626.

Yoon, R.-H. and Ravishankar, S. A. (1996). Long-range hydrophobic forces between mica surfaces in dodecylammonium chloride solutions in the presence of dodecanol. *J Colloid Interf Sci*, 179(2):391–402.

Yotsumoto, H. and Yoon, R.-H. (1993). Application of extended DLVO theory: I. Stability of rutile suspensions. *J Colloid Interf Sci*, 157(2):426–433.

Aalto-DD 57/2012

ISBN 978-952-60-4617-4
ISBN 978-952-60-4618-1 (pdf)
ISSN-L 1799-4934
ISSN 1799-4934
ISSN 1799-4942 (pdf)

Aalto University
School of Chemical Technology
Department of Materials Science and Engineering
www.aalto.fi

BUSINESS +
ECONOMY

ART +
DESIGN +
ARCHITECTURE

SCIENCE +
TECHNOLOGY

CROSSOVER

DOCTORAL
DISSERTATIONS